NASA Contractor Report 166618

Space Shuttle Flying Qualities Criteria Assessment Phase IV

Data Acquisition and Analysis

T. T. Myers, D. E. Johnston, and D. T. McRuer

May 1986

National Aeronautics and
Space Administration

NASA Contractor Report 166618

Space Shuttle Flying Qualities Criteria Assessment Phase IV

Data Acquisition and Analysis

T. T. Myers, D. E. Johnston, and D. T. McRuer
Systems Technology, Inc., 13766 South Hawthorne Boulevard, Hawthorne, California 90250

Prepared for
Ames Research Center
Dryden Flight Research Facility
Edwards, California
Contract NAS2-11431

1986

National Aeronautics and
Space Administration
Ames Research Center
Dryden Flight Research Facility
Edwards, California 93523

TABLE OF CONTENTS

LIST OF FIGURES

LIST OF FIGURES (Continued)

LIST OF FIGURES (Continued)

LIST OF FIGURES (Concluded)

LIST OF TABLES

NOMENCLATURE

AN	Normal acceleration from Cinetheodolite
c.g.	Center of gravity
g	Acceleration due to gravity (32.2 ft/sec^2)
G.S.	Glide slope
h	Altitude
$\dot{h}$	Vertical speed
$\dot{h}_c$	Desired vertical speed
$\dot{h}_e$	Vertical speed error
h_f	Flare initiation altitude
h_o	Altitude at start of shallow glide
h_B	Depth of flare asymptote
$\dot{h}_{TD}$	Vertical speed at touchdown
K	Gain
$K_{\dot{V}}$	Averaged value of -dV/dt
M	Aerodynamic pitching moment; Mach number
n	Load factor
n_z	Load factor in z direction
N_δ^h	Altitude-to-elevator numerator
N_δ^θ	Pitch attitude-to-elevator numerator
Q	Pitching velocity
q	Pitching velocity (pertubation)
$\bar{q}$	Dynamic pressure
q_{TD}	Pitch rate touchdown

s	Laplace Operator
t'_{TD}	Touchdown time measured from flare initiation
T	Time constant; sampling period
T_f	Flare time constant
T_q	Lead time constant in augmentaion system
T_{θ_2}	Lead time constant in short-period θ/δ transfer function for conventional airplane dynamics. Lag time constant between flight path angle, γ, and pitch attitude, θ. $$1/T_{\theta_2} = -Z_w + Z_\delta M_w/M_\delta \doteq -Z_w$$
U_o	Speed in reference condition
V	Speed
V_f	Speed at flare initiation
V_o	Velocity at start of shallow glide
V_T	True airspeed
V_{TD}	Touchdown speed
X_f	Distance traveled in flare
X_g	Distance traveled in shallow glide
X_t	Total distance traveled in shallow glide and flare
Y_{P_h}	Pilot describing function for pilot control action on path deviation
$Y_{p\theta}$	Pilot describing function for pilot control action on attitude
α	Angle of attack
β	Sideslip angle, v/U_o
γ	Flight path angle
γ_o	Selected flight path angle

δ_{RHC}	Rotational hand controller deflection
ζ	Damping ratio
θ	Pitch attitude
θ_c	Attitude Command
θ_e	Attitude Error
ρ	Coherence function (Pg. II-1)
σ	Standard deviation
τ	Time delay
$\phi_{\delta\delta}$	Spectral density distribution of input
ϕ_{qq}	Spectral density distribution of pitch rate
$\phi_{q\delta}$	Cross-spectral density distribution of pitch rate and input
ω	Frequency (Imaginary component of complex variable s)
ω_n	Natural frequency

ACRONYMS AND ABBREVIATIONS

ACAH	Attitude command/attitude hold
ACIP	Aerodynamic Coefficient Identification Package
AFFTC	Air Force Flight Test Center
AGL	Above ground level
ALT	Approach and Landing Test
BET	Best estimated trajectory
BFCS	Backup flight control system
CSS	Control stick steering
DFRF	Dryden Flight Research Facility
EAFB	Edwards Air Force Base
FCS	Flight control system
FFT	Fast Fourier Transform
FREDA	Frequency domain analysis (computer program)
GMT	Greenwich Mean Time
GPC	General purpose computer
HAC	Heading alignment cylinder
HUD	Head-up display
IDH	Interactive data handler
IMU	Inertial measurement unit
JSC	Johnson Space Center
KEAS	Knots equivalent airspeed
LKF	Linearized Kalman Filter
LRC	Langley Research Center
MFP	Multifrequency Parameter Identification Program

MMLE	Modified maximum likelihood estimator
MPDB	Master products data base
NIPIP	Non-intrusive parameter identification program
OEX	Orbiter experiment
OFT	Orbiter Flight Test
OFQ	Flying qualities and flight control system design criteria experiment
OI	Operational instrumentation
PAPI	Precision Approach Path Indicator
PIO	Pilot induced oscillation
RCAH	Rate command/attitude hold
RHC	Rotational hand controller
STA	Shuttle training aircraft
STI	Systems Technology, Inc.
STS	Space Transporation System
TRS	Tape reservation system

SECTION I

INTRODUCTION

This study is a continuation of work initiated under Contracts NAS4-2834, NAS4-2940, and NAS2-11431, Space Shuttle Flying Qualities and Flight Control System Criteria Assessment, Phases I, II, and III. It provides continuation and refinement of a program for the Orbiter Experimental Program (OEX) titled Flying Qualities and Flight Control Systems Design Criteria Experiment (OFQ). The first phase effort, documented in Ref. 1, was devoted to review of existing flying quality and flight control system specification and criteria; review of Shuttle experimental and flight data; identification of specification shortcomings; and preparation of a preliminary OEX approach to produce the optimum use of flight data to develop modified flying qualities criteria for Space Shuttle craft in general.

The Phase I investigation identified several likely problem areas to be addressed in the OEX plan. First, mismatch of Shuttle specification pitch rate response boundaries (and Shuttle response) with available flying qualities data raised the question of whether the specification response boundaries are misplaced or whether the available data base is inadequate for highly augmented relaxed static stability aircraft. The specification boundaries also appeared to allow excessive pitch and roll rate response dead time. Second, comparison of Shuttle characteristics with other criteria, guides, etc., tended to indicate it exhibited excessive longitudinal and lateral effective time delays. This would lower the effective vehicle bandwidth and then reduce pilot-vehicle and autopilot-vehicle attainable closed-loop bandwidth in rolling and path control functions. It would also be expected to produce a tendency for PIO under high stress, precise control situations. Other likely problem areas concerned pilot location effects and hand controller characteristics. While well ahead of the c.g., the pilot is aft of the center of instantaneous rotation for longitudinal control inputs. This location

has consequences on longitudinal path control (possibly quite unfavorable for precise control situations) and lateral acceleration at the pilot station. The rotational hand controller (RHC) displacement/force/electrical command, combined characteristics possibly result in increased pilot control latencies (due to near isotonic properties). This can also affect the control bandwidth and contribute to control difficulties in urgent tasks. Finally, the Phase I effort indicated possible problems concerning off nominal cases of critical aerodynamics variation sets, trim extremes, and reduced surface rates.

The Phase II investigation (Ref. 2) continued the review and analysis of applicable experimental and Shuttle flight data and provided further definition of the Orbiter Flying Qualities Experiment (OFQ) Plan. In particular, the influence of "superaugmentation" on vehicle handling characteristics was continued. It was found that the Shuttle qualifies as a superaugmented vehicle and the form (although not necessarily the numerical value) of the Shuttle specification pitch rate response boundaries may be appropriate for this class of vehicle. Further, elementary superaugmented aircraft such as the Shuttle have unconventional attitude/path response characteristics and zero stick force/speed gradient. Review of STS-1 through -4 crew qualitative assessments indicated flying qualities to be adequate at high altitude and speed, but unconventional and possibly marginal in terminal control (preflare, shallow glide, and final flare).

The OFQ plan was further refined to address the above superaugmentation considerations and special conditions of Shuttle flights which require a somewhat unconventional, indirect, experimentation approach. The indirect approach consists of in-flight experiments combined with a correlated research simulation program. The unconventional features of the approach include the use of non-intrusive flight measurements for effective vehicle and pilot strategy (model) identifications. These flight measurements then can be used to validate simulations for ground experiment programs involving critical flight situations not likely to be permitted (or encountered) on Shuttle flights.

The Phase III study (Ref. 3) encompassed continued analysis of Orbiter STS-4 flight data, conduct of supportive analytic and simulation efforts, and further refinement of the OFQ plan. A major portion of the work was devoted to exploring crucial, but unperfected, flight data measurement and reduction techniques required for the non-intrusive experiment approach. Application of spectral analysis techniques to time history data for the pilot's rotational hand controller (RHC) inputs and vehicle pitch rate response yielded frequency response amplitude and phase data points. Applications of routine parameter identification techniques then produced linearized model transfer function parameters which were in close agreement with the theoretical superaugmentation model derived in Phase II. Application of altitude and sink rate phase plane analysis techniques allowed identification of the preflare, shallow glide, and final flare segments of the landing and provided insight to the control strategy and technique employed by the pilot in each segment. However, confidence in the results was somewhat limited due to problems in extracting sink rate from onboard sensor data contained in the available MMLE flight data tapes.

The purposes of this Phase IV study were to expand the data base through application of the analytical techniques to additional flights and to landing data obtained with the U.S. Air Force cinetheodolite system. Emphasis is placed on the shallow glide, flare, and landing because this is where the unusual flying qualities of superaugmented aircraft become an issue. Three preliminary goals guided the analysis of flight data in Phase IV:

- Identification of the Effective Augmented Vehicle

  While there has been extensive effort to identify the aerodynamic coefficients of the Orbiter airframe from flight data, there has been only one known attempt (Phase III) to directly identify the effective vehicle, as seen by the pilot, which is dominated by the flight control system. This activity is also important to verify analytical models developed in Phase II (e.g., the superaugmented pitch response).

Furthermore, a well defined controlled element model is necessary for the second goal -- pilot technique identification.

- Identification of Piloting Technique

  Identification of piloting technique is more difficult because of technique variations among pilots, pilot remnant, and uncertainty about cues.

- Refinement and Extension of the OFQ Data Handling Procedures

  In addition to obtaining quantitative definition of the vehicle and pilot, refinement and verification of the identification procedures proposed in Phase II has been a primary concern because of the emphasis on non-intrusive techniques.

Section II of this report continues the augmented vehicle pitch response identification with data from two additional flights resulting in almost identical frequency response characteristics as extracted in the Phase III work. Attention is then turned to application of the cinetheodolite data to the phase plane (hodographic) analysis. It is shown that the altitude and sink rate obtained from this source agrees quite well with data obtained by complementary filtered onboard sensor source data. Additionally the cine data are easier to work with and produce auxiliary velocity and distance data not available from the onboard data source tapes.

Section III presents a digest and analysis of STS-2 through -7 landing data. This starts with a review of the flight path landing aids evolution throughout the first seven flights and a digest of information concerning the conditions surrounding each landing. A detailed flight-by-flight analysis of time history traces and hodographs follows and results in identification of possible path control strategies for each landing. Although the hodographs differ markedly across all flights, some significant consistencies in touchdown parameters are noted which provide further insight to possible control loop structures. General trends toward more consistent landings and decreased pilot workload as landing path aids came into service are also indicated.

STS-1 is not included in the Section III analysis because the original archival AFFTC cinetheodolite tape for this flight had passed the time for automatic elimination and had been erased. Another copy of the cine data was available through Rockwell International but this ultimately proved unusable since data in the landing region was missing. This unfortunate set of events lends additional emphasis to the need for the special OFQ flight data archival and processing system outline discussed in Section IV.

Section V is a summary of conclusions and recommendations. The Appendix presents some new approaches to the analysis of pilot strategy for landing with applications to the STS-2 through -7 data. Emphasis is placed on developing theoretical connections between the requirements of a specified task and the implied requirements for flying qualities and flight control system design.

SECTION II

FLIGHT DATA MEASUREMENT AND REDUCTION TECHNIQUES

A. IDENTIFICATION OF ORBITER EFFECTIVE PITCH DYNAMICS

Because of the dominant effect of the FCS on the Orbiter's pitch response, identification of airframe characteristics alone is not adequate to characterize the effective vehicle as seen by the pilot. The superaugmentation model was developed in Phases I and II to deal with this situation. In Phase III the effective vehicle pitch rate response to rotational hand controller (RHC) inputs in landing was extracted from flight data for one flight -- STS-4. This was accomplished by application of a fast Fourier transform spectral analysis technique implemented in a STI Frequency Domain Analysis (FREDA) digital program. The spectral identification of the q/δ_{RHC} describing function requires the δ_{RHC} and q time histories for the approach and landing. The FREDA program obtains the spectral density distributions $\phi_{\delta\delta}$ and ϕ_{qq} and cross spectral $\phi_{q\delta}$ by direct Fourier transform of the time series using the Wiener-Khinchin relationship (Ref. 4). The q/δ_{RHC} describing function is then given by

$$\frac{q}{\delta_{RHC}}(j\omega) = \frac{\phi_{q\delta}(j\omega)}{\phi_{\delta\delta}(j\omega)}$$

The FREDA program produces discrete magnitude and phase angle pairs for q/δ_{RHC}, $\phi_{\delta\delta}$, and ϕ_{qq}. A coherence function

$$\rho^2(\omega) = \frac{|\phi_{q\delta}(j\omega)|^2}{\phi_{qq}(\omega)\ \phi_{\delta\delta}(\omega)}$$

is also computed and gives a measure of the degree to which the output is linearly correlated with the input. A ρ^2 of zero implies no correlation and a ρ^2 of unity indicates perfect correlation between output and input. For vehicle identification, ρ^2 values between 0.8 and 0.9 are generally indicative of meaningful identification.

The FREDA output plots for Columbia STS-4 extending from start of preflare to touchdown, T=30 sec, are shown in Fig. 1. The coherence ρ^2 values are above 0.8 out to approximately 10 rad/sec. Above this frequency the coherence decreases and thus 10 rad/sec is taken as the limit of validity for the frequency response (the describing function plot symbols change when ρ^2 drops below 0.8).

Identification of the effective vehicle transfer function parameter is then accomplished by "fitting" a linear transfer function to the set of discrete magnitude and phase angle points in Fig. 1. This was accomplished in the Phase III work using the superaugmented vehicle transfer function form appropriate for the Shuttle

$$\frac{q}{\delta_{RHC}} = \frac{K(s+1/Tq)\ e^{-\tau s}}{\left[s^2 + 2\zeta\omega_n\ s + \omega_n^2\right]}$$

Table 1 shows a comparison between the theoretical superaugmentation values obtained from a linearized model of the nonlinear digital flight control system and predicted elevon pitching moment aerodynamic coefficient and the values extracted from the STS-4 flight data. Parameter values were extracted with the numerator zero, $1/T_q$, both free and fixed at its theoretical value of 1.5. As noted in Ref. 3, the principal differences between the theoretical values and those from flight lie in the gain (approximately a factor of 2) and in the second-order damping ratio (about 50% higher for the flight data). Possible reasons for these differences were not pursued.

In this Phase IV effort the FREDA program has been applied to the data from Columbia STS-5 and Challenger STS-7. The describing function

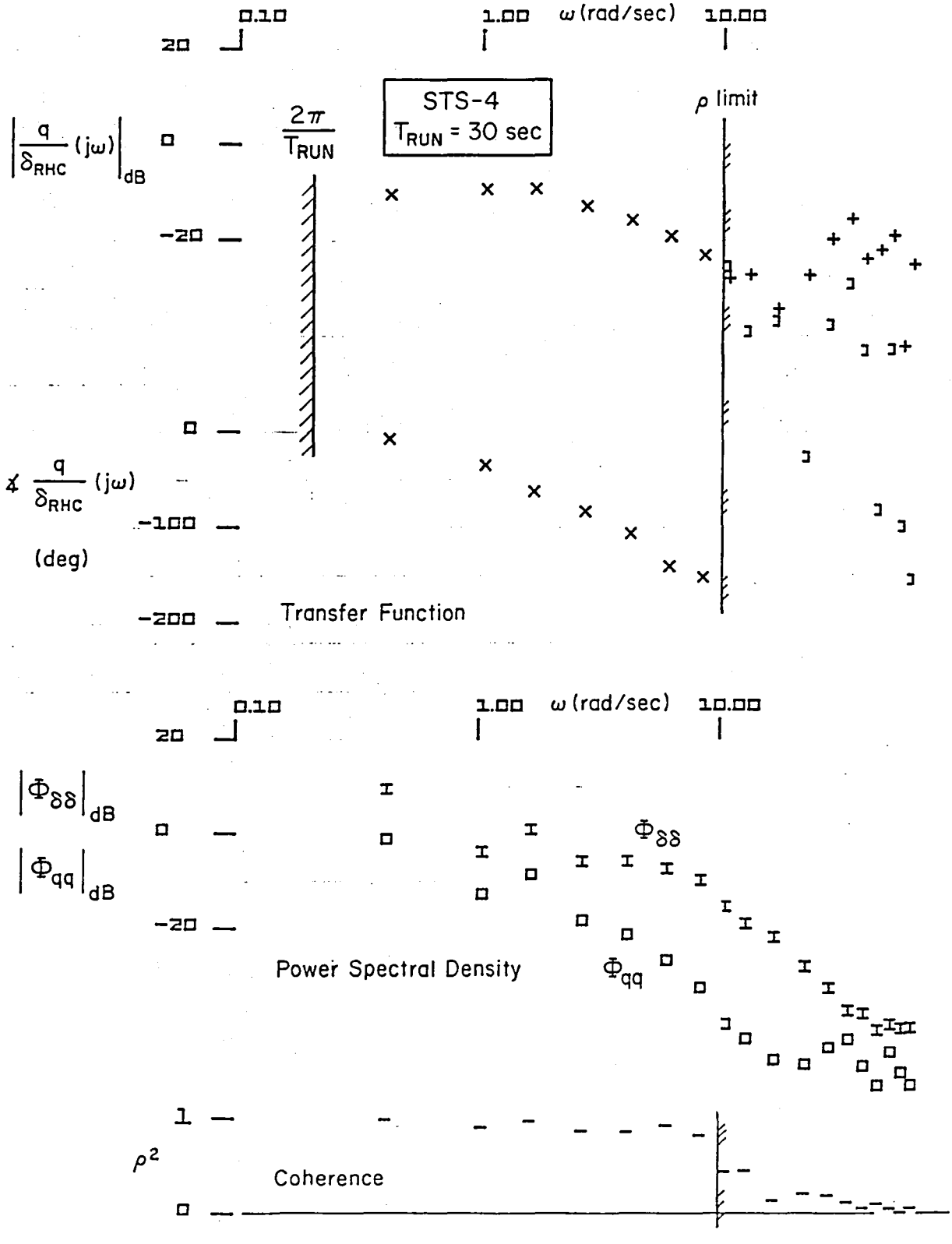

Figure 1. FREDA Output for q/δ_{RHC}, STS-4 Preflare Through Touchdown

TABLE 1. COMPARISON OF PARAMETERS EXTRACTED FROM STS-4 FLIGHT DATA WITH THE SUPERAUGMENTATION MODEL

PARAMETER	SUPERAUGMENTED MODEL	EXTRACTED FROM STS-4 FLIGHT	
		$1/T_q \equiv 1.5$ r/s	$1/T_q$ FREE
$q/\delta_{RHC}(0)$ (rad/sec/rad)	0.17	0.31	0.30
$1/T_q$ (rad/sec)	1.5	1.5	1.03
ζ	0.5	0.74	0.77
ω_n (rad/sec)	1.5	1.68	1.44
τ (sec)	0.174	0.156	0.159

summaries comparable to Fig. 1 are shown for STS-5 and -7 in Figs. 2 and 3, respectively. The discrete frequency response data is superimposed for the three flights in Fig. 4 which also contain the fitted superaugmented form based on the STS-4 data as derived in Phase III. Only those points with a correlation coefficient (ρ) greater than 0.8 are shown. Figure 4 shows that with respect to the major issues in the superaugmentation response, i.e., the effective attitude lead and time delay, there is no indication of a significantly different interpretation than that of Phase III, namely that the effective attitude lead is between 1 and 1.5 rad/sec and thus dominated by the FCS parameter $1/T_q = 1.5$ rad/sec.

The flight data also show essentially no difference between the two Orbiter vehicles. The very close agreement of the data from the three flights thus increases confidence in the technique and results obtained.

B. ALTITUDE/SINK RATE PHASE PLANE ANALYSIS

A major portion of the Phase III work was devoted to pilot control strategy (loop architecture and switching) identification efforts, both

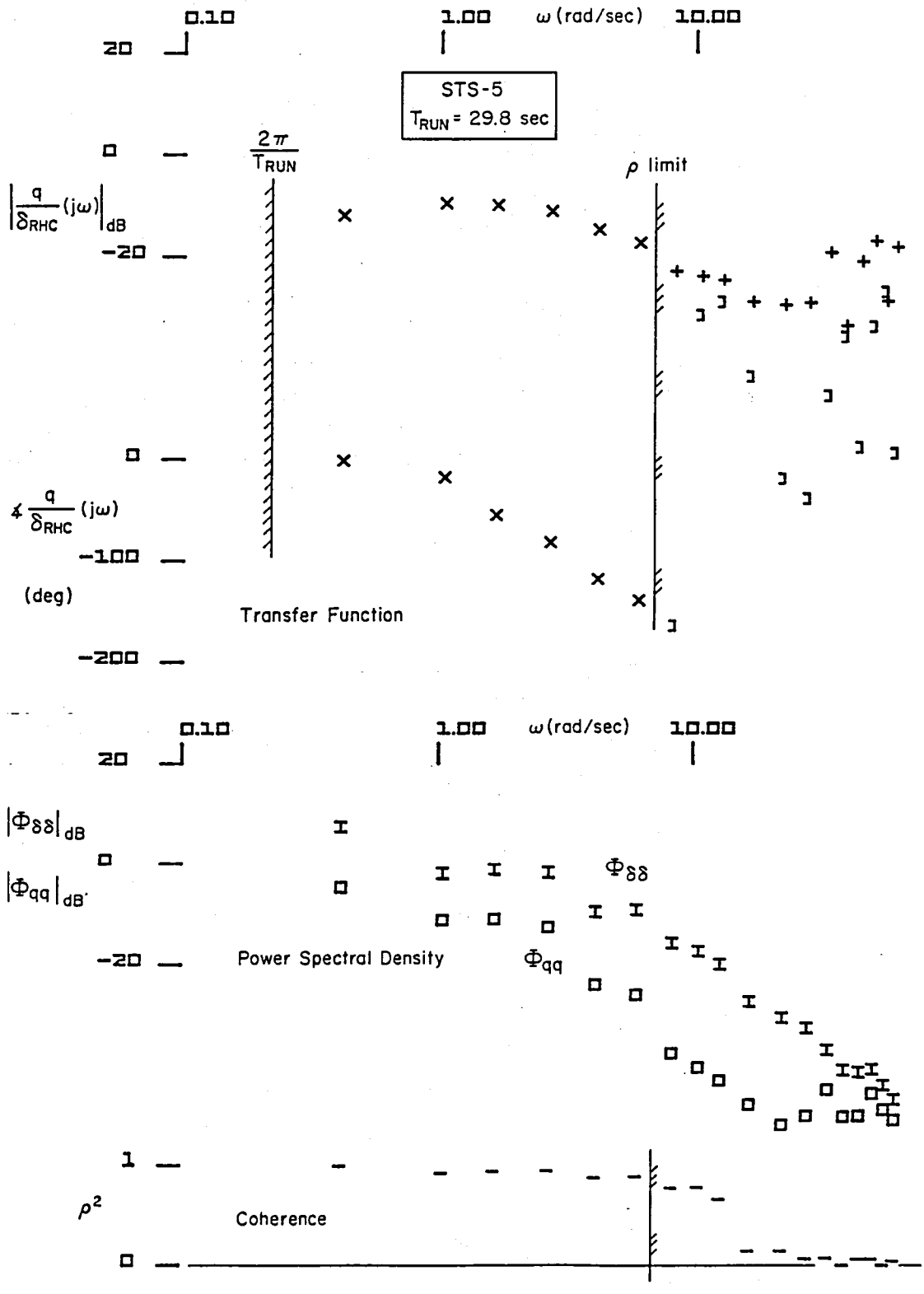

Figure 2. FREDA Output for q/δ_{RHC}, STS-5 Preflare Through Touchdown

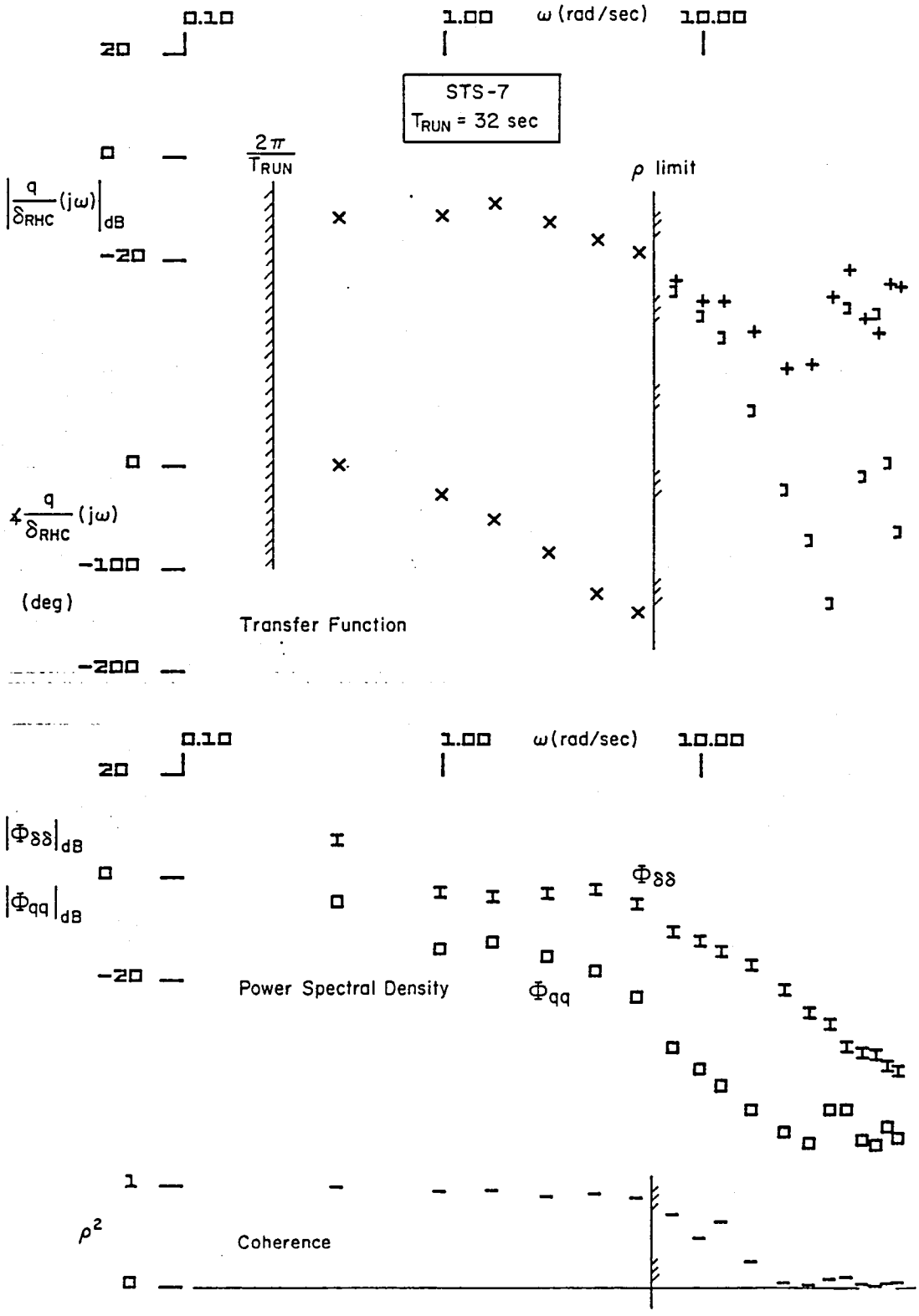

Figure 3. FREDA Output for q/δ_{RHC}, STS-7 Preflare Through Touchdown

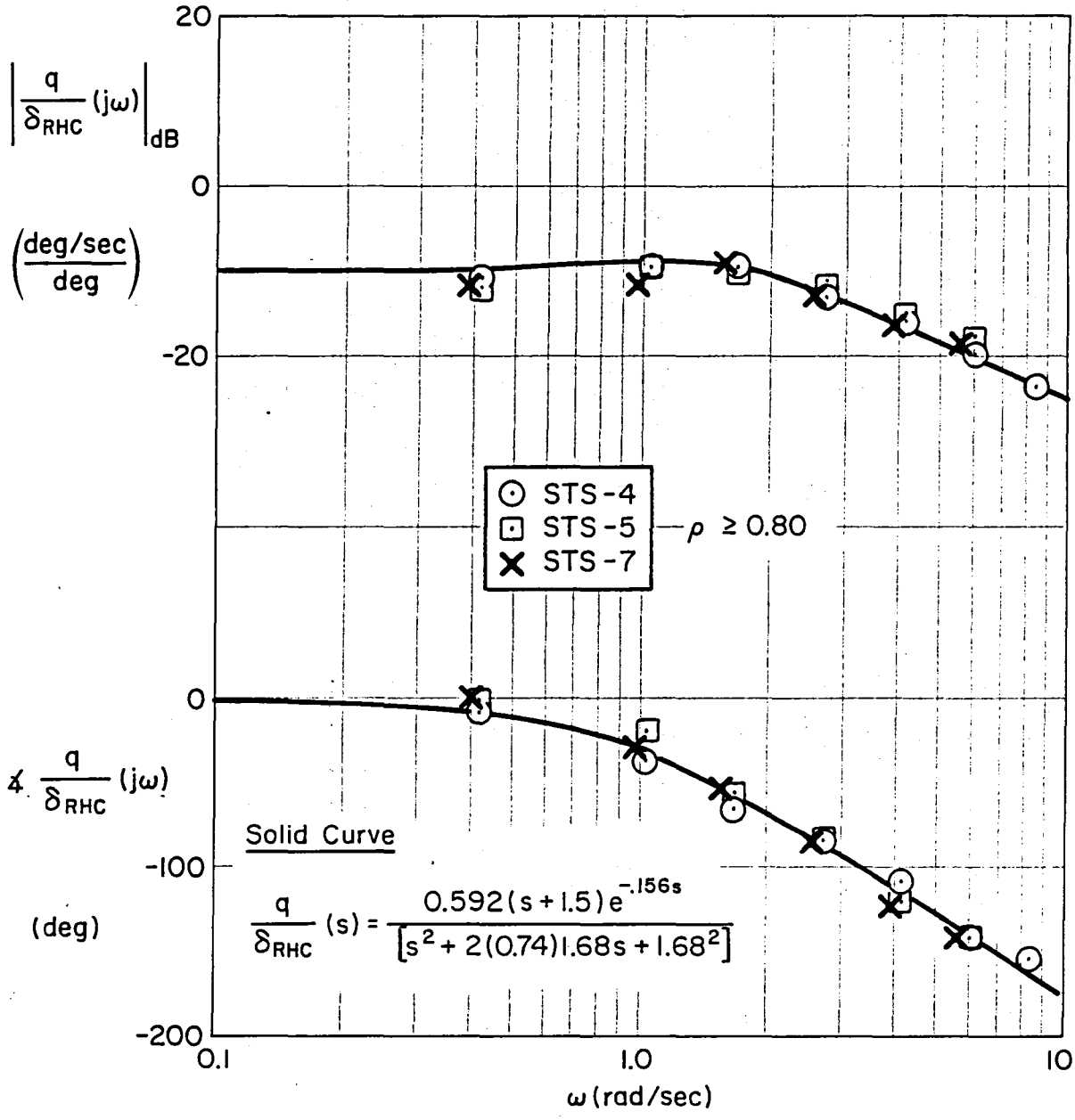

Figure 4. Comparison Between Theoretical Superaugmentation Model and Flight Data

to gain further understanding of pilot technique in landing a superaugmented glider and to refine identification procedures for use in further OFQ experiments. A number of data problems and needs were identified from this Phase III effort. Of these, the one of greatest concern was the need for better altitude and sink rate data from which to extract the landing altitude/sink rate phase plane or hodograph.

The shallow glide and final flare control strategy may be usefully viewed as a trajectory in the altitude/sink rate phase plane shown ideally in Fig. 5. If the shallow glide region has constant flight path angle γ_o as the model implies, the phase plane trajectory will be a straight, sloping line. If the sink rate is constant, the glide trajectory will be horizontal. In the final flare region, if sink rate is scheduled proportional to altitude, the phase plane is a straight line with slope $-1/T_f$. The slope reflects the relative weighting given to arresting sink rate as altitude decreases and therefore can vary significantly. If any other relationship is employed, the phase plane will be curved.

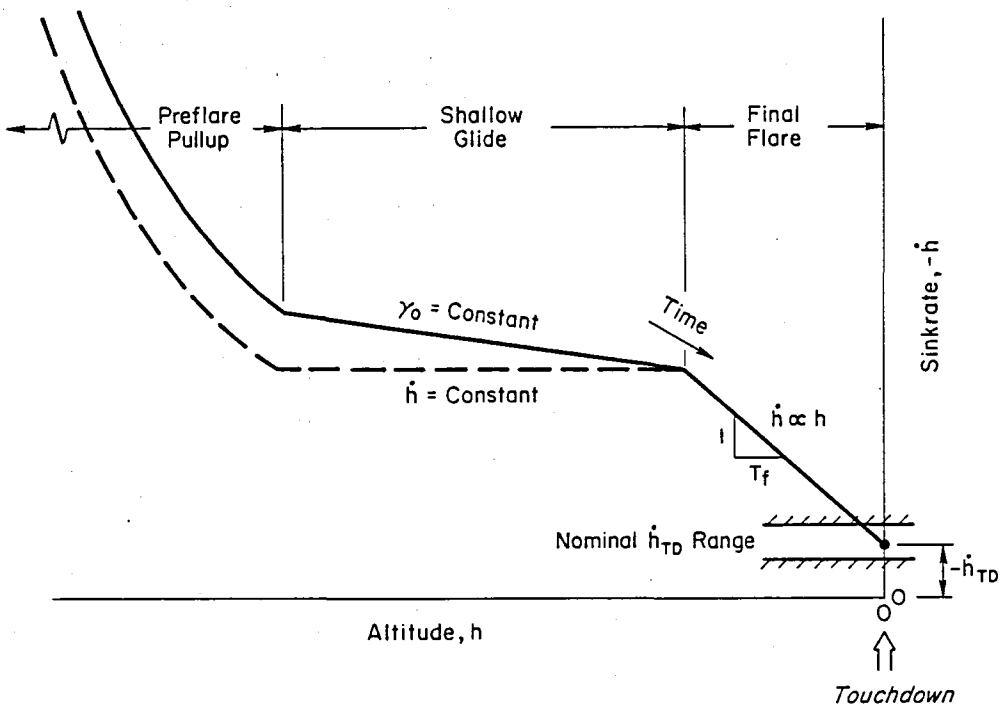

Figure 5. Idealized Altitude/Sink Rate Phase Plane Trajectory for the Shallow Glide and Flare Pilot Model

Application of the phase plane analysis in the preceeding study was complicated by a number of problems with the available STS-4 flight data. The primary source of data for that analysis was the computer file available at DFRF for use with the Modified Maximum Likelihood Estimator (MMLE) program. While the MMLE files were set up for airframe aerodynamic identification, they are usable for preliminary Flight Control System (FCS) and flying qualities studies. However, it was necessary to augment the data available and resolve certain problems before the phase plane analysis could be made.

The MMLE data were plotted as time traces in order to obtain a first cut identification of specific approach and landing segments. In Fig. 6 five time histories are shown from the Phase III data analysis. The time histories are: Rotational Hand Controller (RHC) deflection, pitch rate, angle-of-attack, pitch attitude, and normal acceleration. These traces include the variables pertinent to inner loop (attitude) control. The initial partitioning of these time histories into preflare, shallow glide, and final flare segments is based, in part, on direct examination of the relatively large discrete RHC pulses (cross-hatched in Fig. 6) which appear to initiate significant alteration in vehicle steady state pitch or load factor state.

To consider outer loop (path) control, sink rate and altitude are required since they are essential for the phase plane analysis. Altitude is available on the MMLE file from two sources, the Inertial Measurement Unit (IMU) and the radar altimeter. Unfortunately there is some inconsistency between the two. Further, there is no sink rate data available from the IMU channel and the radar sink rate channel on the STS-4 MMLE file was found to be unusable, due apparently to calibration problems. Thus in Phase III it was necessary to compute sink rate. A radar sink rate plot was created by differentiating the radar altimeter signal. Sink rate was also independently computed from MMLE V_T, θ, and α data $[(\dot{h} = V_T \sin(\theta - \alpha)]$. Finally, another independent sink rate was generated by complementary filtering normal acceleration from the (MMLE) ACIP accelerometer and IMU altitude. The resulting sink rate time traces are shown in Fig. 7 for comparison. The complementary filtered sink rate appears to lie generally between the radar and computed

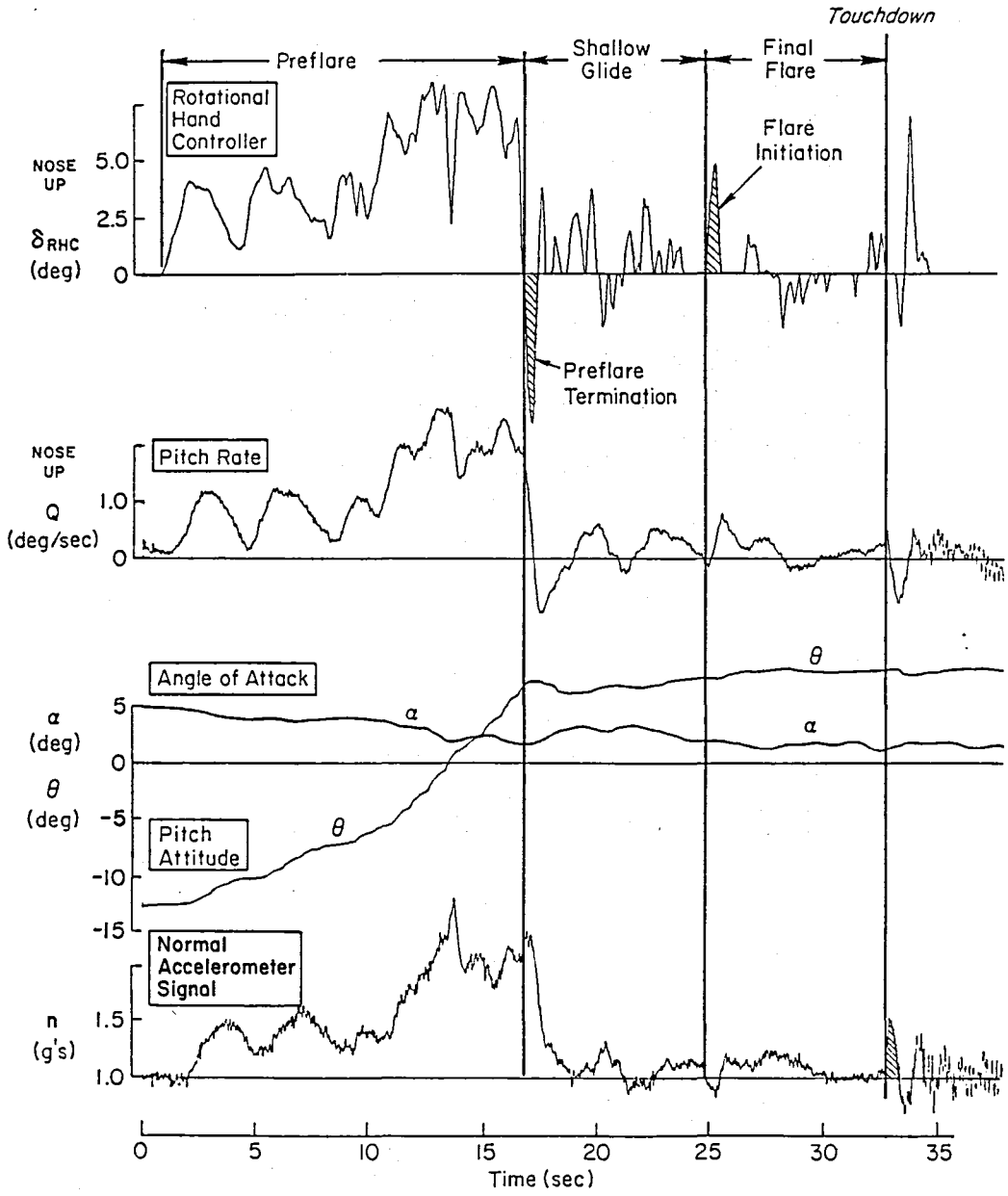

Figure 6. STS-4 Attitude Control Time Histories (from Ref. 3)

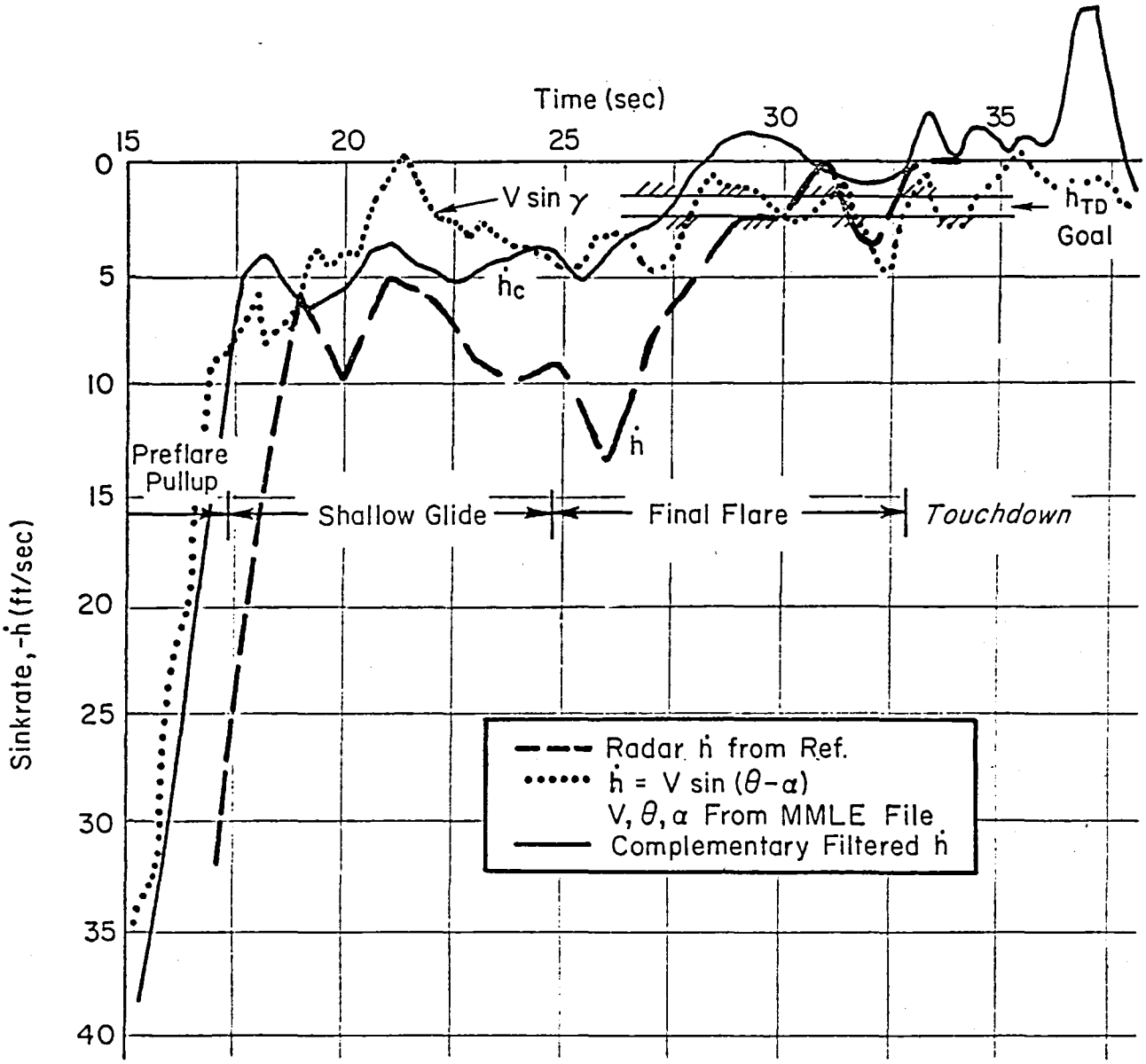

Figure 7. Comparison of Sink Rate Signals (Ref. 3)

sink rates, and was used in the Phase III preliminary analysis to obtain the Fig. 8 STS-4 landing phase plane. This provided encouragement for this non-intrusive approach; however, the need for higher quality altitude and sink rate data was very apparent. In addition, the definition of an effective body reference point becomes very important at altitudes on the order of the Shuttle body length.

For Phase IV higher quality approach and landing measurements from the Air Force Flight Test Center (AFFTC) Contraves cinetheodolite system (Ref. 5) were obtained. This system provides position, rate, altitude, speed, and wind data. Frame-by-frame manual reduction of film from several cinematic cameras is used as raw data to estimate the earth referenced XYZ location of the Orbiter nose, generally at 20 samples per second. The processed data recorded in digital form on magnetic tape was made available through NASA Dryden. This cinetheodolite data has been the primary new data source used in Phase IV.

a. Comparison of Cinetheodolite and MMLE Altitude and Sink Rate Data

As noted earlier, the MMLE data source contains altitude from the onboard radar altimeter and GPC altitude derived from the Navigation Processor. These two onboard altitude signals are compared to the cinetheodolite data in Fig. 9 for the region from the preflare pullup through touchdown. The slow one sample per second rate of the onboard data makes the 20 sample per second cinetheodolite data seem continuous.

It appears in Fig. 9 that there may be some time skew between the onboard measurements (MMLE tape) and the cinetheodolite tape although both are supposedly referenced to Greenwich Mean Time (GMT). No documentation of any procedures for synchronizing the clocks for the MMLE and cinetheodolite data is available. However, since time skews have been a general problem in the Shuttle data acquisition and because an occasional anomaly has been seen in the cinetheodolite data indicating time "gaps," several checks were made of the time references between these two data sources. The only common data between the two systems are the altitude signals and their derivatives. However, the discrepancies noted above between the altitude and sink rate signals preclude

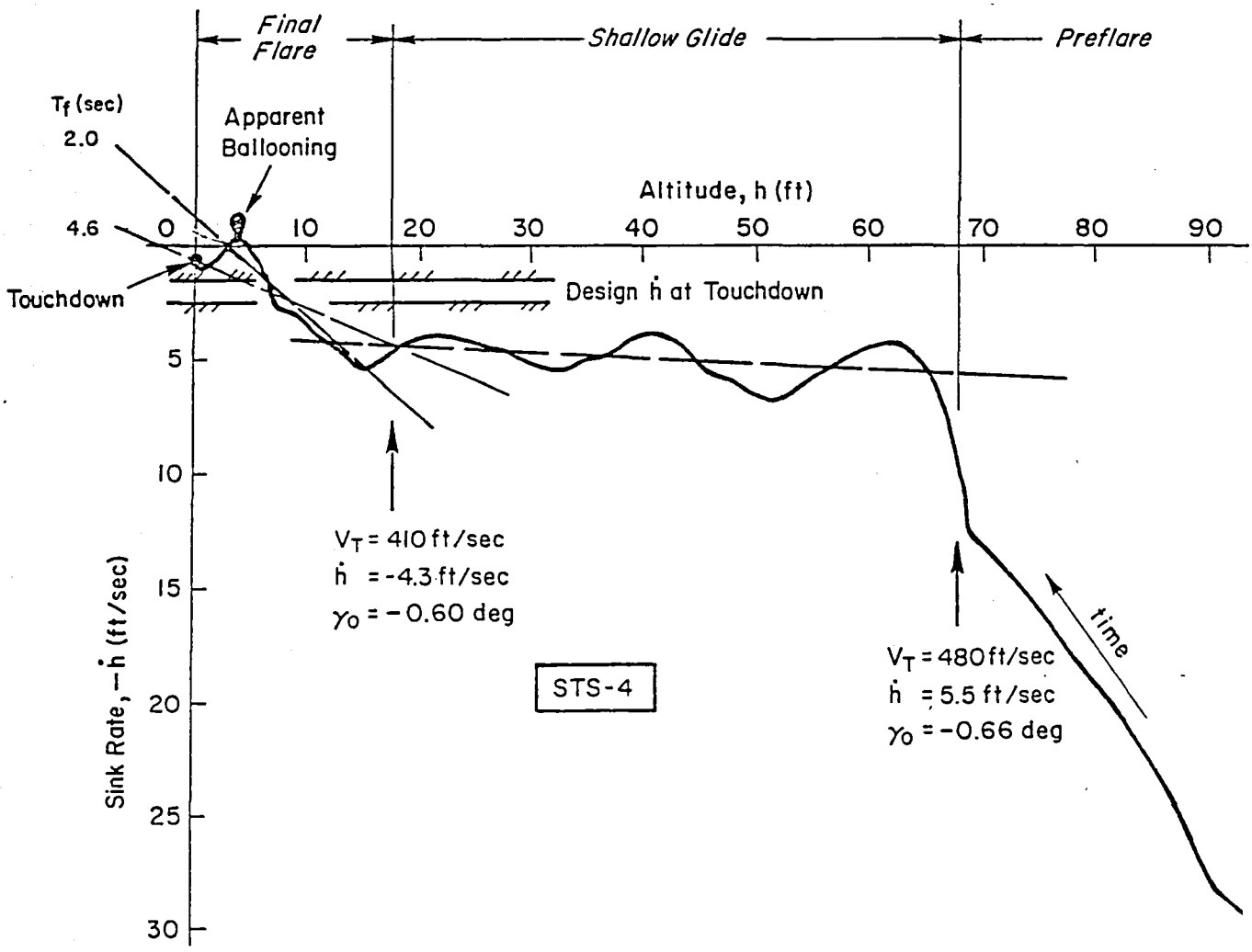

Figure 8. Altitude-Sink Rate Phase Plane Analysis of STS-4 Shallow Glide and Final Flare Complementary Filtered ḣ (from Ref. 3)

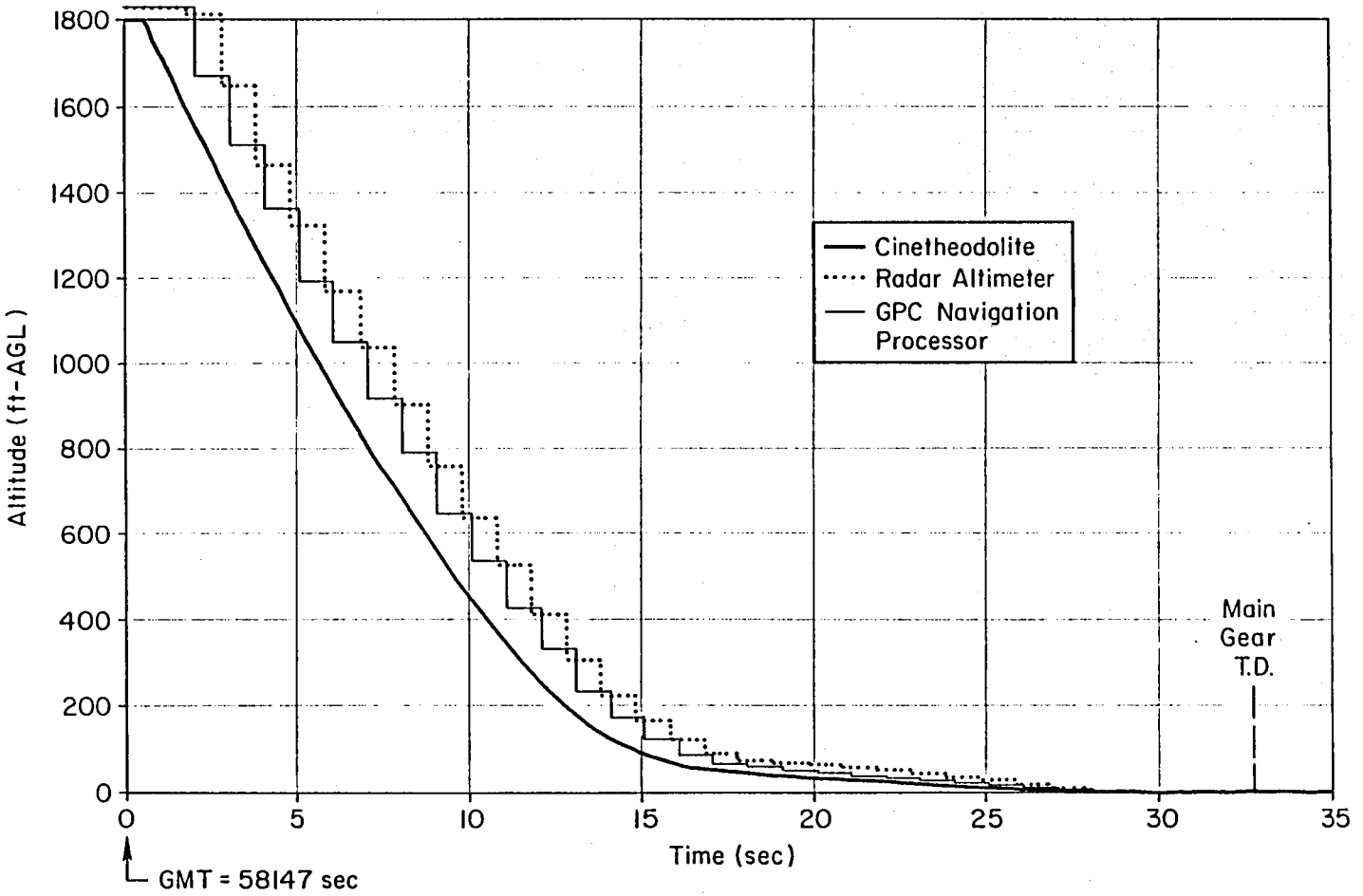

Figure 9. Comparison of Altitude Time Histories from Cine and Onboard Sources, STS-4 Preflare Pullup Through Touchdown

their use for this purpose. Thus the comparison has been based on low frequency correlation of cinetheodolite derived acceleration (at the nose) normal to the earth referenced trajectory (AN) and ACIP onboard normal accelerometer signal. Figure 10 shows a comparison of these plots for STS-4 which indicates a lag in the cinetheodolite clock of 1.25 sec (the low frequency shapes of the two signals have been aligned in the figure). For STS-7 the cine time lag was about 0.5 sec and no shifts were detected in the other four landings.

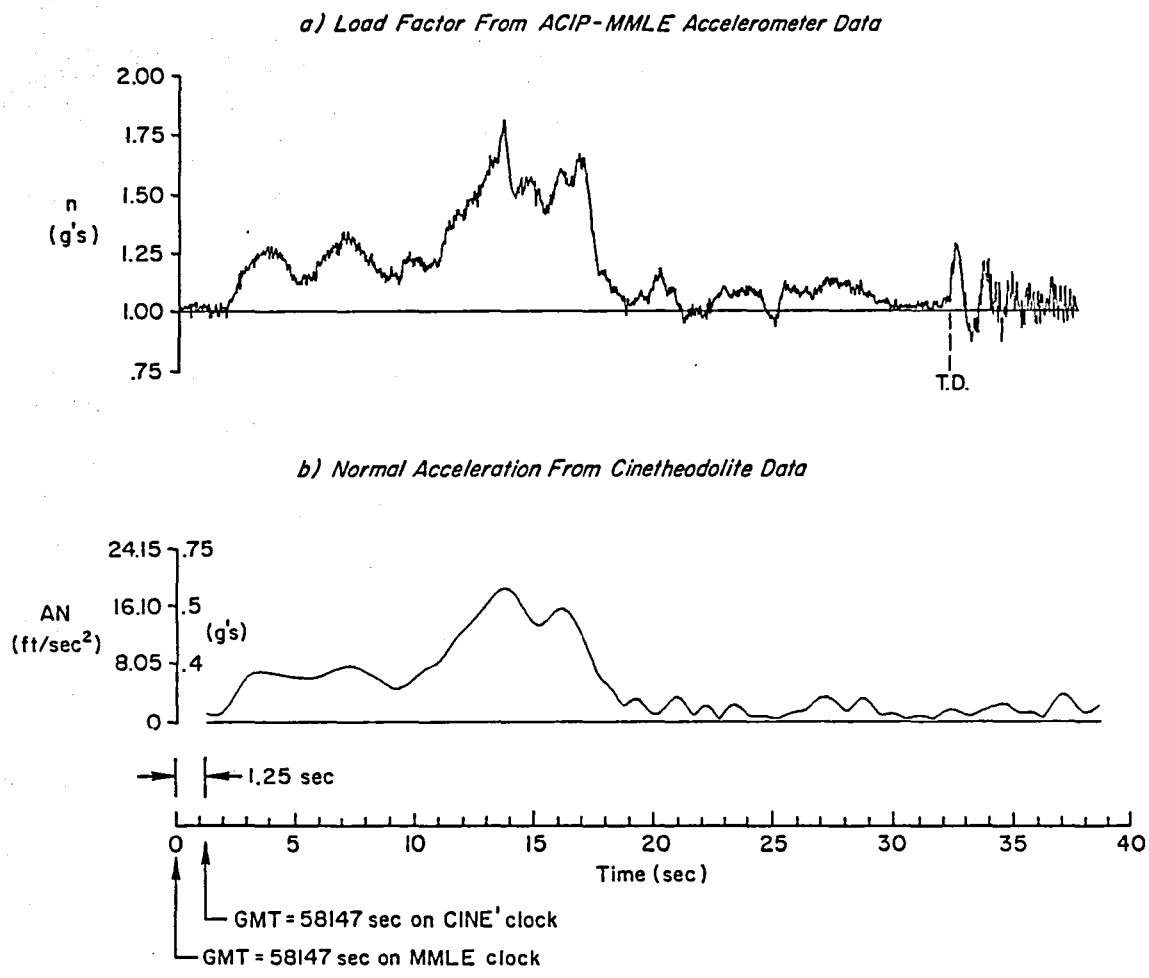

Figure 10. Comparison of Normal Acceleration Time Histories from Cine and Onboard Sources, STS-4 Preflare Through Touchdown

Referring back to Fig. 9, a time shift of 1.25 sec to the right for the cine altitude trace would produce almost exact correlation between the bottom corners of the radar altimeter trace and the cine trace. The cine trace would also pass (approximately) through the mid point of each step in the GPC trace. Thus it is concluded that for STS-4 the cine data should be shifted 1.25 sec.

It is also worth noting in passing that Fig. 10 shows small amplitude, high frequency oscillations of from 4 to 4.5 rad/sec which are not readily apparent in the onboard ACIP normal acceleration signal. This frequency is considerably beyond the Orbiter path response. Also the vehicle center of rotation for elevator deflection inputs lies approximately at the nose and therefore the motion should not represent pitch angular motion. The source of the apparent anomaly has not been determined at this time, however, it may be due to the film reader hunting for the reference point.

Figure 11 is a finer grain comparison of altitude time traces between the radar altimeter, GPC, and cine data for the shallow glide and final flare portions of the STS-4 landing. This shows the influence of Orbiter pitch attitude on the sensed altitude. At 15 sec the Orbiter pitch attitude is about 2.5 deg nose up (see Fig. 6) and it continues to approximately 8 deg nose up just before main gear touchdown. The aircraft nose is then nearly 25 ft in the air at main gear touchdown.

An unspecified smoothing algorithm is applied to the raw cinetheodolite position data. No adverse affects of this algorithm have been indicated in the data analysis and Fig. 12 shows a comparison of the smoothed and unsmoothed altitude data in which the effects appear to be negligible. In fact the two plots appear to be exact overlays.

Figure 13 shows comparisons of the STS-4 cinetheodolite derived altitude/sink rate hodograph and those based upon radar altimeter and complementary filtered sink rate estimates. In Fig. 13a the high sample rate cine data produces obviously superior information compared to the one sample per second radar altimeter signal and derived rate. Signal reference location influence is also apparent in that the radar altimeter hodograph shows a higher sink rate during the later portion of

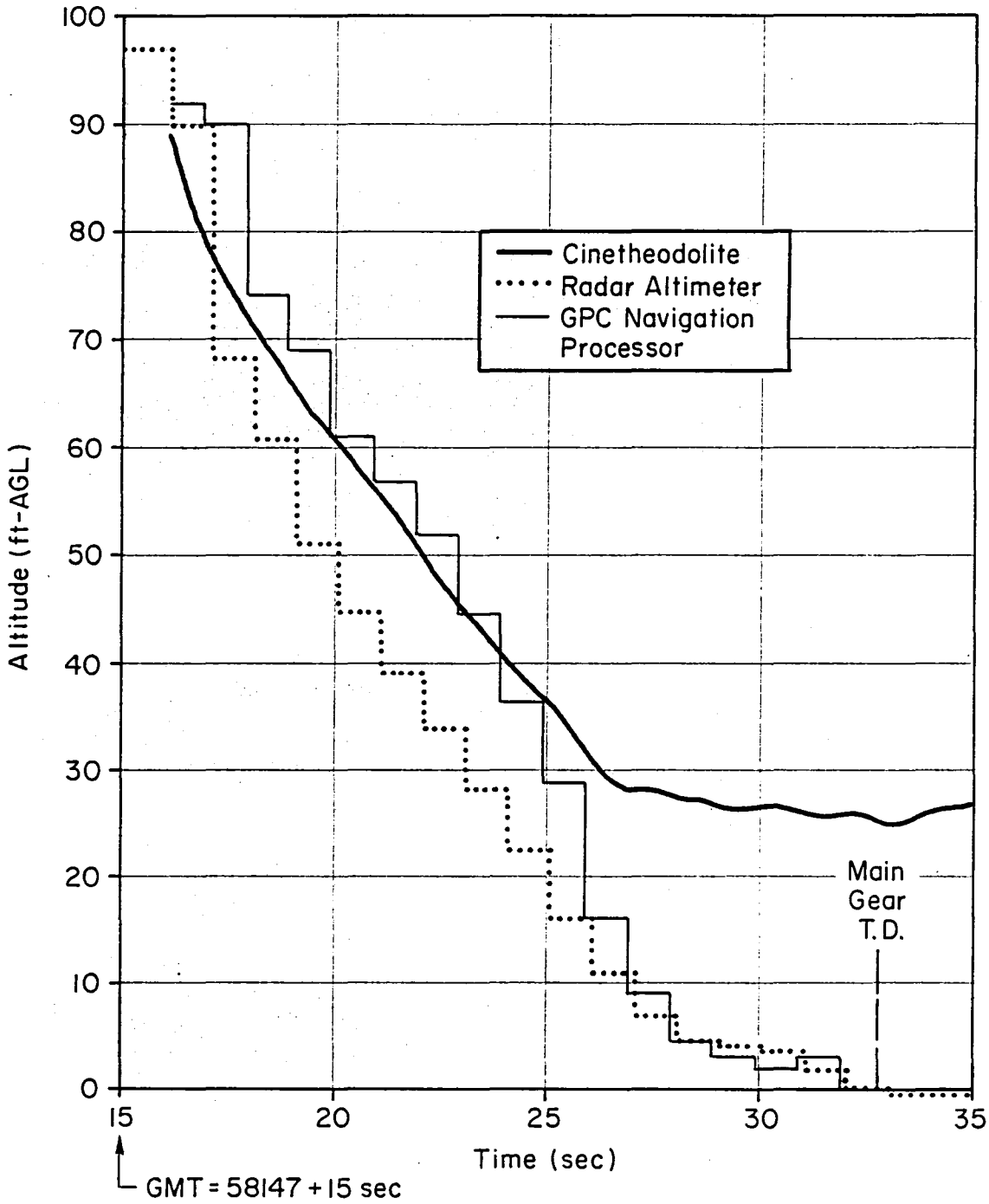

Figure 11. Comparison of Sensed STS-4 Altitude in Shallow Glide and Final Flare

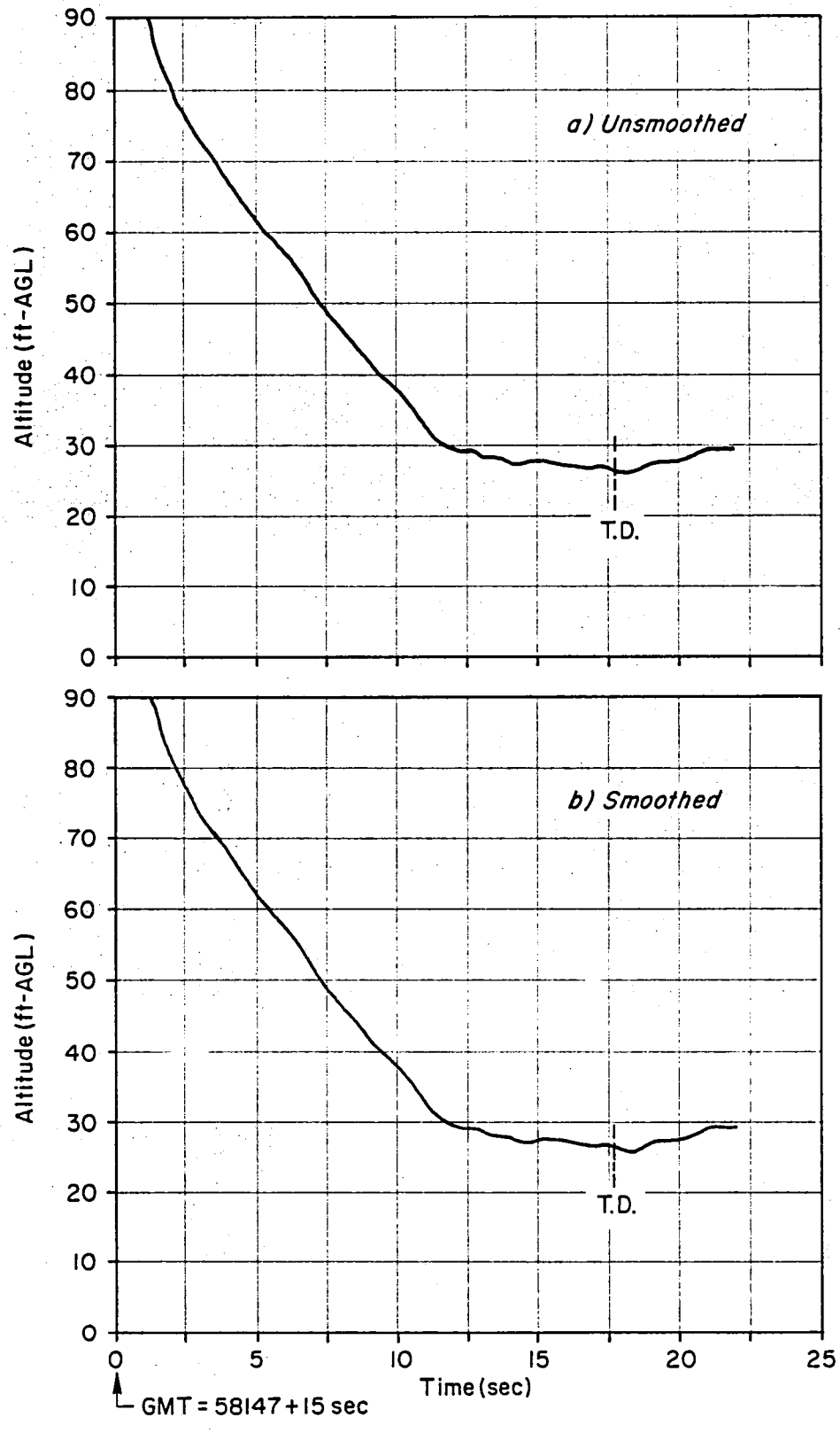

Figure 12. Comparison of Smoothed vs. Unsmoothed Cine Altitude Data, STS-4

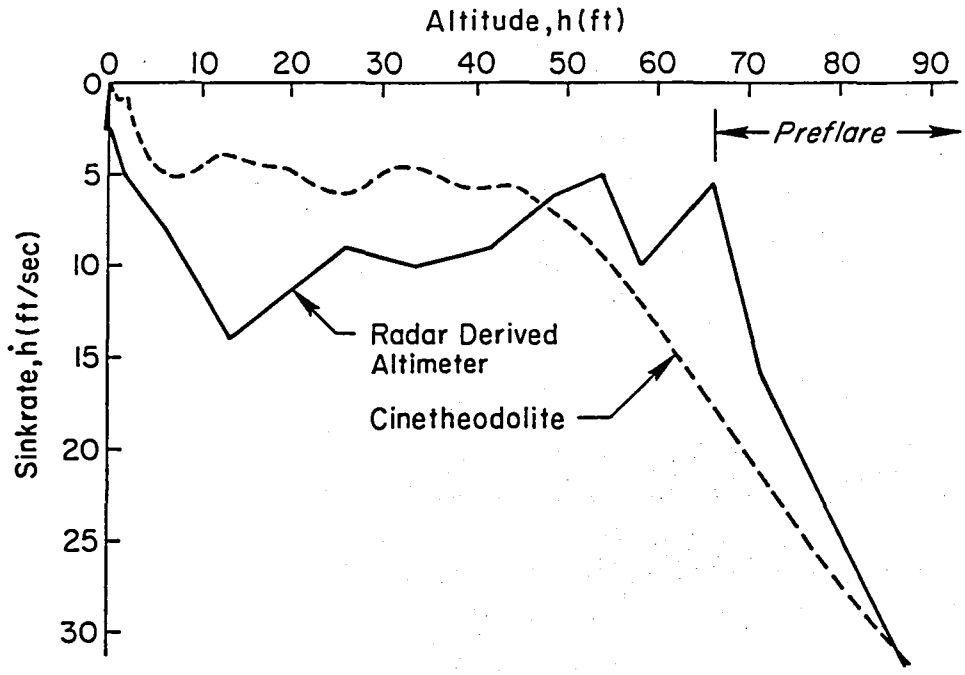

a) Radar Derived vs. Cinetheodolite Data

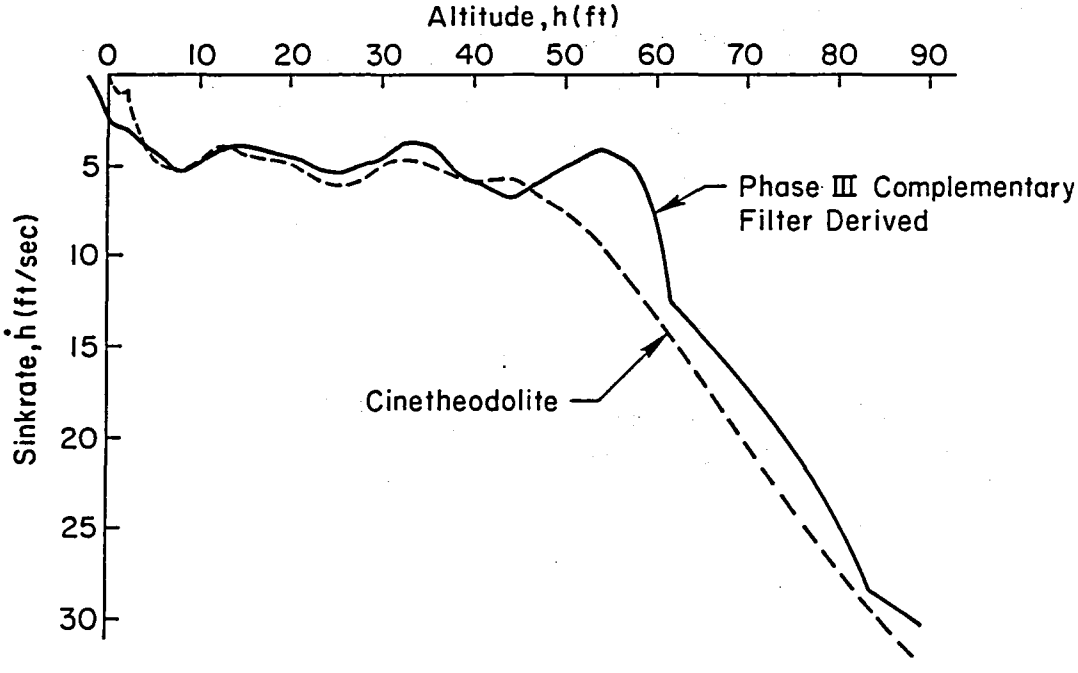

b) Phase III Complementary Filtered vs. Cinetheodolite Data

Figure 13. Comparison of Cinetheodolite Data Hodograph to Phase III Results, STS-4

preflare and shallow glide due to pitch attitude rotation of the vehicle about a point near its nose.

In Fig. 13b it can be seen that the cinetheodolite and complementary filtered signals are generally in good agreement, however, some differences do exist again possibly due to pitching motions. On the basis of this comparison it was decided that the cine data provided valid and direct data suitable for the hodograph analysis although future effort might be suggested to resolve some of the remaining discrepancies (e.g., ground radar).

Determination of touchdown time (of the main gear) presented some practical problems for most flights. In general there is not a reliable, readily available source for this information. The touchdown times for some flights have been reported in Refs. 3 and 6 through 19 although in several cases the times are questionable. It had been hoped that the "weight-on-wheels" discrete would be available from the MPDB data base but this has not yet been obtained. Biases and various differences among the altitude sources available as noted above make the altitude signal far too inaccurate for determination of precise touchdown time. The procedure that has been used in Phase IV is based on the onboard normal acceleration trace. From the early flights in which independent touchdown time information is available, such as STS-4 in Fig. 6, examination of the normal acceleration trace in the region of touchdown showed a distinct positive normal acceleration spike of about two tenths of a g followed by a negative spike and finally a positive rebound. The negative spike apparently is due to landing strut rebound following touchdown. The n signal after touchdown generally shows distinctive high frequency, high amplitude signal content compared to that immediately before touchdown. This is presumably due to structural modes excited by runway roughness. More or less similar touchdown signatures can be identified for STS-2 through -7 at least to the extent of the initial positive spike.

b. Additional Information Obtained from Cinetheodolite Data

Figure 14 shows the time responses of the X and Y (cinetheodolite) ground plane position time histories of the Orbiter STS-4 landing and their crossplot which is the projection of the trajectory on the ground plane. It can be seen that lateral deviation in the landing is negligible. Corresponding data for each flight facilitates determining ground distances covered in each phase of the landing, e.g., glide X_g, flare X_f, and total distance X_t.

In Fig. 15a the cinetheodolite earth referenced velocity V_T is compared to the true airspeed from the MMLE and cinetheodolite data sources. The comparisons are reasonable considering the independent wind measurements. The wind speed in the cinetheodolite data base is shown in Fig. 15b.

Figure 16 shows a trace of the earth referenced total velocity time history in the shallow glide and final flare regions for STS-4. This trace demonstrates the nearly constant deceleration of the Orbiter and lack of influence of pitch attitude. The average slope is fitted to determine the average deceleration, $K_{\dot{V}}$, which plays an important role in the trajectory model equations presented in the Appendix.

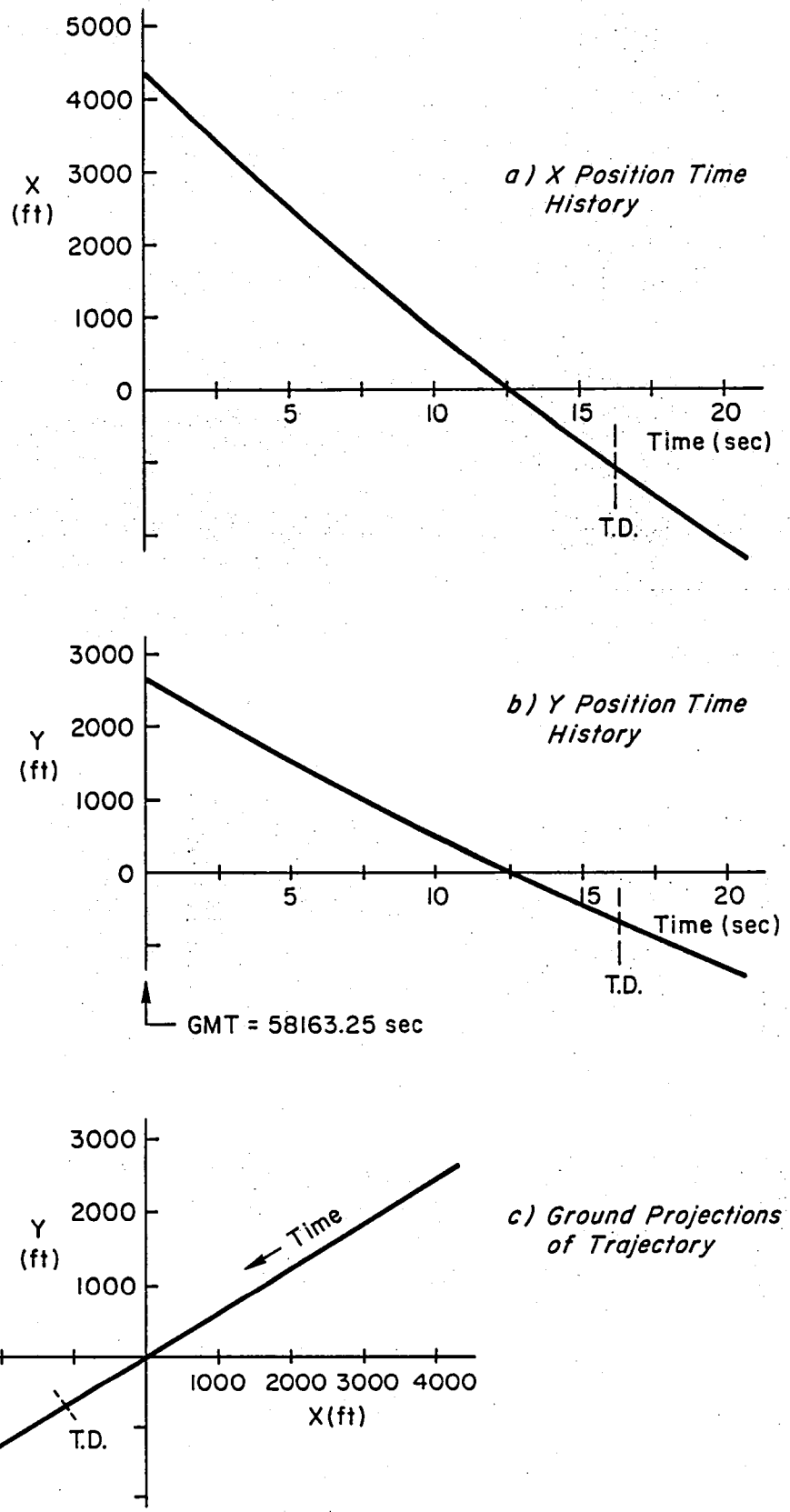

Figure 14. STS-4 Ground Plane Position Time Histories from Cinetheodolite Measurement

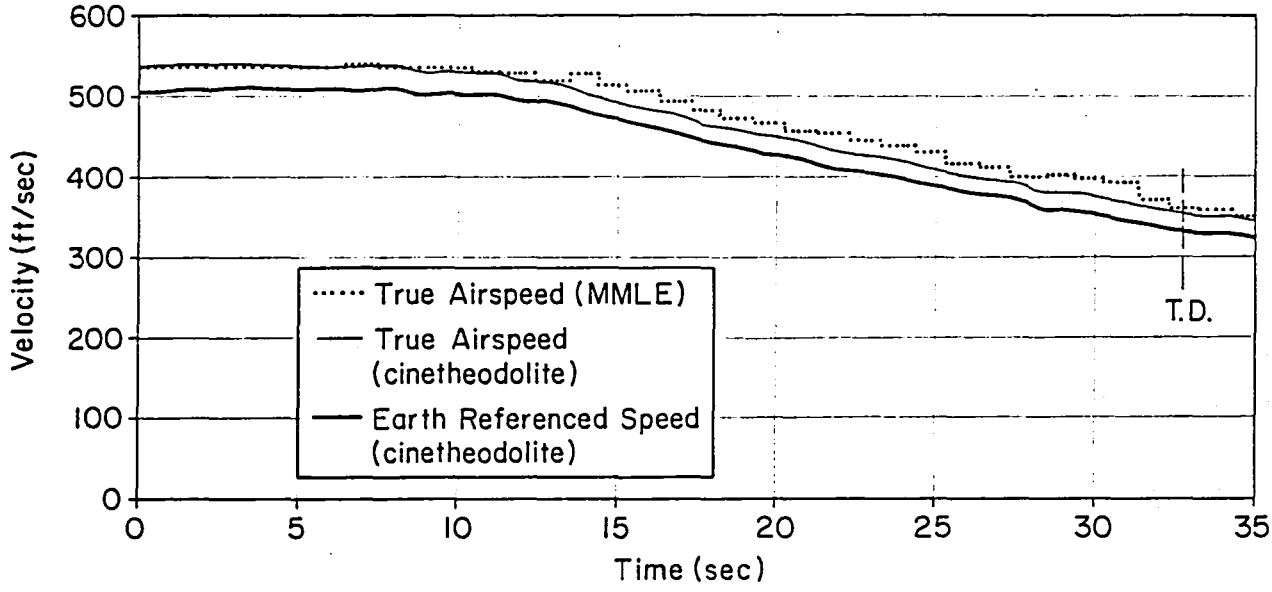

a) Comparison of earth referenced speed with on-board and ground based airspeed measurements

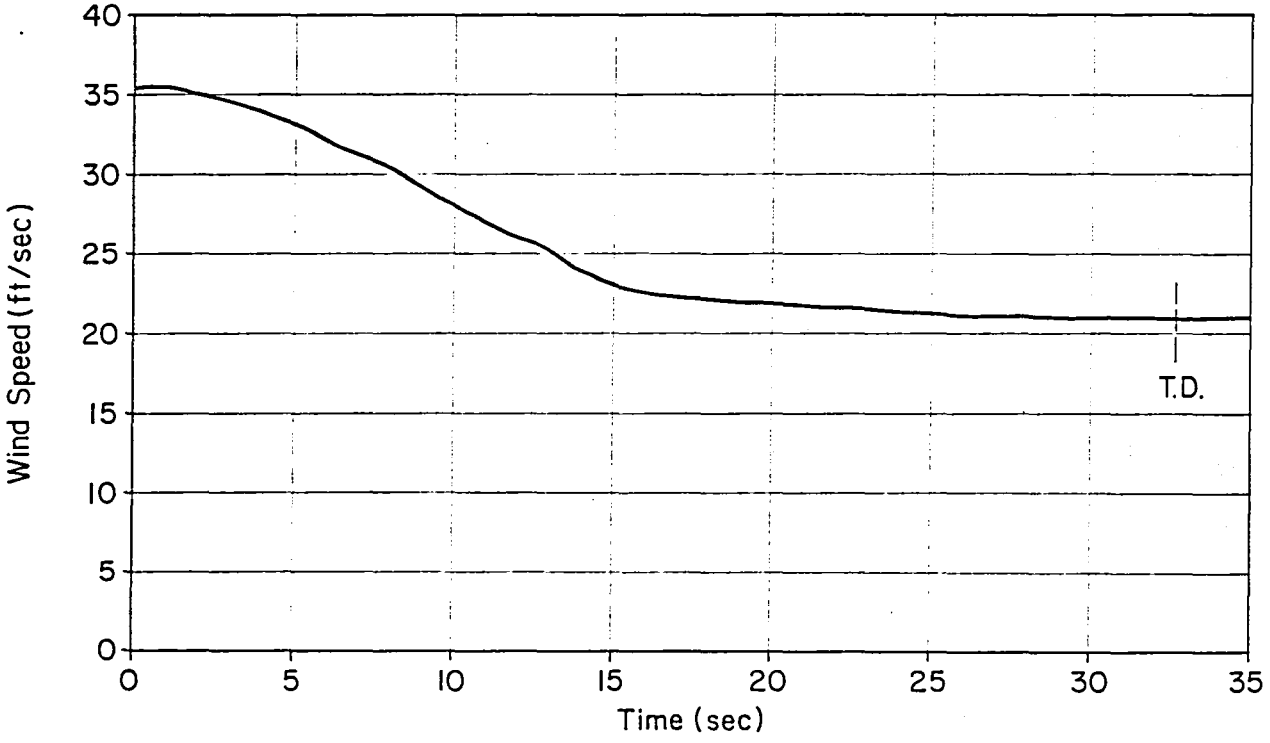

b) Wind speed from cinetheodolite data set

Figure 15. Comparison Between Cine and Onboard True Airspeed and Earth Referenced Speed, STS-4

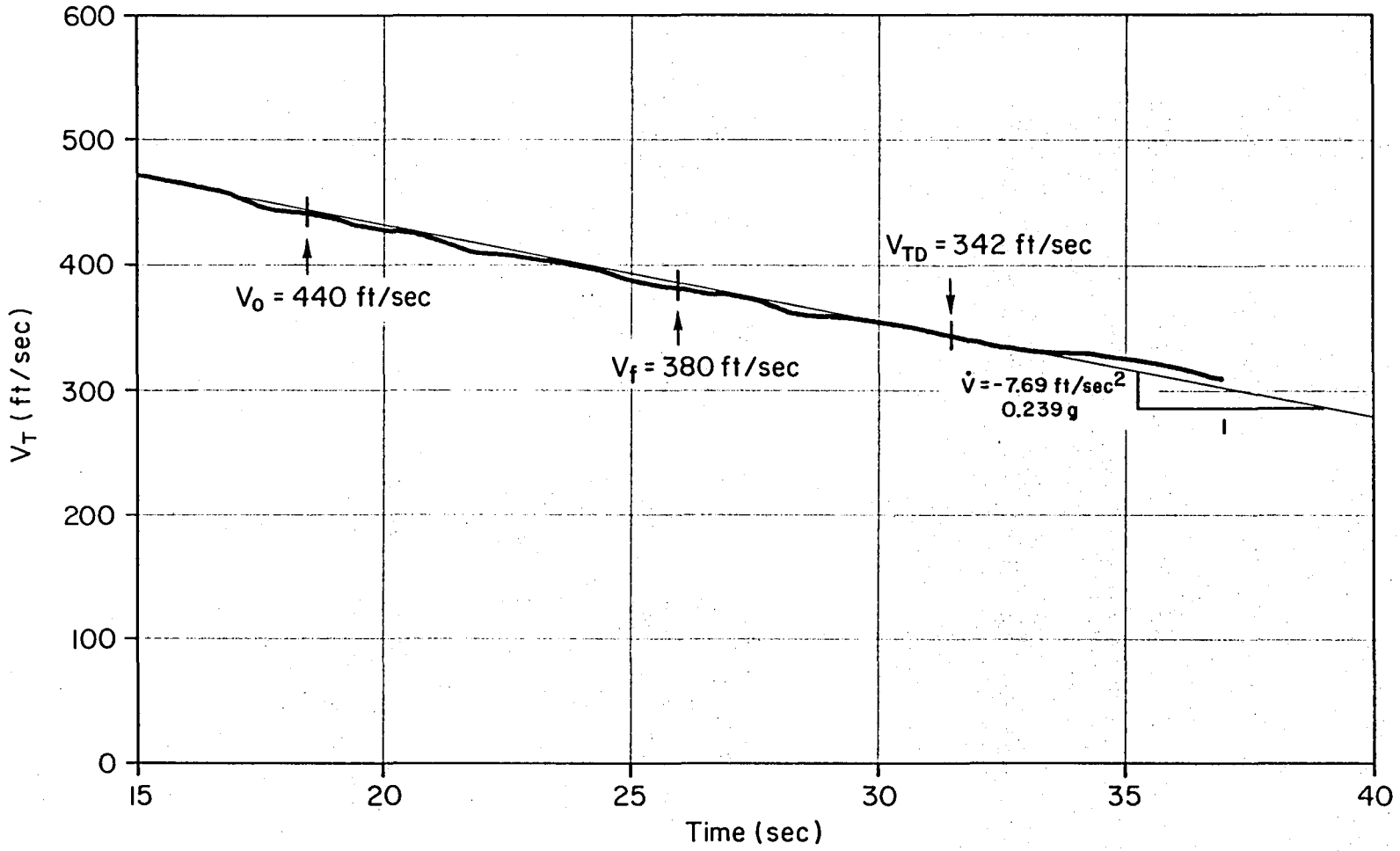

Figure 16. STS-4 Earth Referenced Velocity During Shallow Glide and Final Flare

SECTION III

DIGEST AND ANALYSIS OF STS-2 THROUGH STS-7 LANDINGS

One of the difficulties of the orbital vehicle flying qualities experiment program is that the "experimenter" has no control over the test vehicle configuration or the operational and environmental conditions surrounding the experiment. The transportation system (vehicle, ground aids, operational constraints, etc.) has been in a state of evolution during these first few flights. Furthermore, each landing has been a first for each commander and crew and atmospheric conditions may have played a significant role in several of the landings. It is therefore helpful to identify and track the various aspects which may have influenced the final landing strategy, workload, and performance.

A. EVOLUTION OF FLIGHT PATH AND LANDING AIDS

1. Orbiter Flight Control and Display

The primary change in the Orbiter vehicle occurred for STS-6 and -7 in which the "flight test" vehicle Columbia was replaced by the "operational" vehicle Challenger. Although there were no significant flight control system changes affecting the final approach and landing, the Challenger did introduce the head-up display (HUD).

For the first five landings the principal onboard longitudinal path and energy references were head down instruments: a flight path flight director and airspeed and altimeter indicators for the steep glide (energy management setup) phase; a pitch rate indicator and g-meter for preflare; and airspeed and altitude indicators for shallow glide and final flare. These were supported at all times by pitch attitude display for inner-loop control and out the window ground aim point references for path guidance.

The HUD for STS-6 and -7 added a large selection of head-up status, error, and directive information -- so much so that "declutter" provisions were included to allow elimination of undesired or unnecessary

data and symbology as the various phases of approach and landing are completed. According to Ref. 20 the information displayed for the steep glide slope included: velocity vector (v.v.), flight path angle reference, altitude error, airspeed error, cross track error, speed brake error, and pitch and roll ladder. At 2500 ft altitude new reference markers appear for flight path guidance during pullup to the shallow glide. At 250 ft altitude a GEAR symbol flashes, at 170 ft altitude (5000 ft from runway threshold) radar altitude display starts, and at 100 ft radar altitude is displayed digitally on the right side of the velocity vector and airspeed displayed digitally on the left.

Per Ref. 21, the HUD also provides a computer generated runway symbol which initially informs the pilot that the guidance system speed, distance, etc., are good via the runway symbol being superimposed over the actual runway. During the steep glide, the velocity vector is flown to the steep glide aim point. Preflare or transition to shallow glide slope (and the first declutter) is initiated when path reference markers (which come up from the bottom of the HUD) reach the velocity vector symbol. This signifies the proper altitude and airspeed to initiate transition. The pilot then flies the velocity vector symbol to the path reference markers as they continue to move up the display. Preflare ends when the markers stop moving. The velocity vector should then be directed at the close end of the runway or between the close end and the shallow glide aim point. At this juncture the shallow glide ground aid should signify a 1.5 deg glide slope. The pilot should then minimize pitch inputs but keep the velocity vector symbol and ground glide slope reference steady until reaching the desired flare altitude.

2. Ground Aids for Flight Path Control

Ground aids for manual control of approach and landing have been steadily improved as the program progressed (Ref. 21). For the first few flights the principal ground aids consisted of steep and shallow glide aim markers on the lakebed at Edwards Air Force Base. Two aim makers were provided for the steep glide, one at 7500 ft before the runway threshold for nominal energy approaches and one at 6500 ft in case

the Shuttle should be at a low energy level. The shallow glide slope aim point is 1000 ft beyond the runway threshold.

An additional ground aid for the later portion of the preflare pull-up and shallow glide was then added (Fig. 17). This consisted of a cluster of very high intensity white lights mounted on a pole on the left side of the runway near the runway threshold and a row of similar red lights, also on the left side but perpendicular to the runway at the shallow glide aim point. The height of the pole was selected so that a 1.5 deg glide slope is defined when the white light is superimposed on the red row of lights. This is called the ball-bar aid and is similar in function to the fresnel lens optical landing aid employed on aircraft carriers.

With this ball-bar system, if the white ball appears to be below the red bar, the vehicle is high or on a steeper glide. If the ball is above the bar the vehicle is below the desired 1.5 deg glide slope. Thus this system provides a reference to guide the pilot to the correct termination of the preflare maneuver and to maintain the proper shallow glide in manually controlled flight. It also provides a means of monitoring guidance and control performance for fully automatic landings.

Yet another ground based optical aid for the steep glide slope was added following Mission 5. This consists of red and white high intensity lights located at the steep glide aim point. These are aimed upward at differing angles such that specific glide slopes are defined by the number of red and white lights visible. This is called the Precision Approach Path Indicator (PAPI) and is represented in Fig. 18. The aircraft is on the correct 19 deg steep glide path when the crew can see two white and two red lights.

As a result of these various landing aids being operational with successive flights, the control strategies (path control loop structure, gains, etc.) for preflare and shallow glide would be expected to vary somewhat from flight-to-flight. This will be quite apparent in the later detailed analysis of the STS-2 through -7 landings. It might also be expected that path and landing performance should come closer to

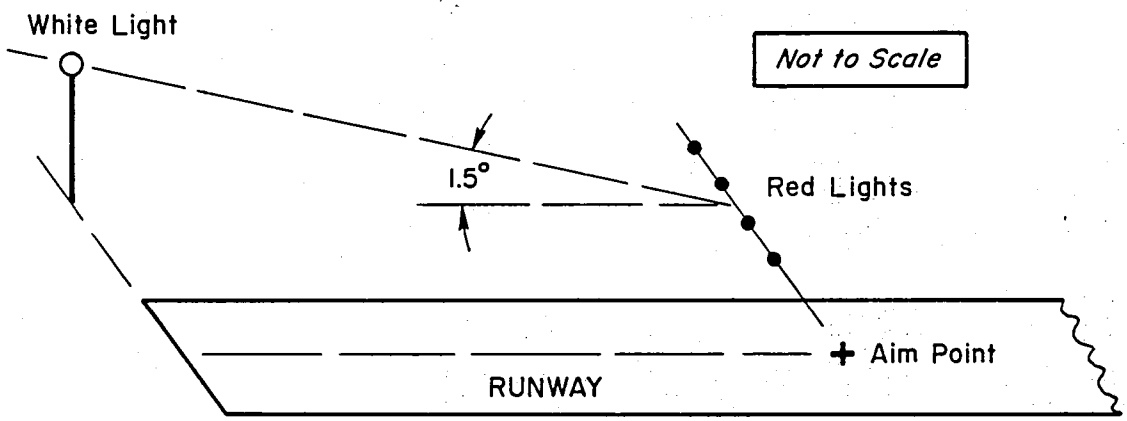

Figure 17. Ball-Bar Shallow Glide Slope Flight Path Aid

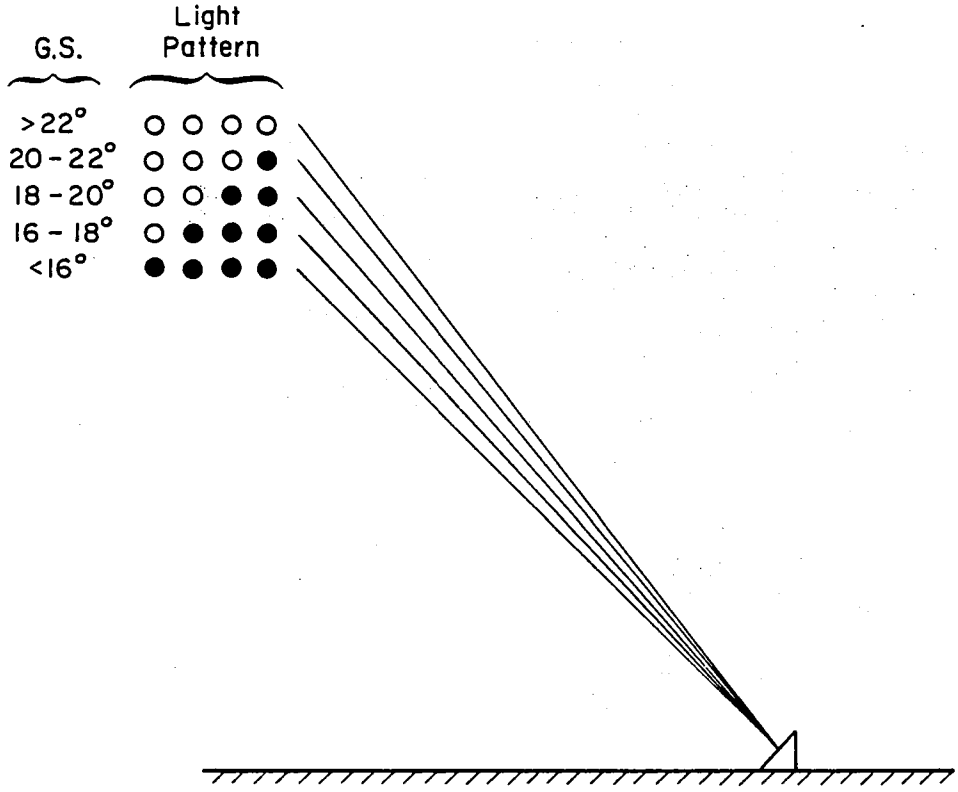

Figure 18. Steep Glide Precision Approach Path Indicator Ground Aid

ideal or target values and become more uniform with each flight. Only the final flare remains essentially the same unaided task for all landings. The exception is HUD direct display of altitude and airspeed information on STS-6 and -7 in place of verbal callouts on previous flights. Even so, the shallow glide and actual flare should be sufficiently similar to start to extract meaningful flying quality information from the ensemble.

B. LANDING CONDITIONS/SITUATIONS

A summary of factors related to the STS-2 through -7 landings, extracted from Refs. 6 through 19 are presented in Table 2. This indicates that there were a minimum of external or head-up landing aids for the first few landings. Also the assistance of the third crew member to reduce cockpit workload was not available until STS-5 and subsequent flights. The commander of STS-4 actually commented that he had difficulty judging preflare and worked hard during the landing. With the additional aids starting at STS-5, one might expect that the pilot workload might be lower with perhaps improved touchdown performance.

The first four flights were considered test flights and there was interest in validating performance of the automatic guidance and path control modes leading eventually to a fully automatic landing. Therefore manual takeover was initiated at different points in the steep glide or preflare on STS-2, -3, and -4. It became apparent on STS-3 that the time required for the pilot to adapt to his closed-loop control task was significant and that early manual takeover was advisable to provide time for the pilot to obtain a feel for the Orbiter response characteristics and settle into the control task. For the latter three flights the crew not only took over manual control for the heading alignment circle (HAC) phase but retained manual control through to touchdown.

The touchdown surface is of interest in that the lakebed offers a much longer and less constrained landing and rollout target than does the concrete runway. Therefore touchdown performance is more important for runway landings. This leads to tighter closed-loop control (as

TABLE 2. ORBITER APPROACH AND LANDING CONDITION SUMMARY

FLIGHT	STS-2	STS-3	STS-4	STS-5	STS-6	STS-7
AIDS						
PAPI LIGHTS	NO	NO	NO	YES	YES	YES
BALL-BAR	NO	NO	NO	YES	YES	YES
HUD	NO	NO	NO	NO	YES	YES
3rd CREWMAN	NO	NO	NO	YES	YES	YES
MANUAL						
TAKEOVER ALT.	2000'	120'	2500'	HAC	HAC	HAC
PREFLARE	1750'	AUTO	?	1750'	?	1750'
TOUCHDOWN						
SURFACE	LAKEBED	SAND STRIP	RUNWAY	RUNWAY	RUNWAY	LAKEBED
DISTANCE	SHORT	SHORT	SHORT	SHORT	SHORT	ON
SPEED	SLOW	FAST	FAST	FAST	FAST	FAST
ENVIRONMENT						
VISIBILITY	CLEAR	BLOWING SAND	CLEAR	CLOUDS ~19K'	CLEAR	CLEAR
WIND	HIGH HEADWIND	HIGH	HIGH	CALM	GUSTY 22 KT HEADWIND	10 KT HEADWIND

demonstrated by the PIO which occurred with the ALT-5 landing) and the need for more precise setup through each of the approach segments leading up to the final flare. Most touchdowns have occurred short of the landing aim point. On STS-2 this might be attributed in part to a low energy state brought about by high winds, an untimely sweep of the speed brake, and re-engagement of the automatic approach/landing system at termination of the HAC. As a result, the crew had to fly a maximum L/D attitude to get to the lakebed. This touchdown was slow and only some 900 ft beyond the runway threshold. The other short touchdowns all occurred at higher than nominal speeds. Pilot comments tend to indicate problems in judging touchdown or in "holding off" touchdown to bleed off airspeed because of being located slightly behind the center of rotation for pitch attitude changes while the main gear is far aft. The pilots not only have problems in judging pitch attitude but also in judging the sinking of the main gear due to small attitude adjustments to "hold off" the sink rate at the cockpit.

Finally, environmental conditions may have contributed to touchdown problems encountered on STS-3 in that the pilot's visibility and depth perception may have been adversely affected by blowing sand. Gusty winds and a large increasing wind shear from 2500 ft to the ground were encountered by STS-6. Also for this flight the outer aim point marker was underwater and the crew was advised to use the inner marker. The crew was then confused as to whether the HUD was aligned to the outer or inner glide slope. This may have increased the workload somewhat.

The foregoing factors should be kept in mind when interpreting the time traces and hodographs for each landing as presented and discussed in the following sections of this report.

C. EXTRACTION OF POSSIBLE CONTROL STRATEGIES

Before getting into time histories and hodographs for each landing it might be useful to review some of the closed-loop control and unique flying quality characteristics of the Orbiter craft. It will be recalled that the preflare, approach, and landing nominally are individual segments which involve different control loop structures. The preflare is a constant pitch rate maneuver and vehicle pitch rate, or its

equivalent is displayed to the pilot (either head down or up). The superaugmented vehicle dynamics response is that of pitch rate command/attitude hold (RCAH). Pilot actuation of the rotational hand controller (RHC) directly commands vehicle pitch rate. During this flight segment one would expect the time traces to show relatively constant RHC, pitch rate, and normal acceleration.

For the shallow glide portion, the control task is more complicated in that pitch control becomes an inner-loop to sink rate or flight path control. The approximate short-term (quasi-steady speed) path to attitude transfer function is

$$\frac{\dot{h}}{\theta} = \frac{sN_{\delta}^{h}}{N_{\delta}^{\theta}} \doteq \frac{U_o}{(T_{\theta_2} s + 1)}$$

where the Orbiter path lag, T_{θ_2} is about 2.0 sec.

A closed-loop pilot vehicle analysis using the theoretical pitch model of Section II-A was accomplished in Ref. 22 (earlier analyses are also shown in Ref. 23) and Fig. 19b shows the closure of the pilot's inner attitude loop for a nominal crossover. The resulting closed-loop attitude mode undamped natural frequency, ω_n', lies between 2 and 3 rad/sec. However, it can be seen that stable closures could be made to $\omega_n' \doteq$ 4 rad/sec, although with corresponding decreases in damping ratio.

Figure 19c shows the closure of the pilot's outer sink rate loop (also from Ref. 22) for the nominal inner-loop closure. The dominant closed-loop modes are the now lightly damped attitude mode, and the lower frequency highly damped path mode. . Thus we might expect the lightly damped attitude mode as a "contaminant," and consequently 2-4 rad/sec spectral components in the q and a_n shallow glide time histories. It may also be evidenced in the $\dot{h}$ time traces and hodographs providing there is sufficient vertical movement of the Orbiter nose due to the pitching motion. Also note that the path mode, which stems from $1/T_{\theta_2}$ and the subsidence, $1/T_{CL}$ resulting from the attitude closure, is restricted to closed-loop responses of the order of 1 to 1.5 rad/sec for

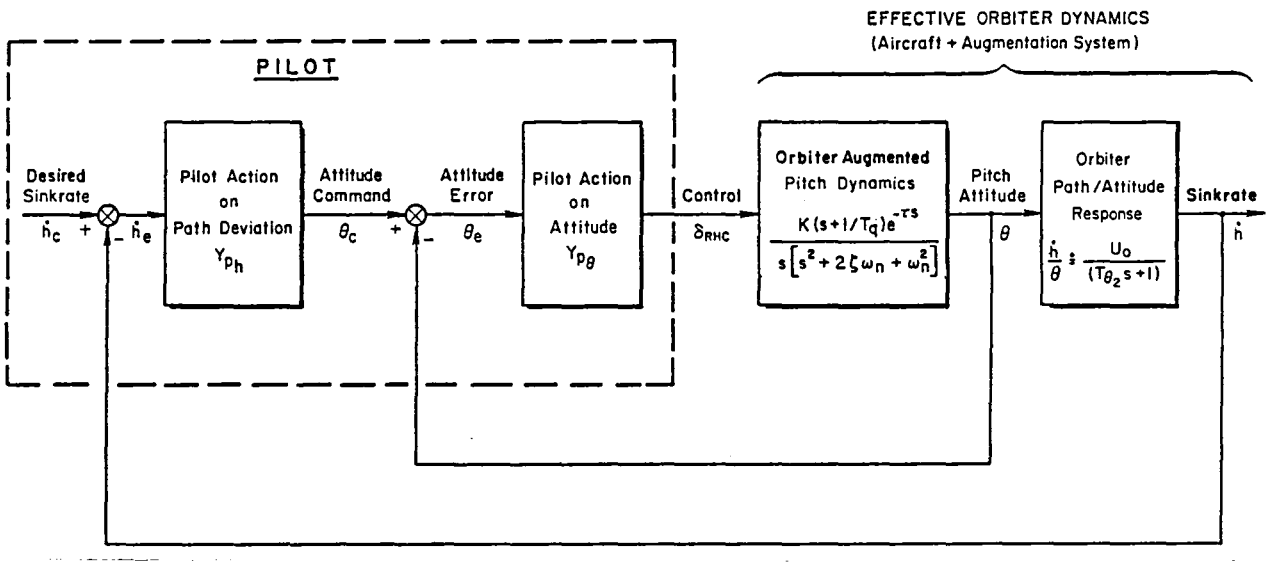

a) Series loop structure for manual control on on the shallow glide

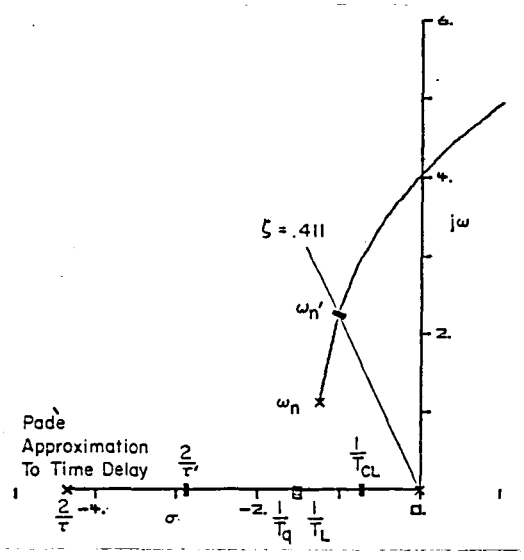

b) Closure of the pilot's inner attitude loop

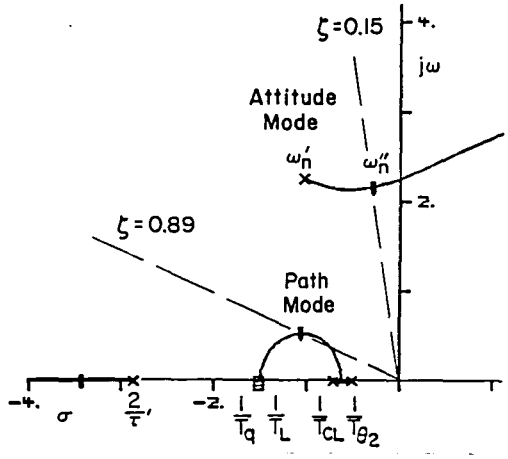

c) Closure of the pilot's outer sink rate loop with the nominal inner loop closure

Figure 19. Model for Attitude and Sink Rate Manual Control During Shallow Glide

this nominal set of attitude and path loop gains. If the attitude loop were to be tightened, the closed-loop pole $1/T_{CL}$ would move further from the origin and this would increase the achievable sink rate control bandwidth. Alternatively if pitch attitude were adjusted in a stepwise manner, the sink rate would change as a first-order response with a time constant of T_{θ_2} = 2 sec. T_{θ_2} thus serves as a limiting factor when the sink rate loop is open, and a governing factor when it is closed.

Perhaps the easiest strategy for the final flare is to change pitch attitude in a stepwise manner and let sink rate decay with the 2 sec (T_{θ_2}) time constant noted above. If sink rate should be controlled in a closed-loop manner as a function of altitude an additional incremental altitude loop (referenced to the desired descending flight path) would be required around the model shown in Fig. 19a. This could result in yet lower path bandwidth or flare response time constants greater than T_{θ_2}. Detection of either of these two path control strategies should be evident from the pilot's RHC inputs. They are also indicated by the flare time constant, i.e., $T_f \doteq T_{\theta_2}$ and little or no RHC activity in the final seconds of the flare indicates precognitive control of sink rate; whereas, a $T_f \neq T_{\theta_2}$ implies closed-loop piloted control of sink rate.

It has been shown in Refs. 22 and 24 that one of the principal differences in the final flare control between conventional aircraft and superaugmented aircraft, such as the Orbiter, is the attitude command/attitude hold (ACAH) nature of the former and the rate command/attitude hold (RCAH) nature of the latter. With ACAH the flare control input is one of relatively continuous nose-up controller deflection and a relaxing of the input to lower the nose. With RCAH the control input becomes pulsive with discrete nose-up or down pulses to adjust pitch attitude. As noted in Refs. 22 and 24, there has been considerable disagreement within the flying qualities and piloting communities as to which type of vehicle is the more desirable. In the Ref. 25 simulation, astronauts generally preferred the RCAH type of control, very possibly because of their extensive training in this type vehicle. However, the results of the STS flights examined here do not show a uniform control technique in the final phases of landing.

1. Time History and Hodograph Views

Time traces and hodographs for the STS-2 through -7 landings are presented in Figs. 20 through 31. The RHC, pitch rate, and normal acceleration time traces are from the MMLE data base. Altitude and vertical speed are from the cinetheodolite data base. Corrections for apparent time shifts between MMLE and cine "clocks" have been made for STS-4 and -7 as discussed previously. The figures which contain only h, $\dot{h}$, and hodograph plots are expanded scale data which covers only the final 10 to 15 sec of the landing. This generally includes the portion of flight which would encompass the end of preflare, shallow glide, and final flare, if such segments are identifiable. It should be noted in the hodographs that the altitude reference point (Orbiter nose) is set to zero ground level at the touchdown point (to remove the 20 to 30 ft nose altitude biases seen in the altitude time histories). If the altitude data were corrected to another reference point (such as the c.g. or main gear) there would be a small change in the hodograph trajectory due to pitch attitude variations before touchdown. Aside from questions of what reference point is relevant for considerations of piloting technique, the variation of altitude and sink rate with reference point is generally a second-order effect. In particular, the variation in sink rate between the nose and the main gear is usually considerably less than 1 fps.

As noted in conjunction with Fig. 6, termination of each path segment and start of the next is generally signalled by a larger than normal RHC pulse which is then followed by a somewhat changed control technique. While for the Fig. 6 case the apparent discrete pilot inputs which terminate the preflare and initiate the final flare appear quite distinct on the RHC trace, gaining confidence that these spikes do represent such precognitive pilot activity requires examining the resulting responses in aircraft attitude and normal acceleration and finally relating these events to "corners" of the hodograph. This process must account at least approximately for the associated vehicle response lags among the state variables. However, by accepting a certain amount of subjectivity and judgment, shallow glide and final flare

initiation points can be defined on the RHC trace for each flight (except STS-2). But tracing these discrete events through the attitude and path responses to the hodograph is complicated since "precognitive" pilot inputs are generally more complex than a series of simple impulses. Thus the effective lag between an identified RHC "event" and the resulting response in the hodograph varies somewhat. After some iteration the shallow glide and final flare initiation response points were defined as ⓪ and ⓕ respectively on the hodographs. There is an inevitable subjectivity and uncertainty in the extracted parameters which might ultimately be improved by the use of more sophisticated identification algorithms and computational procedures, however, such steps were felt to be inappropriate at this early stage of analysis. Thus the approach here has been to make a simple best estimate of the basic model parameters and then examine the implications for the six flights. The most fundamental test of the validity of the parameter extraction process is whether or not gross inconsistencies and obvious impossibilities are implied downstream in the analysis.

In all flights, an attempt is made to identify each sequential segment; although in some instances the short time span between ⓪ and ⓕ make it unlikely that the segments are indeed separable rather than one continuous flare to touchdown.

The flights will be analyzed individually in the following:

1. STS-2 - The onboard data recording system suffered data dropout during most of the time segments of interest (Fig. 20). However, the relatively smooth responses of the pitch rate and normal acceleration traces are indications the initial preflare was accomplished by autoland. Reversion to manual occurred at about 16 or 17 sec on the trace time scale. The flight segments are identified on the basis of the Fig. 21 $\dot{h}$ time trace in which the sudden oscillation is interpreted as an attempt to terminate the preflare and initiate shallow glide. However, the short time span of this transient certainly leaves it open to question. If one assumes the final flare was initiated at ⓕ, the average slope for the hodograph between that point and touchdown produces a flare time constant of 2 sec which is the same as the T_{θ_2} path

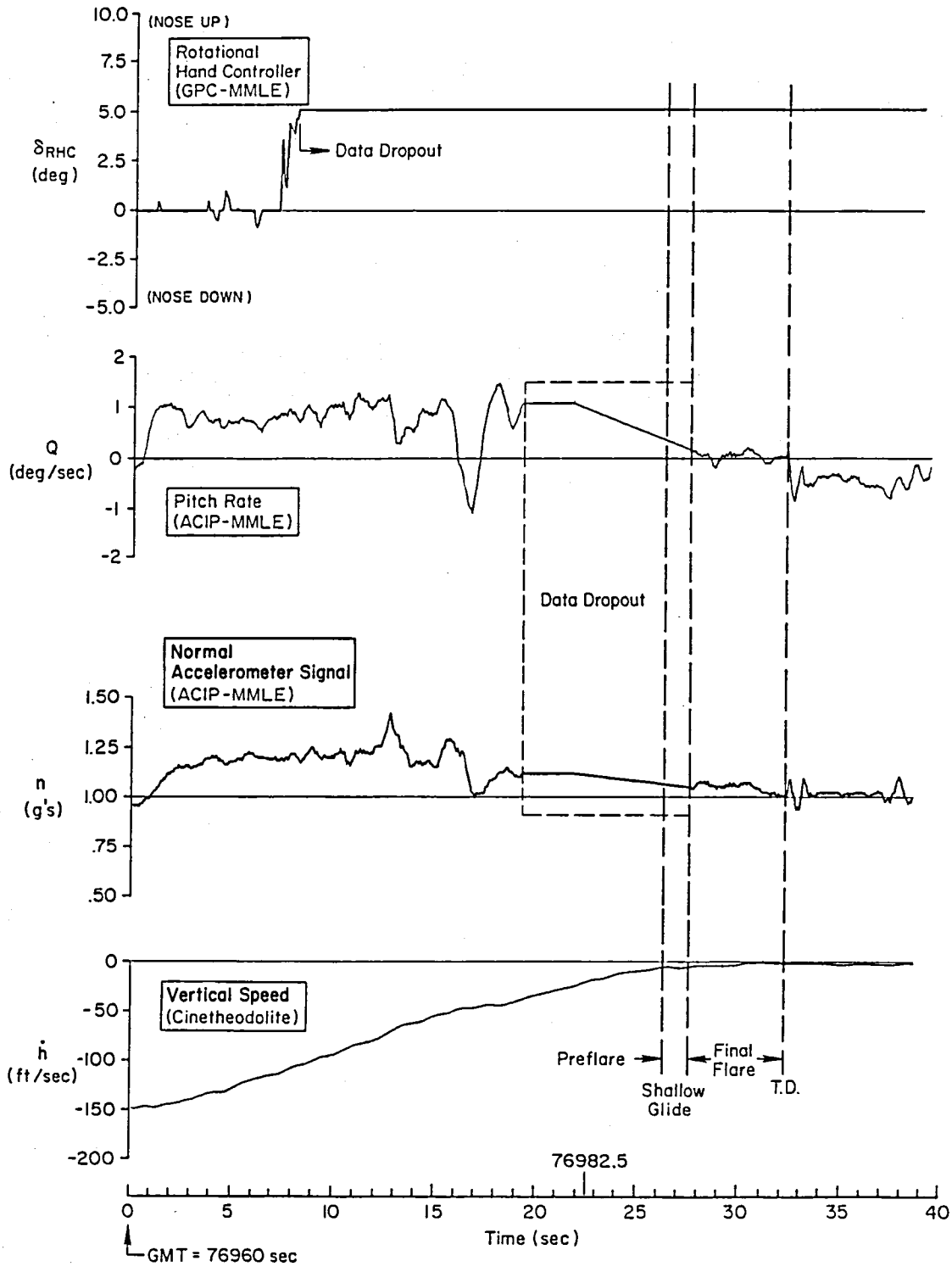

Figure 20. STS-2 Preflare Through Touchdown Time Traces

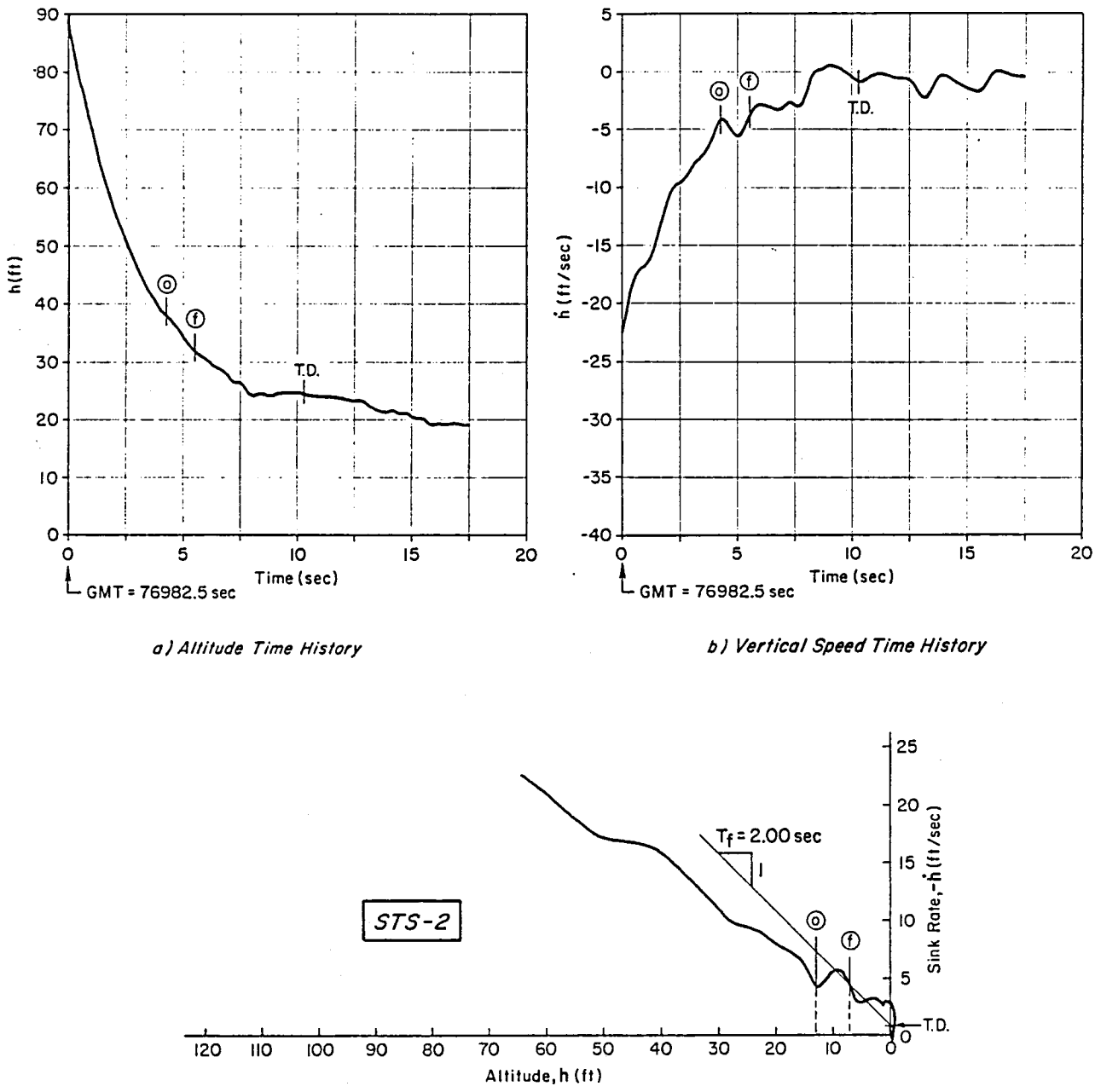

Figure 21. STS-2 Preflare Through Touchdown Hodograph

time constant. If one assumes the path to be one continuous flare, the average slope produces a $T_f \doteq 2.75$ sec. Since this flight was low on energy and barely made the runway threshold, it is presumed the landing was in reality one continuous flare and the roughly 3.5 rad/sec oscillations at 5 sec before touchdown reflect a tightening of attitude control as the vehicle approached touchdown.

2. STS-3 - The first 20 sec of the Fig. 22 time traces again reflect autoland operation. At 20 sec, the commander took over manual control and made several large nose-down and up inputs prior to touchdown at about 30 sec. The initial input appears to be to stop the preflare, increase sink rate, and avoid ballooning. This is followed by a large pilot induced oscillation to touchdown. Two aspects of the RHC inputs are of particular interest. First, there is an absence of the pulse and wait type control which one would expect with rate command/attitude hold type inner-loop control when path control is well in hand. Second, the large one and one-half cycle input oscillation at about 1.6 rad/sec may indicate the pilot was concentrating on gaining direct control over altitude or sink rate and may have dropped the inner attitude closure.

The h, $\dot{h}$, and hodograph traces of Fig. 23 also reflect the rather unstable nature of the STS-3 landing. The hodograph seems to indicate an attempt to establish a shallow glide at the rather high sink rate of 15 ft/sec. This was followed by the 4 to 4.5 rad/sec oscillation between 6 and 8 sec on the $\dot{h}$ time history. This frequency is too high to be a path mode response and indeed is not apparent in the n trace of Fig. 22. Therefore the oscillation preceeding point ⓕ on the traces and hodograph may be some anomaly of the cine measurement of nose movement. The large amplitude oscillation from point ⓕ to touchdown (last 2.5 or 3 sec) is visible in the $\dot{h}$ and n traces and apparently was an attempt to arrest the high sink rate. Note that within this time frame the vehicle could have touched down at a sink rate anywhere from 0 to 7.5 ft/sec. The flare time constant averaged about 2 sec while arresting the sink rate from -15 ft/sec to the -2.5 ft/sec at touchdown.

It appears from the hodograph that there was sufficient time following manual takeover to establish a shallow glide at a sink rate of about -10 ft/sec and then a smooth flare to touchdown. However, it is also apparent that the pilot RHC inputs were overly large, perhaps because he had not established a "feel" for the aircraft response, and the situation rapidly deteriorated following the initial large nose-down input. This has implications for the safety of any last second manual takeover from an autoland system failure and for much earlier takeover on other flights in order for the pilot to adapt to the landing control task.

3. STS-4 - This was the first runway landing at Edwards and was accomplished with only the external aim point aids. The time traces of Fig. 24 reflect the early manual takeover for STS-4 in which the pilot performed the preflare, shallow glide, and final flare. The traces show that the preflare was accomplished in a two step sequence with the initial pitch rate averaging about 0.7 deg/sec and then increasing to about 2 deg/sec. This is consistent with the pilot's comments (Ref. 12) that he had trouble judging the preflare, that he started preflare but it felt "hard" so he relaxed and then did another preflare when he had better "visual." The RHC trace for the shallow glide slope segment shows a transition from essentially continuous rate command type control to a rapid pulsing type control. This is followed by two nose-up pulses to initiate final flare and several small nose-down corrective pulses.

The traces and hodograph of Fig. 25 show the late part of the preflare, a definite shallow glide with a sink rate of about -5 ft/sec, and a final flare with time constant of about 1.26 sec. This T_f value and the pilot's RHC activity clearly indicate closed-loop control of sink rate throughout the flare.

4. STS-5 - This flight also landed on the runway at Edwards and was the first to have the ball-bar shallow glide aid. The traces of Fig. 26 cover preflare, shallow glide, and final flare. It is somewhat difficult to detect where preflare ends and shallow glide begins on these traces. This would tend to indicate the pilot was following the ball-bar aid since its purpose is to guide a smooth transition from steep to shallow glide slope. The pilot also commented that he had no problem judging preflare (Ref. 16).

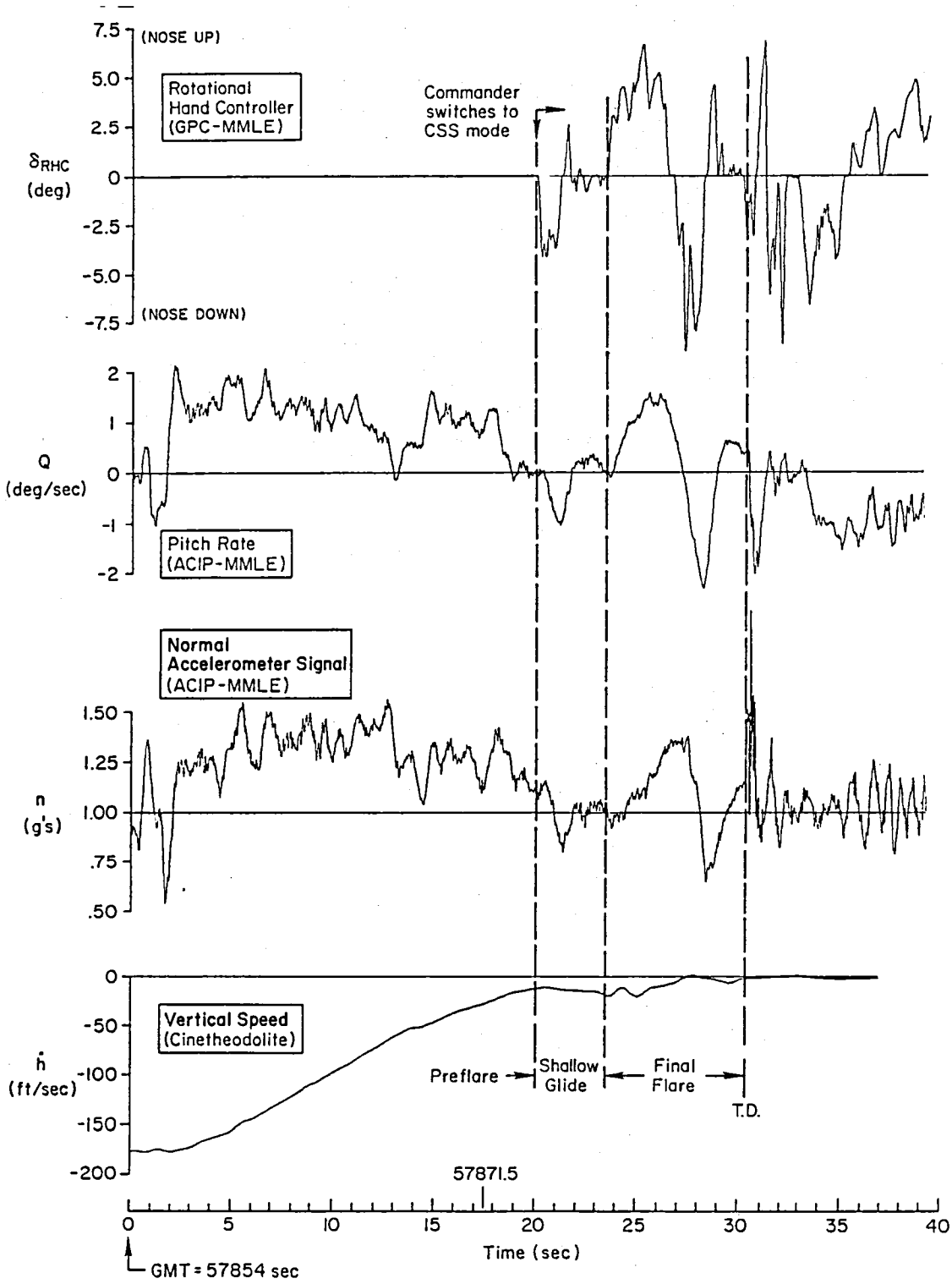

Figure 22. STS-3 Preflare Through Touchdown Time Traces

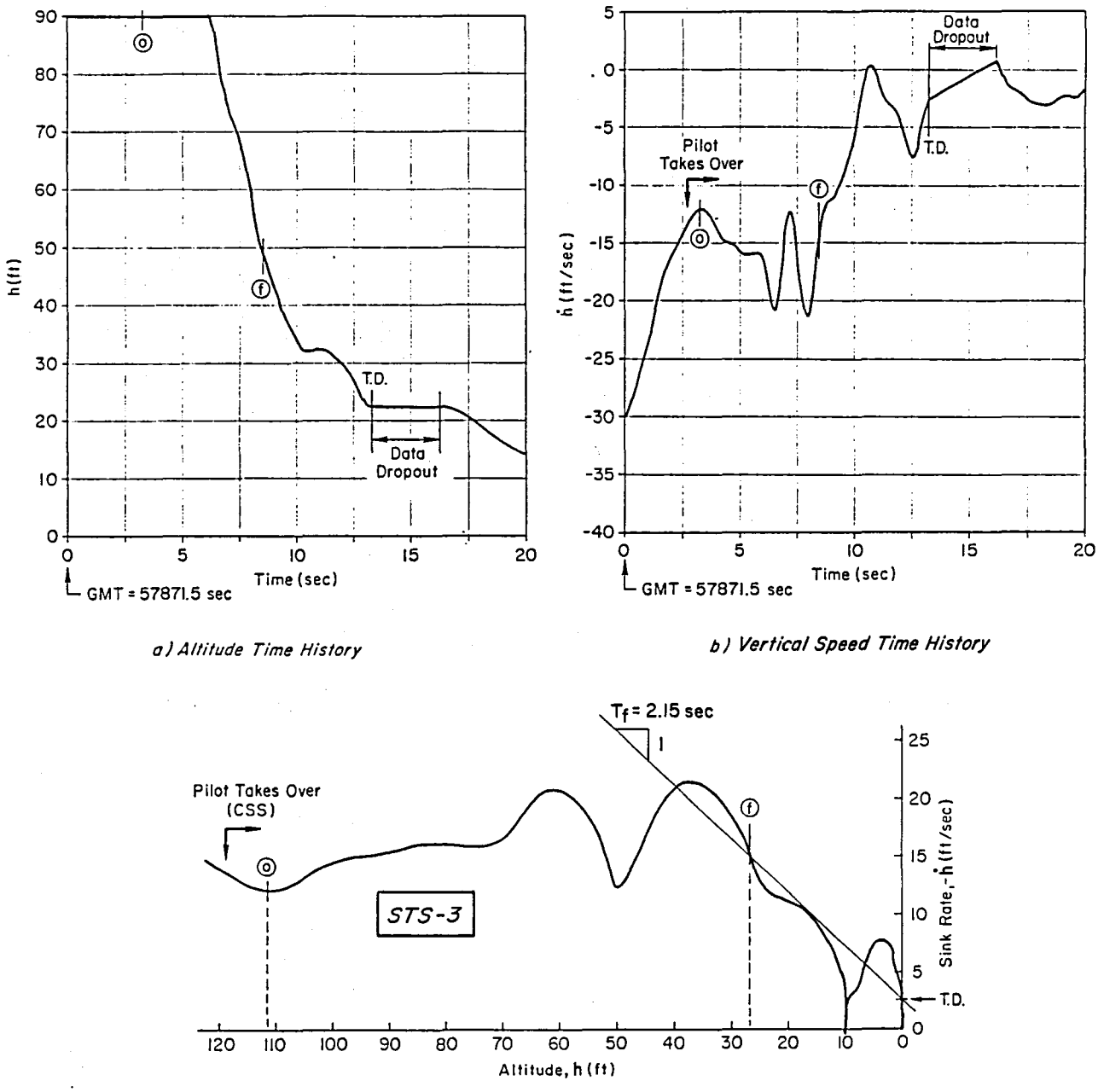

a) Altitude Time History

b) Vertical Speed Time History

Figure 23. STS-3 Preflare Through Touchdown Hodograph

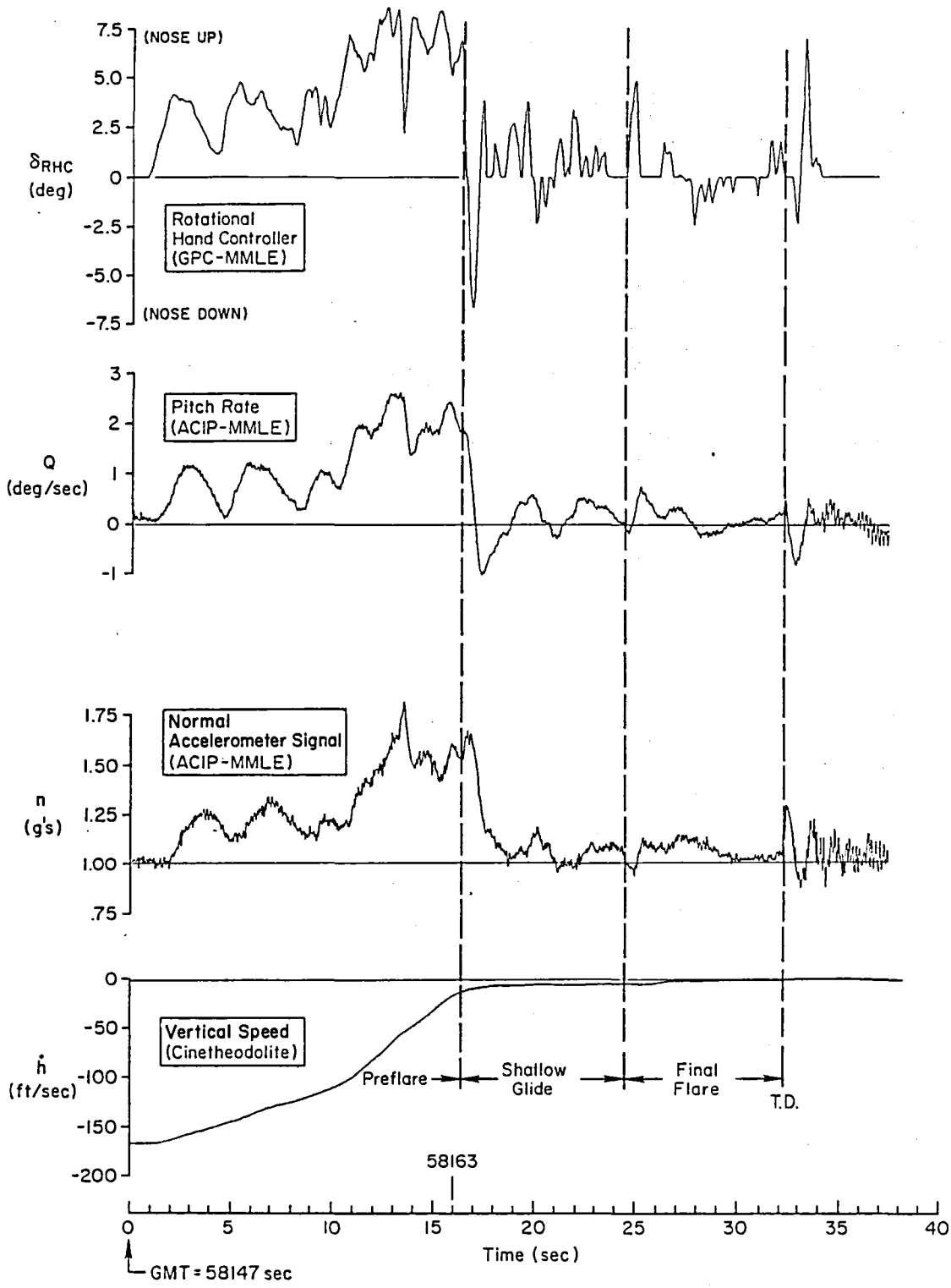

Figure 24. STS-4 Preflare Through Touchdown Time Traces

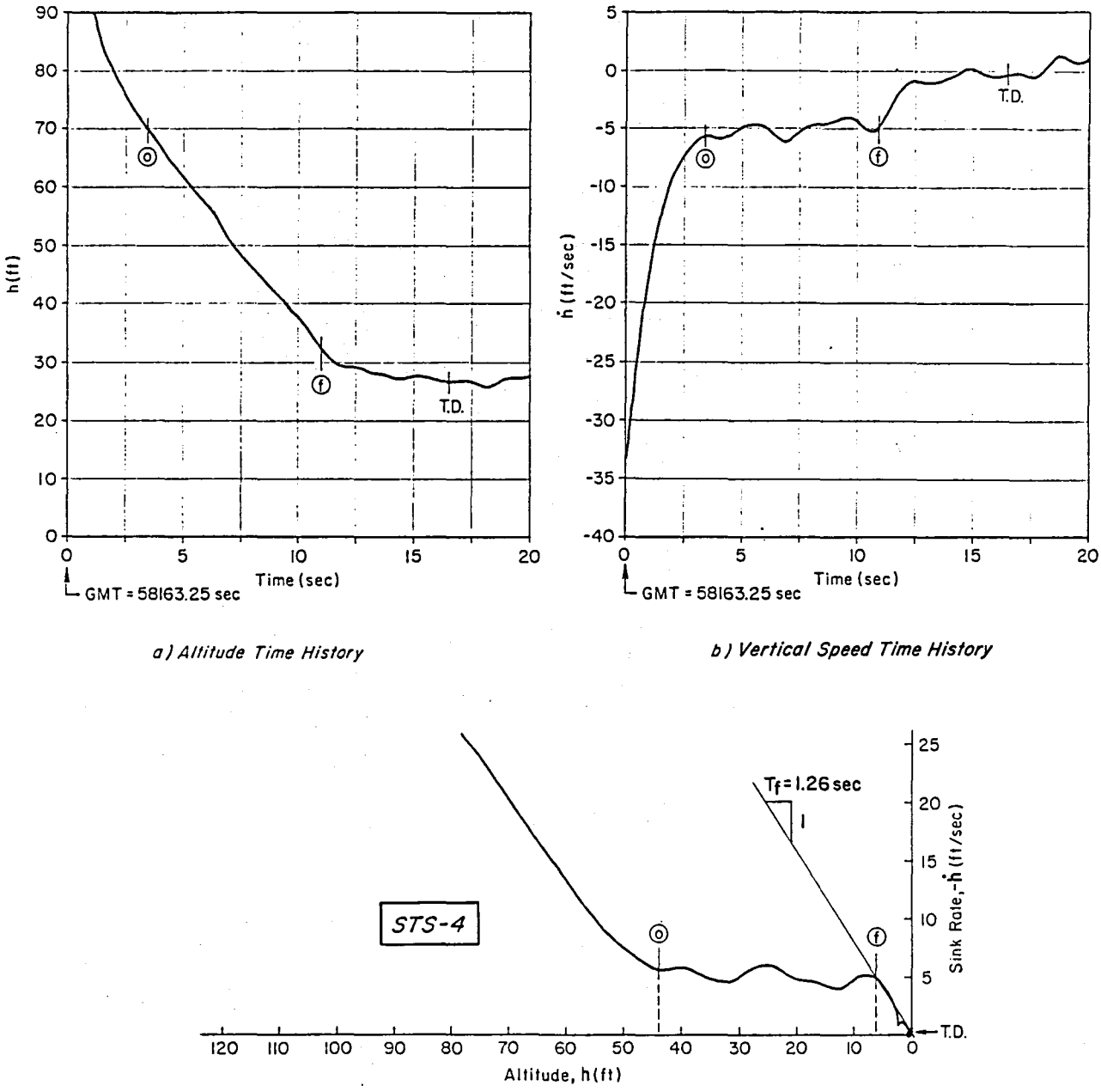

a) Altitude Time History

b) Vertical Speed Time History

Figure 25. STS-4 Preflare Through Touchdown Hodograph

By the time the shallow glide slope was reached, the pilot had adopted the pulse control technique. The transition to final flare was accomplished by a series of up-down-up pulses after which the vehicle was allowed to settle to touchdown in the attitude hold mode. Note there were essentially no pitch attitude commands for the final 5 sec of the landing.

The time history and hodograph plots of Fig. 27 do not show such decisive phases as seen in the STS-4 landing. It appears that the shallow glide was initiated at about -10 ft/sec sink rate, but from then on it is not clear whether separate segments were actually achieved. It does appear the pilot was attempting to slowly decrease sink rate prior to initiating final flare. The $T_f \doteq 2.85$ sec flare time constant and the nearly passive RHC indicate that pilot control of the flare itself was nearly precognitive during its last half.

5. STS-6 - This flight landed on the runway at Edwards with the aid of the PAPI lights, ball-bar system, and HUD. It is relatively easy to identify preflare, shallow glide, and final flare in the time traces of Fig. 28. There is a distinct transition to pulse type control for the shallow glide slope and landing. Again there is essentially no RHC activity for the last 5 sec prior to touchdown.

The time histories and hodograph of Fig. 29 also show very decisive segments for this landing. The shallow glide is held quite precisely at -10 ft/sec until final flare which is initiated at a nose altitude of about 50 ft. The final flare is almost an ideal exponential with a time constant of 2.42 sec.

Based on the minimum RHC activity in Fig. 28 and the smooth transitions and segments of Fig. 29, it appears that the ground based landing aids and HUD have reduced the control workload significantly.

6. STS-7 - This flight was diverted at virtually the last minute from landing at Kennedy to the lakebed at Edwards. The PAPI and ball-bar ground aids were available, and it was the second landing with the HUD. The time traces of Fig. 30 show a gradual change in RHC activity from continuous rate command to distinctly pulsive rate command/attitude

hold control. Thus, there is little to distinguish separate path segments. The time histories and hodograph of Fig. 31 provide additional clues to indicate a transition occurs between ⓪ and ⓕ from the preflare to an apparent final flare. There is a hesitation at a sink rate of about -12 ft/sec which suggests start of shallow glide, but this is followed immediately by a flare with a time constant of 4.6 sec. Since this landing is on the lakebed where there is little concern for touchdown point and landing roll, it appears the pilot was concentrating on achieving a specific touchdown sink rate (and possibly speed). The lightly damped path oscillation at about 2.3 rad/sec (also discernable in the pitch rate of Fig. 30) and the rapid RHC pulsing suggests a rather tightly closed sink rate loop which results in an almost neutrally stable pitch mode (see Fig. 19c). This terminal RHC activity and the $T_f \doteq 4.6$ sec flare time constant make it very clear that the pilot was in closed-loop control throughout the flare.

Figure 32 is a composite of the STS-2 through -7 hodographs which provides yet another perspective among the landings. There is considerable similarity in the two lakebed landings (STS-2 and -7) in that neither has a discernable shallow glide phase but rather one almost continuous flare. It is likely the control strategy and loop structure were the same in both. The three runway landings (STS-4, -5, and -6) are similar in that each has a fairly distinct shallow glide at a sink rate of -10 ft/sec or less followed by a flare at close to the vehicle path response time constant. While there appears to be little difference in task accomplishment between these three hodographs, the time traces for the pilot's RHC inputs in Figs. 24, 26, and 28 indicate a definite decrease in activity and therefore workload as the landing aids (ground and HUD) came into use. The STS-3 landing bears little resemblance to the others due to the late manual takeover and over-control problems. Again all of the above has obvious implications on pilot workload, landing performance, and possible safety for emergency landings at less well-equipped or more restricted landing sites.

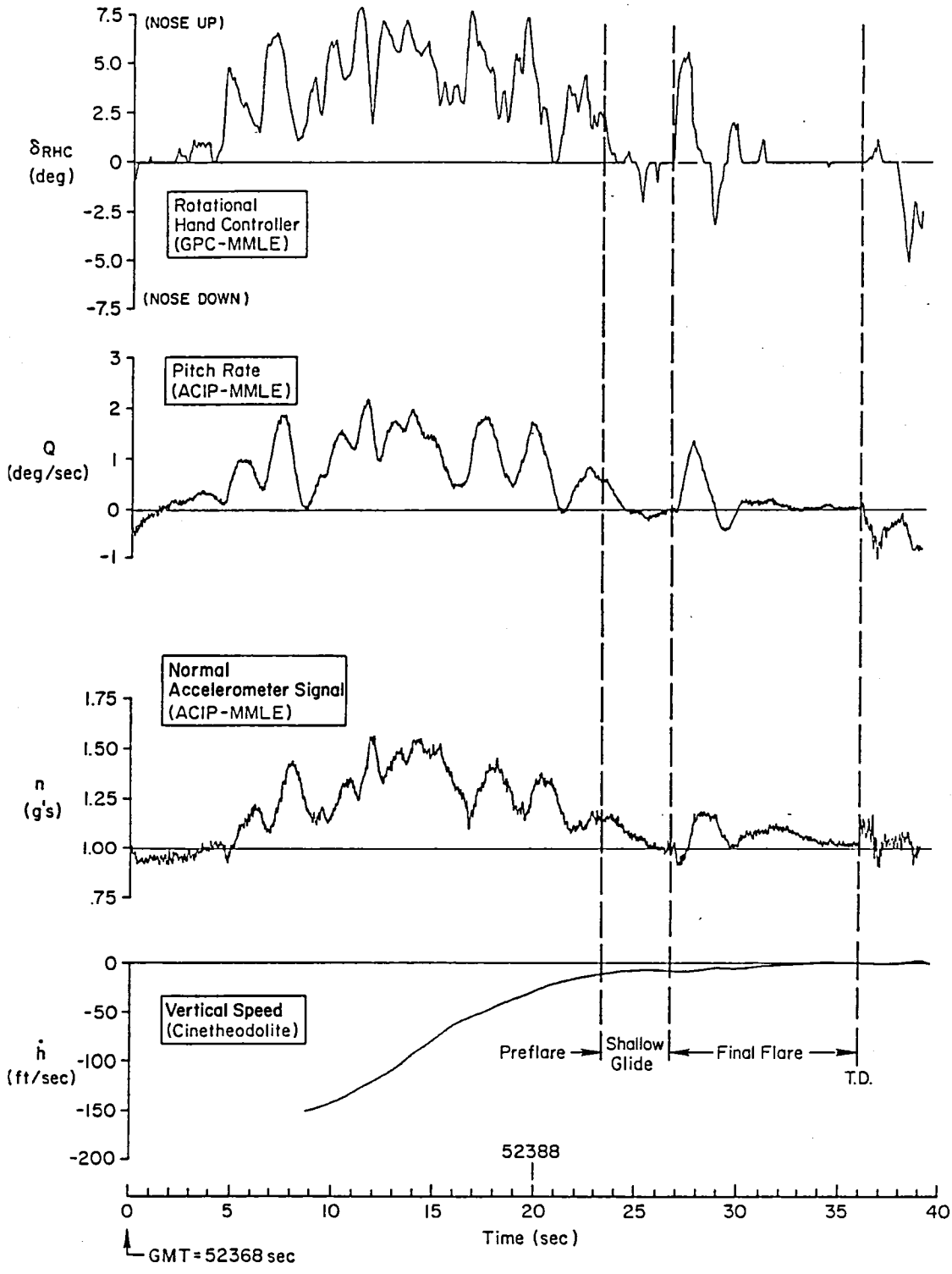

Figure 26. STS-5 Preflare Through Touchdown Time Traces

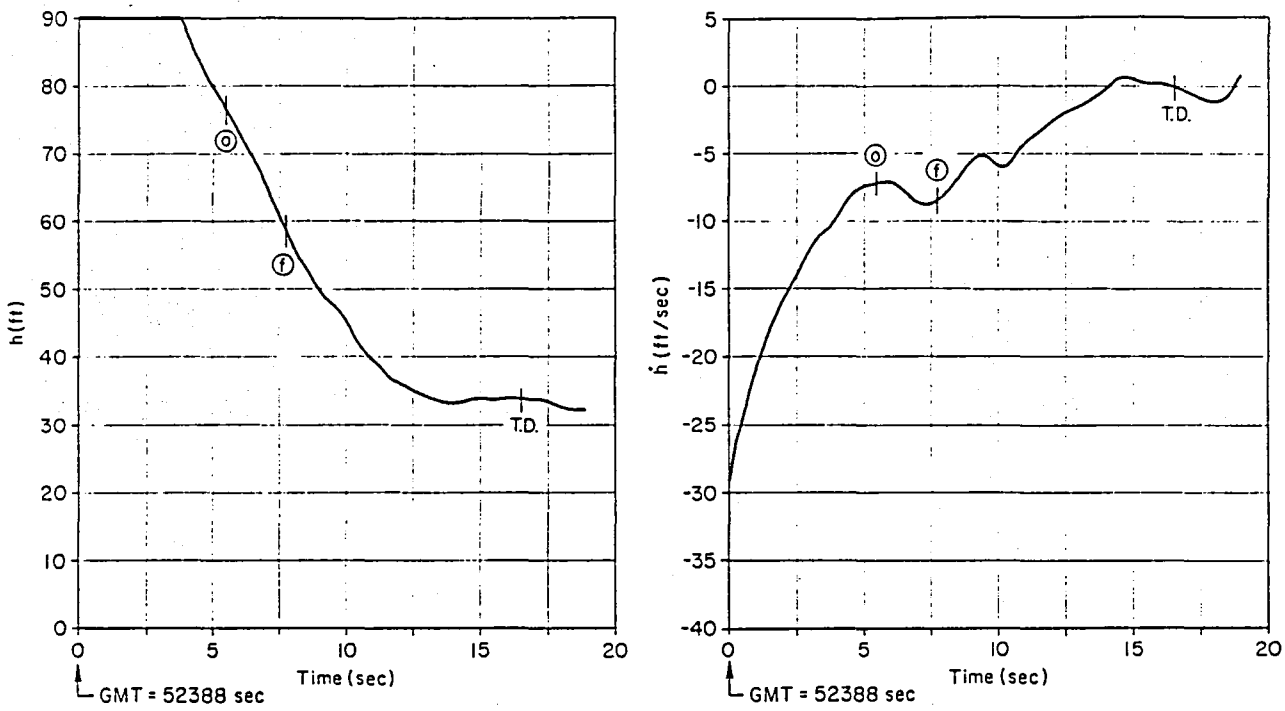

a) Altitude Time History

b) Vertical Speed Time History

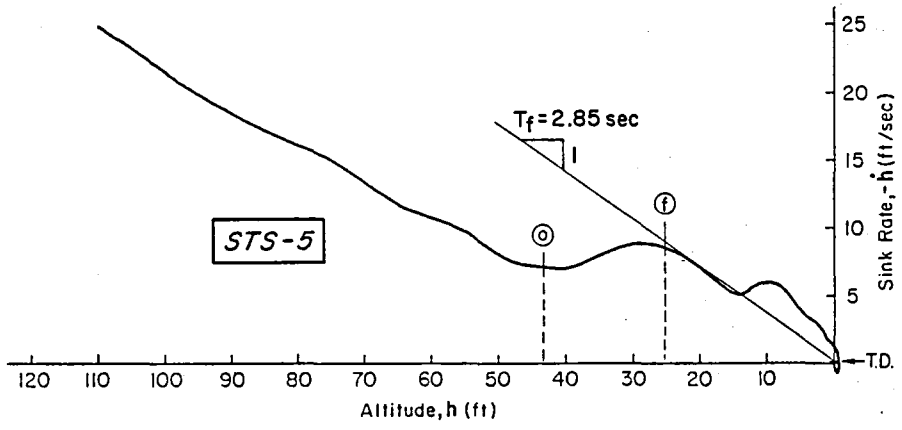

Figure 27. STS-5 Preflare Through Touchdown Hodograph

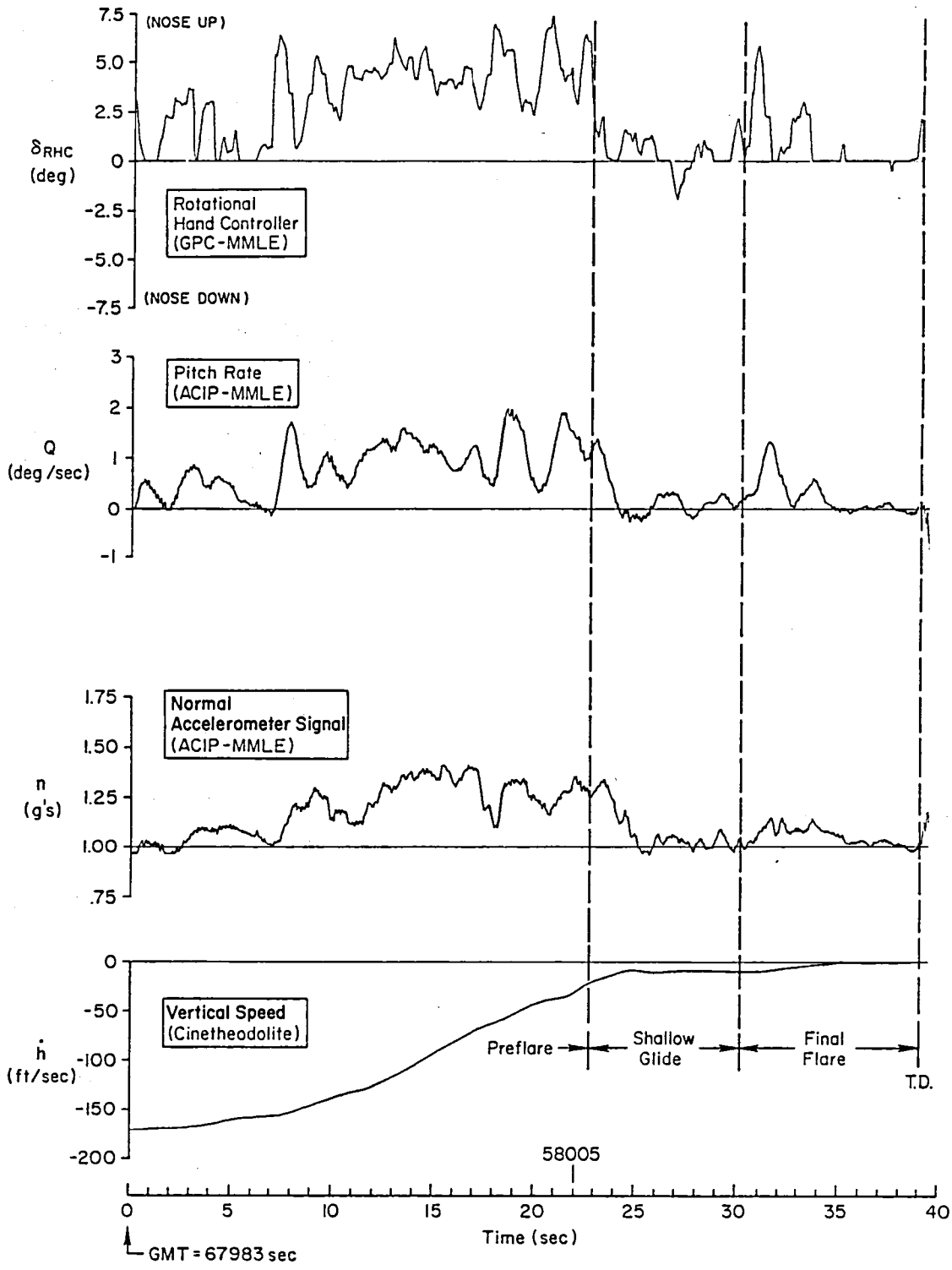

Figure 28. STS-6 Preflare Through Touchdown Time Traces

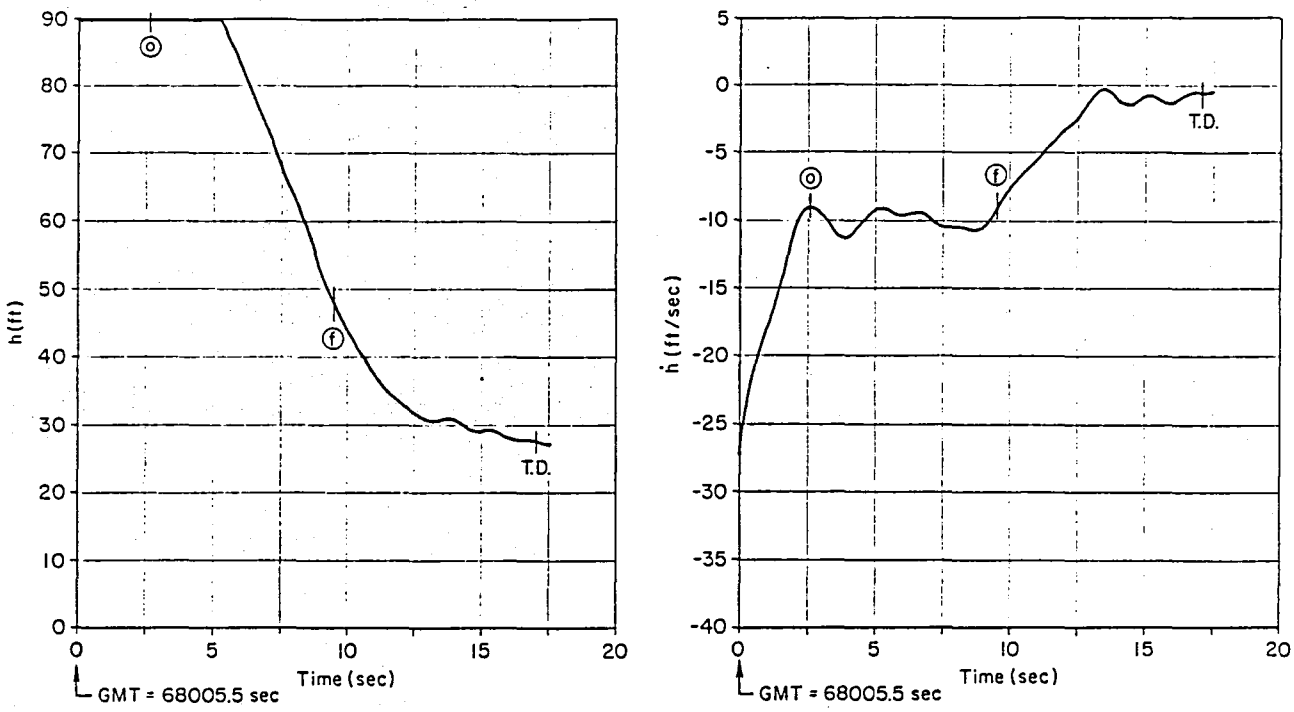

a) Altitude Time History

b) Vertical Speed Time History

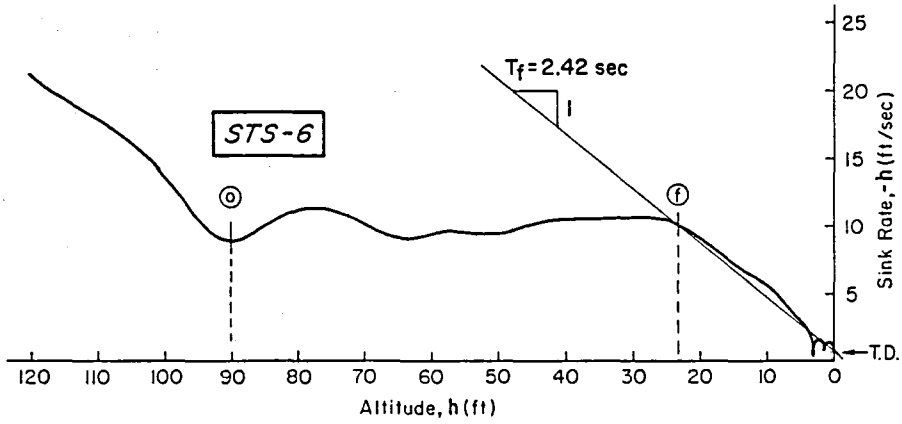

Figure 29. STS-6 Preflare Through Touchdown Hodograph

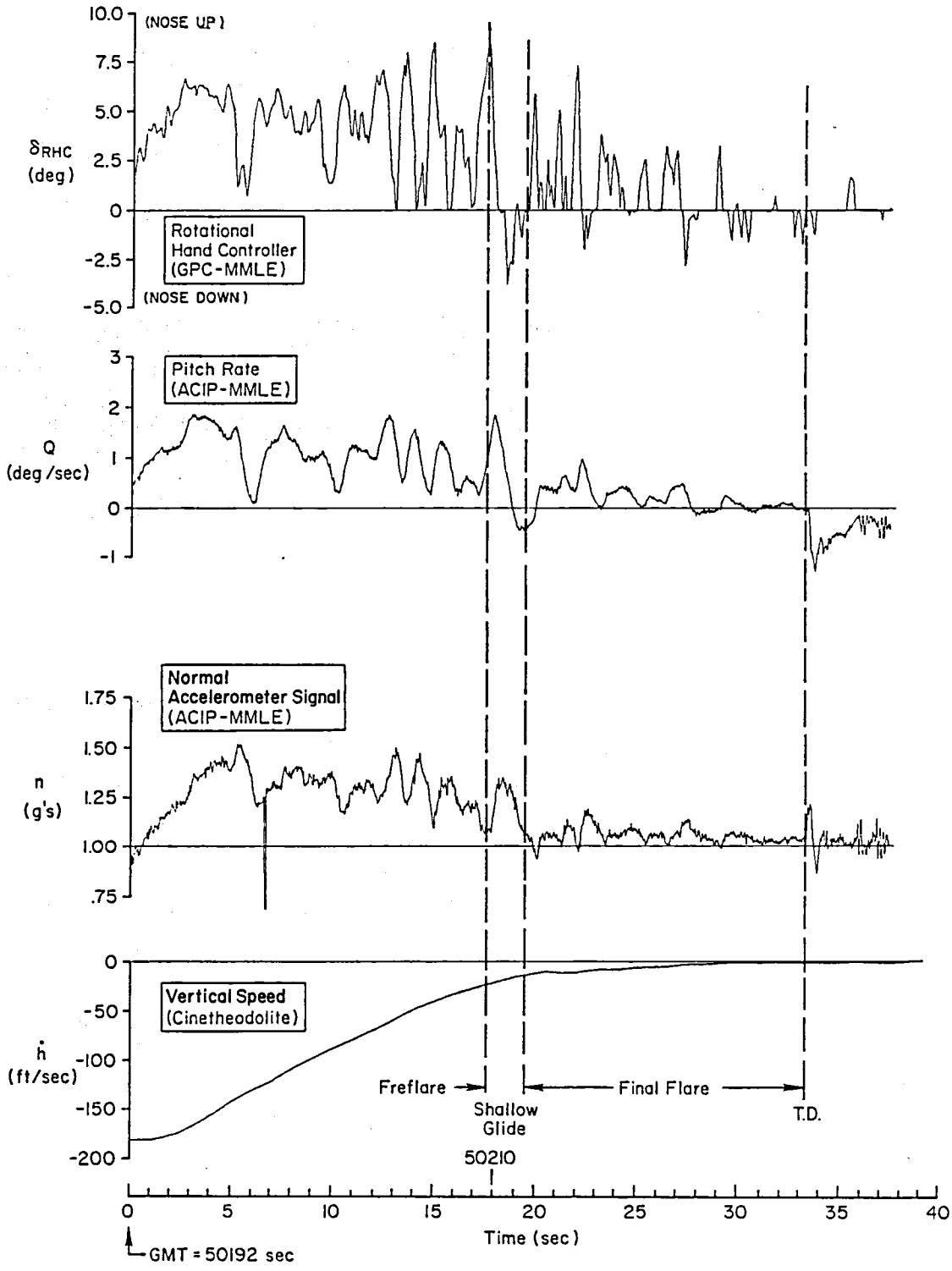

Figure 30. STS-7 Preflare Through Touchdown Time Traces

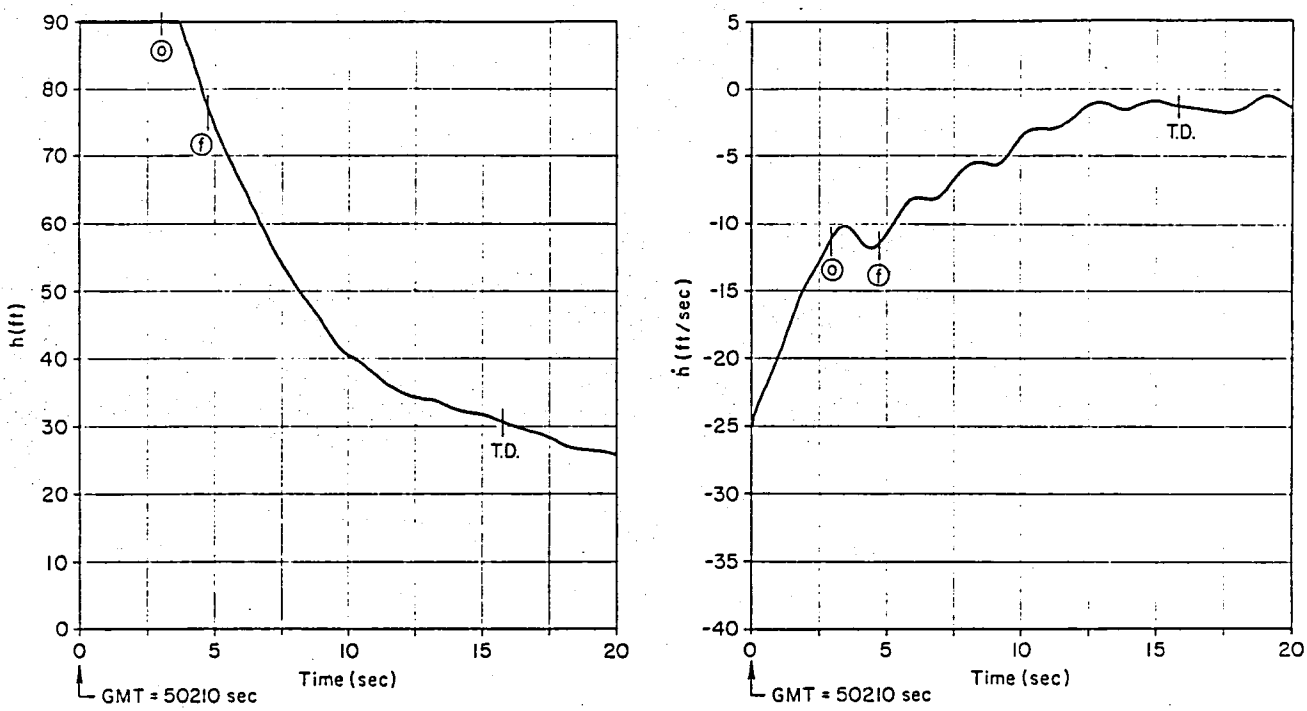

a) Altitude Time History

b) Vertical Speed Time History

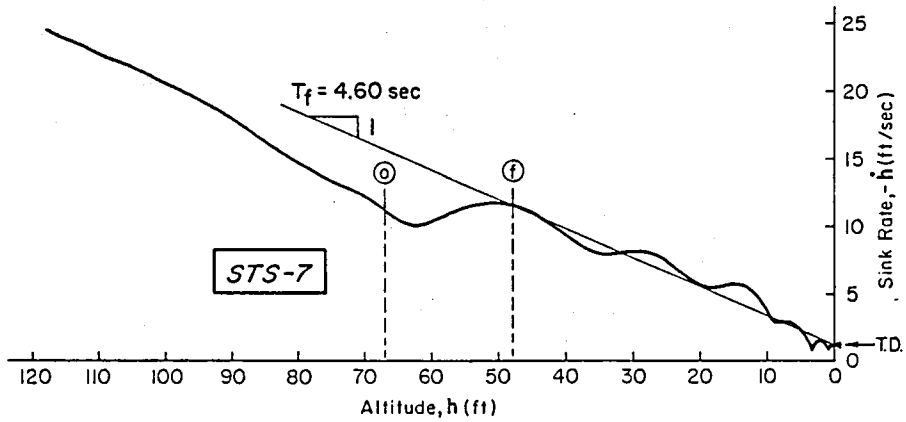

Figure 31. STS-7 Preflare Through Touchdown Hodograph

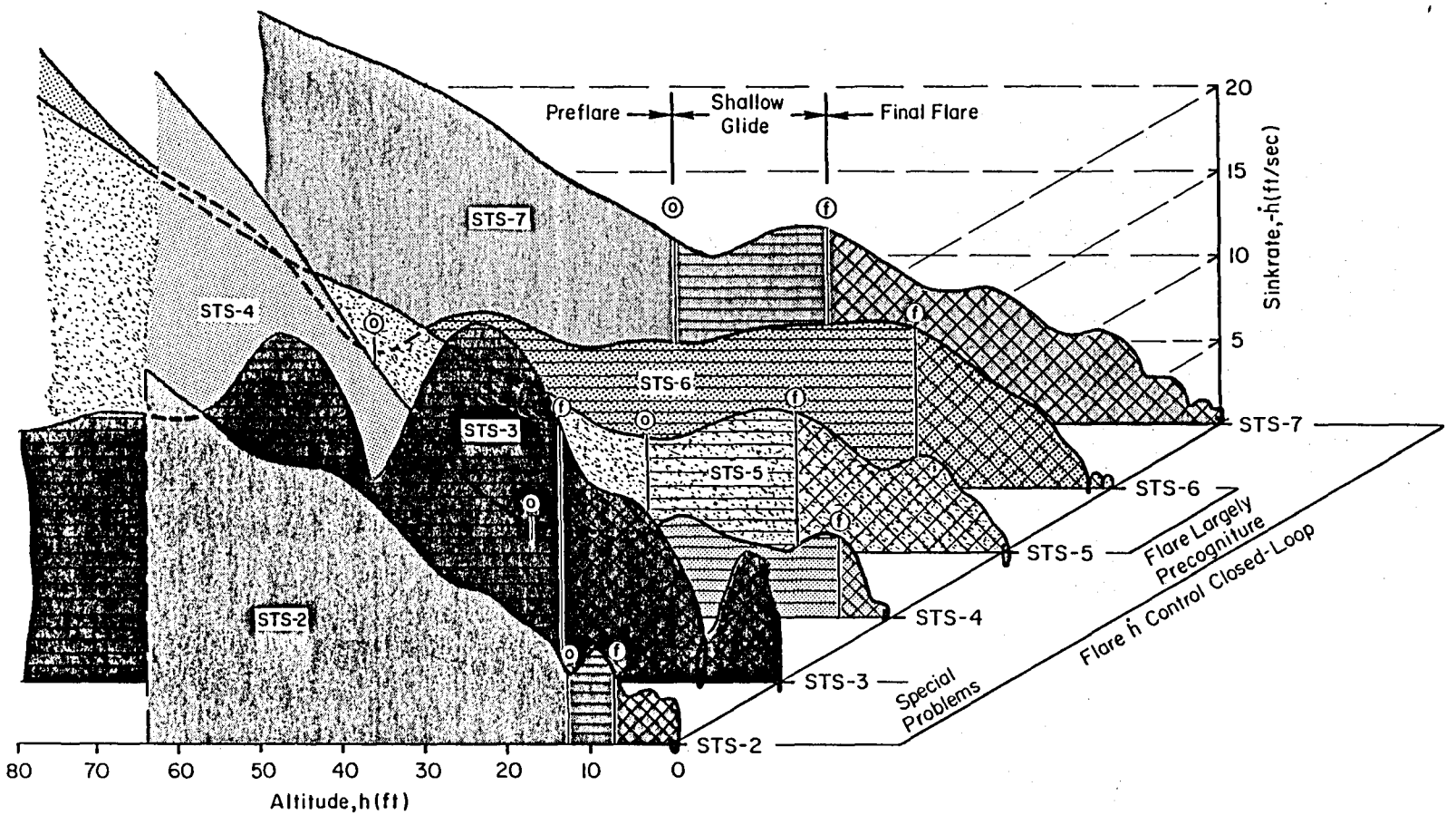

Figure 32. Composite of STS-2 Through -7 Approach and Landing Hodographs

2. Touchdown Performance Parameter Summary

The values of touchdown sink rate at the nose, $\dot{h}_{TD}$, speed, V_{TD}, and glide and flare distance, X_T, derived from the STS-2 through -7 cinetheodolite data are summarized in Table 3. The distance is measured from the assumed end of preflare as identified from the hodographs. In addition, touchdown sink rate at the nose was translated to the main gear based on vehicle geometry and pitch rate. Main gear sink rate, vehicle speed, and glide distance at touchdown are also plotted in bar chart form in Fig. 33. Various constraints were established for $\dot{h}_{TD}$ and V_{TD} in Phase II (Ref. 2) and these are listed in Table 4 and shown as boundaries in Fig. 33. These constraints are best estimates based on Autoland design information and do not necessarily reflect the latest Shuttle mission policies. More importantly, they do not necessarily drive the pilots, who have internal criteria we are trying to discover in this study! However, they provide a consistent representative set for comparison.

The touchdown sink rate summary in Fig. 33a indicates that all landings were well within the 6 fps (crosswind) sink rate limit and only the STS-3 landing exceeded the assumed nominal region. However, that landing could have exceeded the 6 fps limit if the vehicle had touched down about 1 sec earlier. All of the other landings have sink rates below 1.5 fps and tend to indicate a target value close to 1 fps. Indeed, a major conclusion to be derived from these data is that the touchdown sink rate when STS-3 is excluded is remarkedly uniform for all flights -- mean $\dot{h}_{TD} \doteq 0.86$ ft/sec with a standard deviation of 0.38 ft/sec. These are shown on Fig. 33a, and differ markedly from the autoland based nominal. The pilots were able to achieve this low and uniform value via adoptive control of pilot-vehicle system "architecture" (i.e., adopting precognitive or closed-loop control as needed) and of sink rate pilot gain sensitivity (i.e., T_f) when the control is closed-loop.

The touchdown speed summary in Fig. 33b shows that the 225 kts touchdown speed limit was exceeded only in the STS-3 landing. Three flights were slightly higher and two slightly lower than the nominal

TABLE 3. SUMMARY OF TOUCHDOWN SINK RATE AND SPEED

Mission	$\dot{h}_{TD}$ nose (fps) Cine	q_{TD} (deg/sec) MMLE	$\dot{h}_{TD}$ wheels (fps)	V_{TD} (fps) Cine	X_T (ft) Cine
STS-2	-0.70	0.10	-0.84	314.00	1990
STS-3	-2.50	0.40	-3.04	398.00	4023
STS-4	-0.40	0.40	-0.94	342.00	4966
STS-5	-0.20	0.05	-0.27	348.00	4251
STS-6	-0.50	0.00	-0.50	305.00	5061
STS-7	-1.40	0.00	-1.40	357.00	5057
Mean	-0.95	0.16	-1.17	344.00	4225
Std Dev	0.79	0.17	0.91	30.35	1078

TABLE 4. CONSTRAINTS ON TOUCHDOWN PARAMETERS ADOPTED FROM AUTOLAND DESIRES

Design sink rate at TD: $-1.5 \text{ fps} \geq \dot{h}_{TD} \geq -2.5 \text{ fps}$

Maximum sink rate at TD: $\dot{h}_{TD} = -9 \text{ fps}$

Maximum sink rate at TD, crosswind: $\dot{h}_{TD} = -6 \text{ fps}$

Nominal V_{TD} = 195 kts (329 fps)

Maximum V_{TD} = 225 kts (380 fps)

Minimum $V_{TD} \equiv 0.9$ nominal V_{TD} (296 fps)

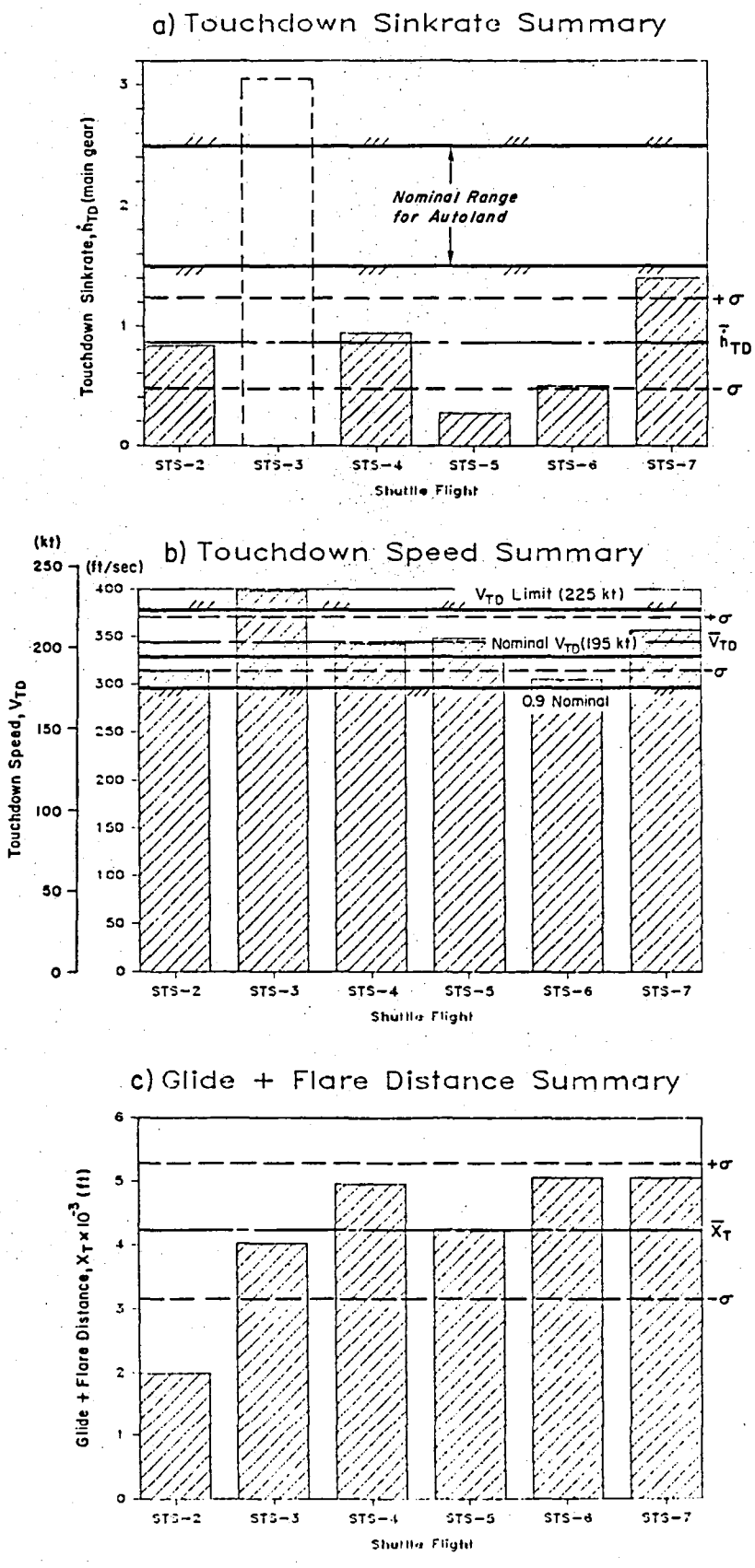

Figure 33. Touchdown Parameter Summary Chart

195 kts. One standard deviation in the achieved touchdown speed is less than the 30 kt difference between the upper limit and nominal V_{TD} values. If STS-3 is again excluded, the mean $V_{TD} \doteq 333$ ft/sec with a standard deviation of 22.5 ft/sec.

Figure 33c compares the total distance traveled from the end of the preflare pullup (as identified in the hodographs) to touchdown. Establishing absolute constraints for distance is more difficult than for $\dot{h}_{TD}$ and V_{TD} since reference must be made to the runway threshold. Further the effective distance constraints certainly vary more among the flights especially between lakebed and runway landings.

STS-2 was known to be low on energy and this is reflected in both V_{TD} and X_T. Despite this (and with the exception of STS-3) touchdown performance is quite consistent and adequate with respect to the Table 4 constraints. When it is recognized that this performance is attainable with both precognitive and tight closed-loop control of sink rate, this implies excellent and flexible performance for the pilot-vehicle system.

The data of Fig. 33 also tends to indicate that most importance is being attached to touchdown sink rate, with touchdown velocity also being weighted heavily. The latter is consistent with Ref. 21, in which it was stated that the difficulty of runway landings was reduced by setting V_{TD} criteria rather than X_{TD}.

3. Other Path Parameter Summaries

The fact that the crews of STS-2 through -7 appear to have used distinctly different landing strategies while achieving acceptable landing performance in all cases provide some interesting answers to old questions. Some specifics include:

- There are distinct variations in landing techniques, ranging from precognitive, nearly open-loop control, to tight closed-loop control.
- The differences in technique can be quantified and identified.
- Pilots can achieve remarkably uniform touchdown sink rates, which are, perhaps, less than those considered to be nominal for autoland systems.

On the other hand, there are still some unresolved questions about how the task constraints, pilot guidance strategies, and flight mechanics impact the orbiter's pitch and path dynamics and flying qualities requirements.

While there is value in focusing on the details of the individual flights and seeking explanations of pilot behavior on a flight-by-flight basis, such conclusions strictly speaking, apply only to the individual flights and not to the characteristics of the vehicle in general. Our approach to obtaining answers to the above questions is based on use of the pilot-vehicle-task model evolved in Phases II and III (Refs. 2 and 3). A primary motivation for use of such a quantitative model is the desire to draw conclusions which apply to the Orbiter and landing task as a whole. This is done by considering the ensemble of approaches and landings.

A first cut at quantifying the task model, determining sensitivities, margins for error, etc., which can then be used to establish potential flying qualities criteria is presented in the Appendix. The elements of the shallow glide and flare landing model are summarized in Fig. A-2. This model has intentionally been maintained as simple as possible and involves only about a half dozen parameters. These are obtained from the cine time traces at the times identified as initiation of shallow glide ⓘ and final flare ⓕ in the hodographs. The parameters thus extracted are summarized in Table 5 and Figs. 34 and 35.

Figure 34a compares the initial glide speeds for STS-2 through -7 and shows fairly high consistency -- particularly after STS-3. However, there is considerable variation in the initial glide altitude (Fig. 34b) even when the anomalous STS-3 case is neglected.

Figure 34c shows the shallow glide slope variable. The shallow glide slope is difficult to extract precisely from the flight data; these values were obtained by averaging $\dot{h}/V$ over the shallow glide region. The values obtained are all less than the nominal 1.5 deg except for STS-3 and show a significant variation range. Note that after the HUD became available on STS-6 and -7, the shallow glide is close to the nominal -1.5 deg.

TABLE 5. SUMMARY OF GLIDE AND FLARE MODEL PARAMETERS EXTRACTED FROM SHUTTLE FLIGHT DATA

Mission #	V_o fps Cine	h_o ft Cine	γ_o deg Cine	$K_{\dot{V}}$ ft/sec^2 Cine	V_f fps Cine	h_f ft Cine	T_f sec Cine	X_g ft Cine	X_f ft Cine
STS-2	355.00	13.00	-0.82	6.78	342.00	7.50	2.00	451.00	1539.00
STS-3	470.00	111.00	-1.70	7.41	432.00	27.00	2.15	2100.00	1923.00
STS-4	440.00	43.70	-0.73	7.69	380.00	6.20	1.26	2985.00	1981.00
STS-5	443.00	43.00	-1.07	7.84	412.00	25.00	2.85	933.00	3318.00
STS-6	412.00	89.70	-1.46	8.00	360.00	23.20	2.42	2593.00	2468.00
STS-7	451.00	66.50	-1.42	7.84	439.00	47.50	4.60	775.00	4282.00
Mean	428.50	61.83	-1.20	7.59	394.17	22.73	2.55	1639.50	2585.17
Std Dev	37.07	32.99	0.35	0.41	36.17	13.80	1.04	965.28	942.33

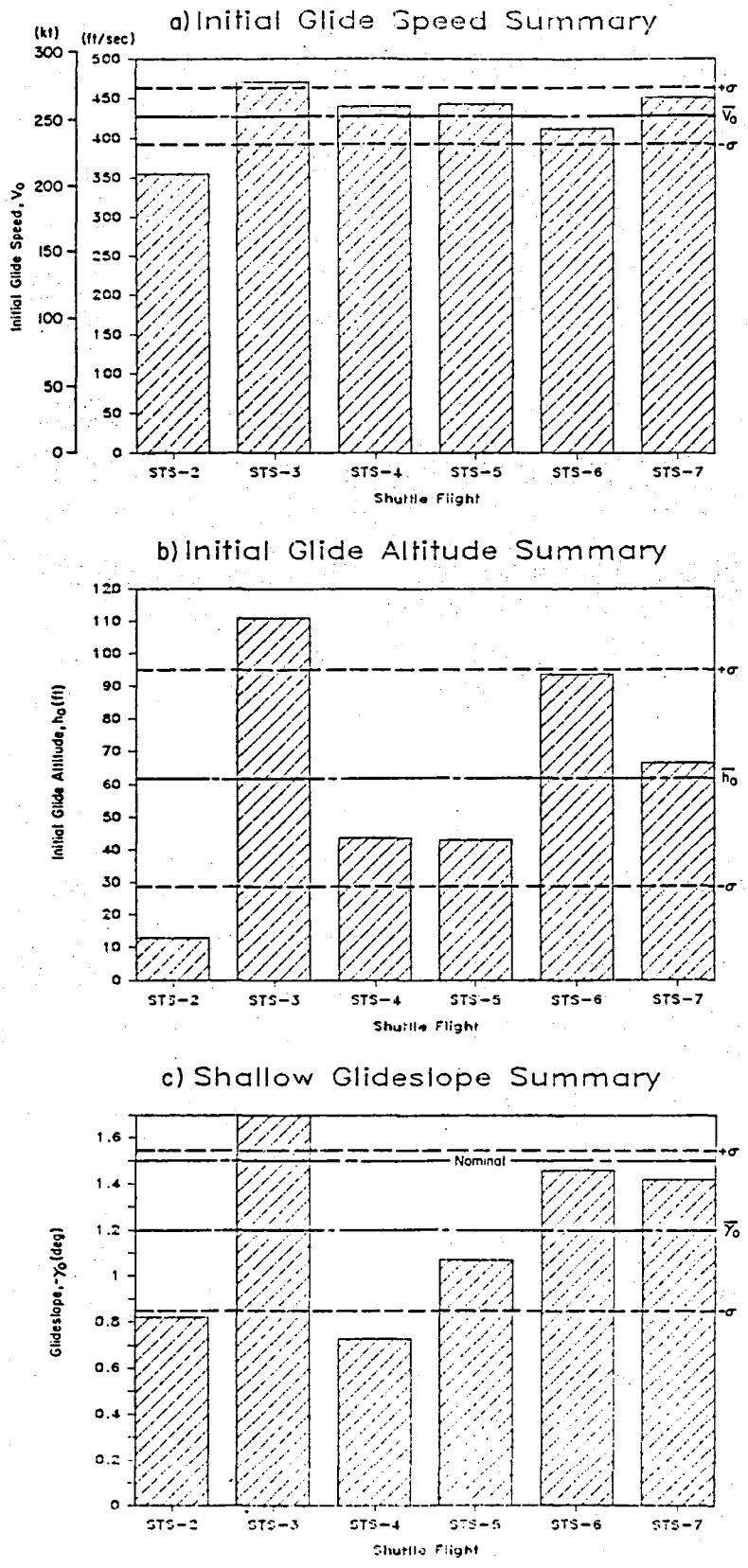

Figure 34. Summary of Shallow Glide Parameter Values

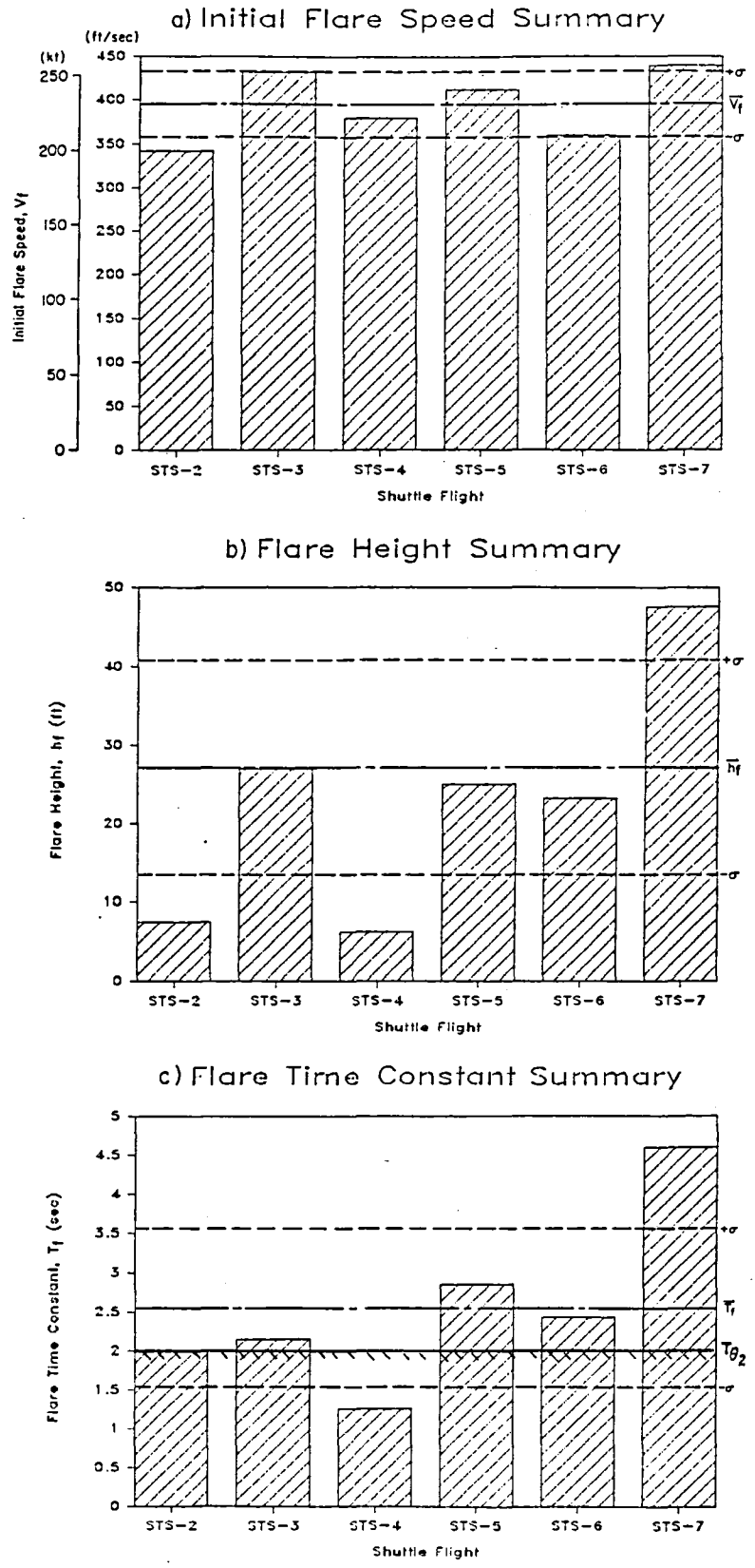

Figure 35. Summary of Final Flare Parameter Values

The initial flare speed summary of Fig. 35a shows variation similar to that of the V_o summary in Fig. 34a and the V_{TD} summary of Fig. 33b. This is consistent with the constant deceleration model following the conclusion of preflare. Velocity at any point in the trajectory is thus a function of time, and touchdown time is controlled via sink rate.

The flare height summary of Fig. 35b shows considerable variation over the 6 flights and does not appear related to h_o. This is to be expected since not all flights exhibited shallow glide of significant duration.

The key control variable which the pilot selects in the hypothesized multistage landing strategy is the flare time constant, T_f. This is of particular interest because it represents the outer loop guidance requirement most likely to be influenced by the available path response characteristics of the aircraft and ultimately the attitude bandwidth. T_f can be varied by the pilot by appropriately weighting his gain on sink rate relative to that on path deviation. Thus, the "flare time constant" in closed-loop control is directly adjusted by the sink rate feedback. In precognitive control T_f approaches T_{θ_2}. The "available" range of T_f is likely to be a critical point for flying qualities of the Orbiter in landing. The inner-loop manual control model assumes closure of a pitch attitude loop during the final flare at least after a precognitive flare initiation pulse. The vehicle can respond to flare law requirements as long as the flare time constant required is greater than the flare time constant available, i.e., the "path lag" T_{θ_2}. Thus we expect to find flare time constants not less than T_{θ_2} which for the Shuttle in landing is about 2 sec. This reference "boundary" is indicated in the flare time constant summary of Fig. 35c, and reveals that the observed flare time constants are all near to T_{θ_2} except for the STS-4 and -7 landings. In the STS-4 landing (Fig. 25), if the initiation of final flare ⓕ had been selected at 10 sec on the trace instead of 11 sec, T_f would be very close to 2 sec. These data for STS-2 through -6 may then actually validate the theoretical path time constant value of 2 sec.

T_{θ_2} is not a "hard" limit since the pilot can attempt to flare faster than T_{θ_2}, as he may have in STS-4. It does represent a reference beyond which we may expect that the pilot will have increased difficulty in achieving the desired flare performance and consequently may be dissatisfied with the vehicle flying qualities in landing. The real question of interest here is to define the circumstances under which a pilot might be forced to "push the T_{θ_2} limit" to achieve a satisfactory landing (i.e., within the touchdown constraints). Note in this respect that the two lowest flare time constants (Fig. 35c) occur for the two lowest flare initiation altitudes (Fig. 35b). This very well might be related to the lack of shallow glide flight path guidance aids in these early flights. In the last three flights the magnitude of h_f and T_f appear almost directly related. Perhaps an earlier (higher) flare initiation would have produced a larger T_f.

From a flying-qualities-in-flare standpoint presumably a "good" aircraft will possess a T_{θ_2} value which suffices for an adequate flare time constant in its own right for precognitive control. Further for closed-loop flares, the pilot should have a wide range (margin) of T_f well above T_{θ_2} for which he can achieve a landing which satisfies the basic touchdown constaints. These conditions appear to be present in the Orbiter so the flying qualities are certainly adequate or more than adequate for the landing task.

SECTION IV

PLAN FOR OFQ ARCHIVE DATA BASE AND INTERACTIVE HANDLING PROCESS

Because of the critical importance of rapid, efficient manipulation of flight data for the OFQ work, a portion of the effort has been devoted to defining requirements and planning an OFQ data handling "structure." Not all of this structure has been implemented in Phase IV but the overall plan is summarized here for future reference. Details of the data processing actually performed in the Phase IV work is also discussed.

A. GENERAL OFQ DATA PROCESSING NEEDS

The basic approach to the OFQ puts great emphasis on flexibility and eclectic use of data processing tools. Supporting software has been planned and partially developed. There are four primary considerations for achieving these capabilities.

- Extracting a data subset for specific analyses: an important first step in any OFQ work item is the extraction of a Shuttle approach and landing data subset as a working file. This requires defining a "time slice" in the trajectory and selecting specific variables of interest.

- Flexible execution of specialized data manipulation: emphasis is put on the capability to easily perform data operations such as axis and reference point transformations, complementary filtering, etc. The point of view here is that, because of the nature of the work, data manipulation needs cannot be defined far in advance and "canned" in specialized FORTRAN code. Instead a flexible "calculator" mode is desired in which variable time history vectors can be operated on in a sequence of arbitrary but well motivated operations.

- Graphic display and analysis: much of the OFQ work puts particular emphasis on qualitative insights to pilot control strategies and Shuttle response, which implies a strong need for flexible, interactive graphics.

- Special analysis procedures: in addition to a variety of ad hoc analyses, several specific procedures are important. These include altitude-sink rate hodographs, cross-spectral analysis for effective vehicle dynamics identification, and the use of the NIPIP program for pilot strategy identification.

B. OFQ FLIGHT DATA SOURCES

Five independent sources of Shuttle flight data of possible interest for the OFQ are identified below. The data available from each data source is indicated in Table 6. Only the MMLE and cinetheodolite data sources have been used in the Phase III and IV analysis to date.

1. Modified Maximum Likelihood Estimator (MMLE) Data Files

Specialized data files have been generated for Orbiter entry and landing phases for use in the NASA DFRF identification of aerodynamic coefficients. These files form an excellent starting point for flying qualities OEX data files. The primary data sources are onboard sensors from the Aerodynamic Coefficient Identification Program (ACIP), the Navigation and Guidance General Purpose Computer (GPC), and the Backup Flight Control System (BFCS) computer. The flight variables available on the DFRF MMLE file are indicated in Table 6. Since the primary use of this data file is in extraction of airframe aerodynmaic coefficients, emphasis is on airframe response and control surface deflection variables; however, limited data is available on manual controller deflections as well as some flight control system discrete data.

2. Cinetheodolite Tapes

The cinetheodolite system is operated by the Air Force Flight Test Center (AFFTC). Some documentation of the system and the data output is available through Refs. 5 and 27. Data apparently can be obtained from altitudes corresponding to the Shuttle entering the EAFB area through touchdown. Frame-by-frame manual reduction of film from several cinematic cameras is used as raw data to estimate the earth referenced XYZ

TABLE 6. SUMMARY OF SHUTTLE FLIGHT DATA DESIRED AND SOURCES FOR OFQ

VARIABLE	MMLE FILES				TAKEOFF & LANDING TOWER TAPES	CINETHEODOLITE TAPES	BEST ESTIMATED TRAJECTORY DATA (DFRF & LRC) FILES	NASA JSC MPDB TAPES
	ACIP	GPC	OI	BFCS				
TRANSLATIONAL ACCELERATION A_Z A_Y A_Z								MOST ON-BOARD SIGNALS EXCEPT FROM ACIP
ANGULAR ACCELERATION $\dot{P},\dot{Q},\dot{R}$								
TRANSLATIONAL RATE (AIR DATA) $\alpha,\beta,\dot{H},V_{TRUE},V_{EAS},\dot{q},\dot{M}$								
TRANSLATIONAL RATE (EARTH REFERENCED) $\dot{X}$, $\dot{Y}$, $\dot{Z}$								
ANGULAR RATE P,Q,R								
EARTH REFERENCED POSITION X, Y, H								
EULER ANGLES ψ, θ, ϕ								
CONTROL SURFACE DEFLECTION δ_e, δ_a, δ_r, δ_{SB}, δ_{BF}								
MANUAL CONTROLS (COMMANDER AND PILOT SEPARATE) $\delta_{Q_{RHC}}$, δ_{PRHC}, δ_{PED}, δ_{SBC}, δ_{BFC}								
MANUAL TRIM CONTROLS								
SWITCHES AND FCS DISCRETES								
DISPLAY AND HUD VARIABLES								
WIND DATA								

location of the orbiter nose, generally at 20 samples per second. It also is possible to obtain the location of a second reference point on the body for use in estimating vehicle attitudes, however this has not been done for the OFT landings. Some undocumented optical distortion apparently occurs near the ground. A variety of rates and accelerations are estimated in the data reduction program based on the position data (see Table 7). Data from meteorological sources on the ground and at altitude are used to estimate rates and accelerations referenced to the airmass (see Table 6). Copies of the digital magnetic data tapes for STS-1 through -7 were made available by the AFFTC and archived in the DFRF Tape Library.

3. Takeoff and Landing Tower Tapes

Earth referenced XYZ position of the Orbiter is also available from the Edwards Takeoff and Landing Tower system but only for runway landings and for a much lower altitude range than that of the cinetheodolite data. However, the accuracy is apparently higher than that of the cinetheodolite system. No documentation of this system has been obtained. The data tapes for STS-4, -5, and -6 have also been obtained from the AFFTC and are archived in the DFRF Tape Library. However, initial attempts to access the files were unsuccessful and because of the success obtained with the cinetheodolite data, this data set has not yet been used.

4. JSC Master Products Data Base (MPDB)

The MPDB is a very large and sophisticated computerized archive, which serves Shuttle operational needs at NASA JSC and is the "official" flight data archive for the Space Transportation System. There are unique data in this archive of particular interest for the OFQ. These include: switching discretes (as between AUTO and CSS modes), the "weight-on-wheels" signal (which would be valuable for precise determination of touchdown), display signals (including the HUD) and mass properties (i.e., weight, c.g., and moments of inertia). Because of difficulties in directly accessing this data from JSC, data subsets relevant to flying qualities/flight control work have been obtained from the

TABLE 7. LIST OF PARAMETERS AVAILABLE FROM CINETHEODOLITE TAPE

LIST OF AVAILABLE PARAMETERS							
NO.	NAME	UNITS	DESCRIPTION	NO.	NAME	UNITS	DESCRIPTION
1	HMS	HMS	Time in Hours, Minutes and Seconds	53	AYZ	Ft/Sc2	Acceleration in the YZ-Plane
2	INDEX		Index Number	54	AT	Ft/Sc2	Tangential Acceleration
3	ELAPS	Sec	Elapsed Time in Seconds from Zero Time	55	AN	Ft/Sc2	Normal Acceleration
4	SECS	Sec	Time in Total Seconds	56	AWT	Ft/Sc2	Tangential Acceleration-Wind Corrected
5	X	Feet	X-Unsmoothed (EAST)	57	AWN	Ft/Sc2	Normal Acceleration-Wind Corrected
6	Y	Feet	Y-Unsmoothed (NORTH)	58	AXP	Ft/Sc2	Acceleration along the VA Vector
7	Z	Feet	Z-Unsmoothed (UP)	59	AYP	Ft/Sc2	Acceleration Horizontally Perpendicular to the VA Vector
8	XSM	Feet	X-Smoothed (EAST)	60	AZP	Ft/Sc2	Acceleration Perpendicular Upward to the VA Vector
9	YSM	Feet	Y-Smoothed (NORTH)	61	HORD	Feet	Horizontal Distance
10	ZSM	Feet	Z-Smoothed (UP)	62	ARCD	Feet	Arc Distance
11	LAT	Deg	Latitude	63	HORDW	Feet	Horizontal Distance-Wind Corrected
12	LONG	Deg	Longitude (+WEST)	64	ARCDW	Feet	Arc Distance-Wind Corrected
13	ALT	Feet	Altitude	65	ACCGD	Feet	Accumulated Ground Distance
14	RHO	Sl/Ft3	Air Density	66	QC	Lb/Ft2	Impact Pressure
15	PA	MBS	Ambient Pressure	67	QDP	Lb/Ft2	Dynamic Pressure
16	TA	Deg C	Ambient Temperature	68	RLD		Lift to Drag Ratio
17	WD	Deg	Wind Direction	69	CDS	SqFt	Drag Area
18	WV	Ft/Sec	Wind Velocity	70	CD		Coefficient of Drag
19	WX	Ft/Sec	X-Component of Wind Velocity	71	KD		Ballistic Coefficient of Drag
20	WY	Ft/Sec	Y-Component of Wind Velocity	72	HV	Deg	Heading with Respect to Y-Axis
21	VX	Ft/Sec	X-Component of Velocity	73	HVN	Deg	Heading with Respect to North
22	VY	Ft/Sec	Y-Component of Velocity	74	HVW	Deg	Heading with Respect to Y-Axis-Wind Corrected
23	VZ	Ft/Sec	Z-Component of Velocity	75	HVNW	Deg	Heading with Respect to North-Wind Corrected
24	ROC	Ft/Sec	Rate of Climb	76	VNO	Ft/Sec	Northward Velocity at the Object
25	VWX	Ft/Sec	X-Component of Velocity-Wind Corrected	77	VEO	Ft/Sec	Eastward Velocity at the Object
26	VWY	Ft/Sec	Y-Component of Velocity-Wind Corrected	78	VZO	Ft/Sec	Upward Velocity at the Object
27	AX	Ft/Sc2	X-Component of Acceleration	79	HVO	Deg	Heading with Respect to North at the Object
28	AY	Ft/Sc2	Y-Component of Acceleration	80	EL	Deg	Elevation Angle
29	AZ	Ft/Sc2	Z-Component of Acceleration	81	AZY	Deg	Azimuth Angle with Respect to Y-Axis
30	AV	Ft/Sc2	Vertical Acceleration	82	AZN	Deg	Azimuth Angle with Respect to North
31	SR	Feet	Slant Range	83	AR	Ft/Sc2	Radial Acceleration
32	GR	Feet	Ground Range	84	KAPPA	Deg	Direction of Radial Acceleration
33	XZR	Feet	Range in the XZ-Plane	85	OMEGA	Dg/Sec	Angular Rate of Pull-up
34	YZR	Feet	Range in the YZ-Plane	86	PITCH	Deg	Pitch Angle
35	RN	Feet	Range in the Northward Direction	87	YAW	Deg	Yaw Angle
36	RE	Feet	Range in the Eastward Direction	88	FPA	Deg	Flight Path Angle
37	VN	Ft/Sec	Northward Component of Velocity	89	DVA	Deg	Dive Angle
38	VE	Ft/Sec	Eastward Component of Velocity	90	XINV	Feet	X-Coordinate of VT Intercept with the XY-Plane
39	VT	Ft/Sec	Total Velocity	91	YINV	Feet	Y-Coordinate of VT Intercept with the XY-Plane
40	VA	Ft/Sec	Total Velocity-Wind Corrected	92	VXP	Ft/Sec	Velocity along the SR Vector
41	VG	Ft/Sec	Ground Velocity	93	VYP	Ft/Sec	Velocity Horizontally Perpendicular to the SR Vector
42	VXZ	Ft/Sec	Velocity in the XZ-Plane	94	VZP	Ft/Sec	Velocity Perpendicular Upward to the SR Vector
43	VYZ	Ft/Sec	Velocity in the YZ-Plane	95	HORIZ	Deg	Horizontal Angle between the VT and SR Vectors
44	VWXY	Ft/Sec	Velocity in the XY-Plane-Wind Corrected	96	VERT	Deg	Vertical angle between the VT and SR Vectors
45	VWXZ	Ft/Sec	Velocity in the XZ-Plane-Wind Corrected	97	SPACE	Deg	Space Angle between the VT and SR Vectors
46	VWYZ	Ft/Sec	Velocity in the YZ-Plane-Wind Corrected	98	PALT	Feet	Pressure Altitude
47	ROD	Ft/Sec	Rate of Descent	99	AZATT	Deg	Azimuth Attitude Angle
48	VS	Ft/Sec	Speed of Sound	100	ELATT	Deg	Elevation Attitude Angle
49	MACH		Mach Number	101	VATT	Deg	Vertical Attitude Angle
50	AM	Ft/Sc2	Acceleration Magnitude (Total Acceleration)	102	ELDMP	Deg	Dumped Elevation Angle
51	AXY	Ft/Sc2	Acceleration in the XY-Plane	103	RBO	Deg	Bearing of Origin with Respect to Heading with Respect
52	AXZ	Ft/Sc2	Acceleration in the XZ-Plane				to North-Wind Corrected

AFFTC. This approach has the added advantage that a tape reading program for the CYBER computer developed by AFFTC is also available. Copies of these tapes have been delivered to DFRF.

5. The Best Estimated Trajectory (BET) and the DFRF Linearized Kalman Filtered (LKF) Air Data Tapes

The DFRF LKF air data (Ref. 28) is an extension of the original BET data developed at NASA Langley for each Shuttle landing. This is data from four sources merged through a linearized Kalman filter to obtain a best estimate of vehicle and wind velocities. These data have not yet been necessary at the level of the Phase IV analysis, however, they have potential value for future work.

C. A PROTOTYPE FOR AN OFQ DATA HANDLING SYSTEM

Figure 36 shows a prototype structure for the OFQ data analysis system that has been developed in Phase IV for planning purposes. This structure is intended to be implemented by linking a number of basically independent FORTRAN programs, many of which exist and have been exercised by STI or DFRF to some extent. One of the main functions of this system is to combine the large volume of variously formatted Shuttle data from a variety of sources to produce the specialized data subset needed for a particular analysis. Thus the system consists of a hierarchy of "archive" and "working" files interconnected by specialized data handling software. As the data flows through the system from the original sources to ultimate use, the data files become smaller and the data handling software becomes (ideally) more interactive. The components of the Fig. 36 system are detailed below.

1. Data Source - Computer Interface

The integration of the five OFQ data sources on the primary DFRF computer (upper left in Fig. 36) is indicated in greater detail in Fig. 37. Once data tapes are logged into the DFRF Tape Library they can be accessed for use on the CYBER by use of the Tape Reservation System (TRS) -- the standard CYBER tape handing utility. Actually reading

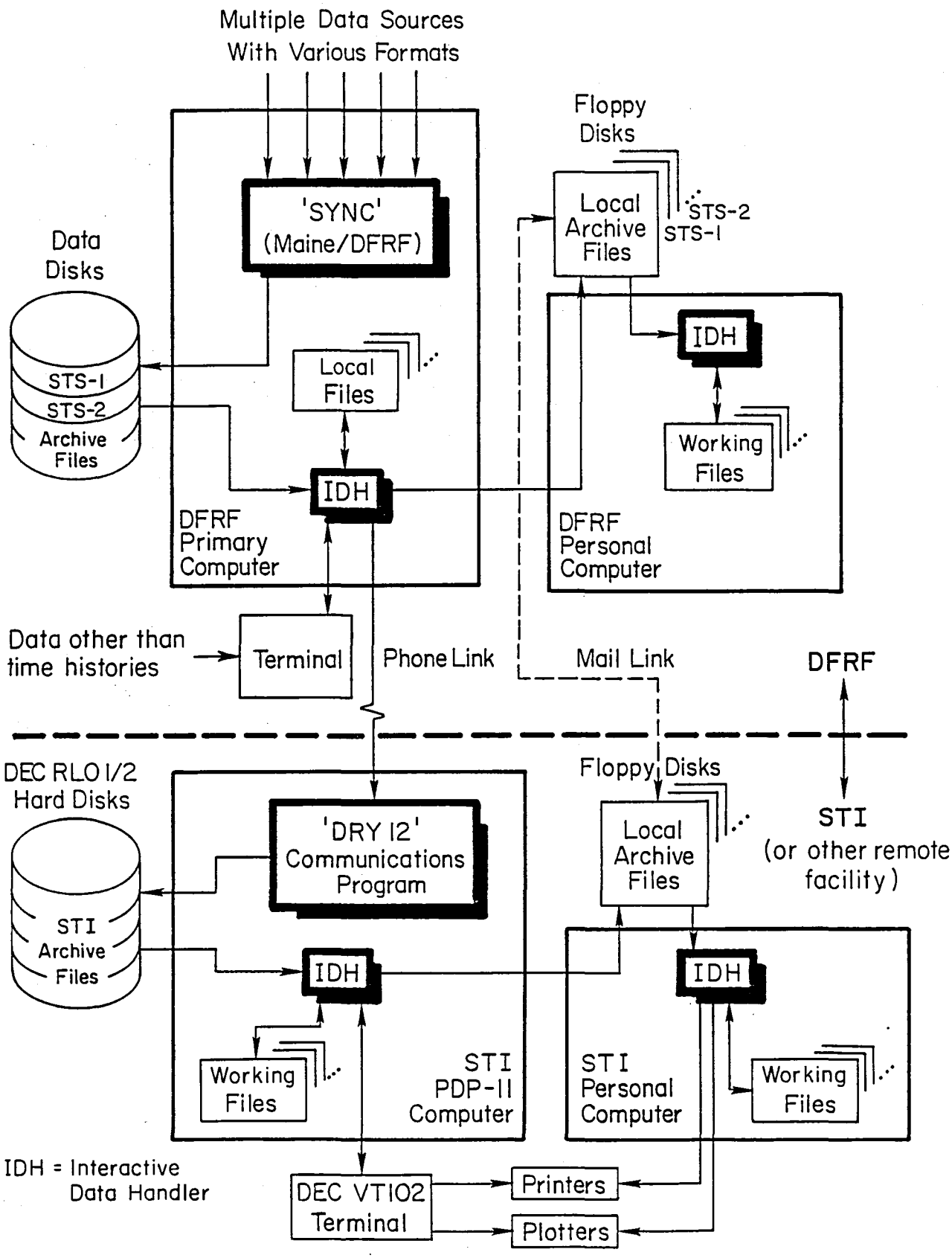

Figure 36. Prototype Structure for OFQ Data Processing

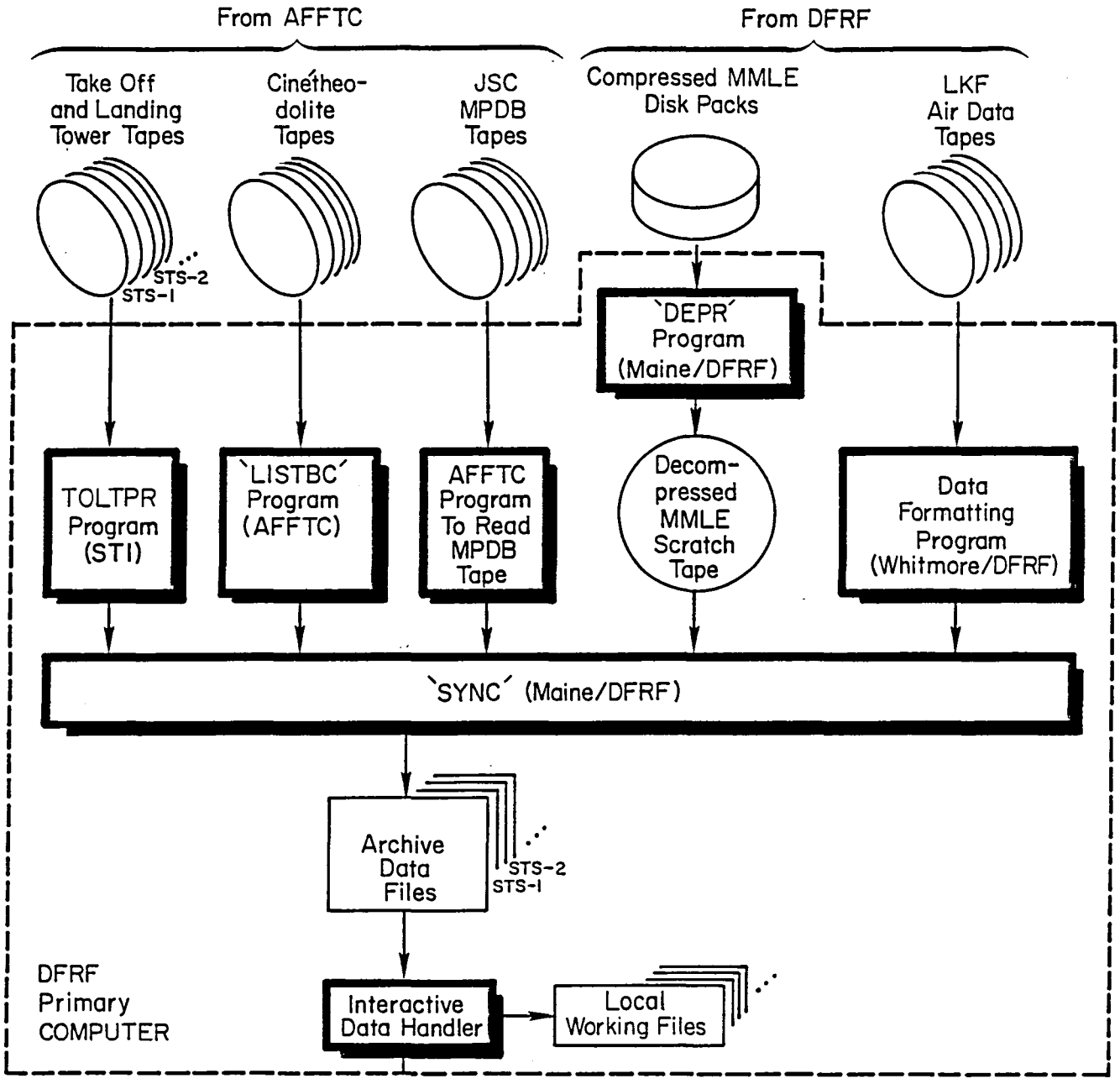

Figure 37. Shuttle Flight Data Sources for the OFQ Archive Files

tapes and storing data on file requires a unique tape reading program for each data source. The five tape reading programs have been obtained from several sources as discussed below.

- MMLE Database Access -- The MMLE data is archived at DFRF in compressed form with each channel represented at its own sample rate. To use the compressed MMLE data, it must first be decompressed by use of the "DEPR" program developed by R. E. Maine. The decompressed data file, which is very large, must then be written to a (two-reel) tape file. A subset of this data can then be obtained using a data handler program (IDH in Fig. 36).

- Cinetheodolite Tape Reading -- An AFFTC FORTRAN program, "LISTBC," for reading the cinetheodolite tapes was obtained through DFRF. This program was modified by STI to make it more suitable for extracting short "time slices."

- Takeoff and Landing Tower Tape Reading -- Two FORTRAN subroutines and brief documentation for reading the "TOLT" tapes have been obtained from the AFFTC and used to create a program (TOLTPR) which has not yet been exercised.

- MPDB Tape Reading Program -- The program developed by the AFFTC to read the JSC MPDB tapes has been delivered to DFRF with the MPDB data tapes but has not yet been exercised.

- LKF Air Data Tapes -- A FORTRAN 77 program to read the LKF air data tapes is listed in Ref. 28 but has not yet been exercised.

2. OFQ Archive Files

The first part of the Fig. 36 process is the creation of master archive files on the DFRF primary (CYBER or ELXSI) computer from the various Shuttle flight data tapes. The primary purpose of these archive files is to collect the OFQ-relevant time history data for each Shuttle landing into readily accessible files with a single time reference and sample rate and correction for time skews. Combining extensive data from the several data sets with various time references and sample rates can be done using the "SYNC" program (Fig. 37) developed at DFRF,

Ref. 29. This program has been exercised from STI in simple tests on the DFRF CYBER. However, because the SYNC program is somewhat complex, it has proven easiest so far to transfer individual file subsets to STI and combine them with simpler special purpose programs.

Experience to date has confirmed the importance of maintaining flexibility in organizing and using the data processing system. Much of this is provided through the CYBER Tape Reservation System. However, some effort is required by novice users (especially at outside facilities) to access and use data tapes productively. Thus one of the appeals of the archive files is simplification of this data access process. However, the archive files may become extensive in time and a storage efficient alternative might be to archive the instructions for generating specific files in a file of descriptive text and job control code. The original data tapes could thus serve as the primary archive if desired.

Regardless of where an archive or working file resides in the system, what is to be contained in the file and the logical (as distinct from physical) data structure is of fundamental importance. Figure 38 shows a prototype logical data structure. It is important that the data handling software accept archive files with or without all six of the component blocks and that the files contain documentary (text) information as well as time history data. The first block in Fig. 38, the File-Wide Text Block, would contain descriptive text referring to the overall data set. This might begin with an identifier line and include particulars of the flight such as pilot comments, unusual events, or new FCS features. The File-Wide Constants Block would contain the information to define constants which apply to the file as a whole such as weight, moments of inertia, c.g. position, etc. Each constant entry might contain a number, a name, engineering units, and descriptive text. The third data block, the Variable Directory, would provide the basis for a directory display for the user selecting variables for a working file. The Variable-Specific Text Block is analogous to the first block, but contains descriptive material for each variable in the directory, e.g., notes on problems with specific sensors. The Variable-Specific

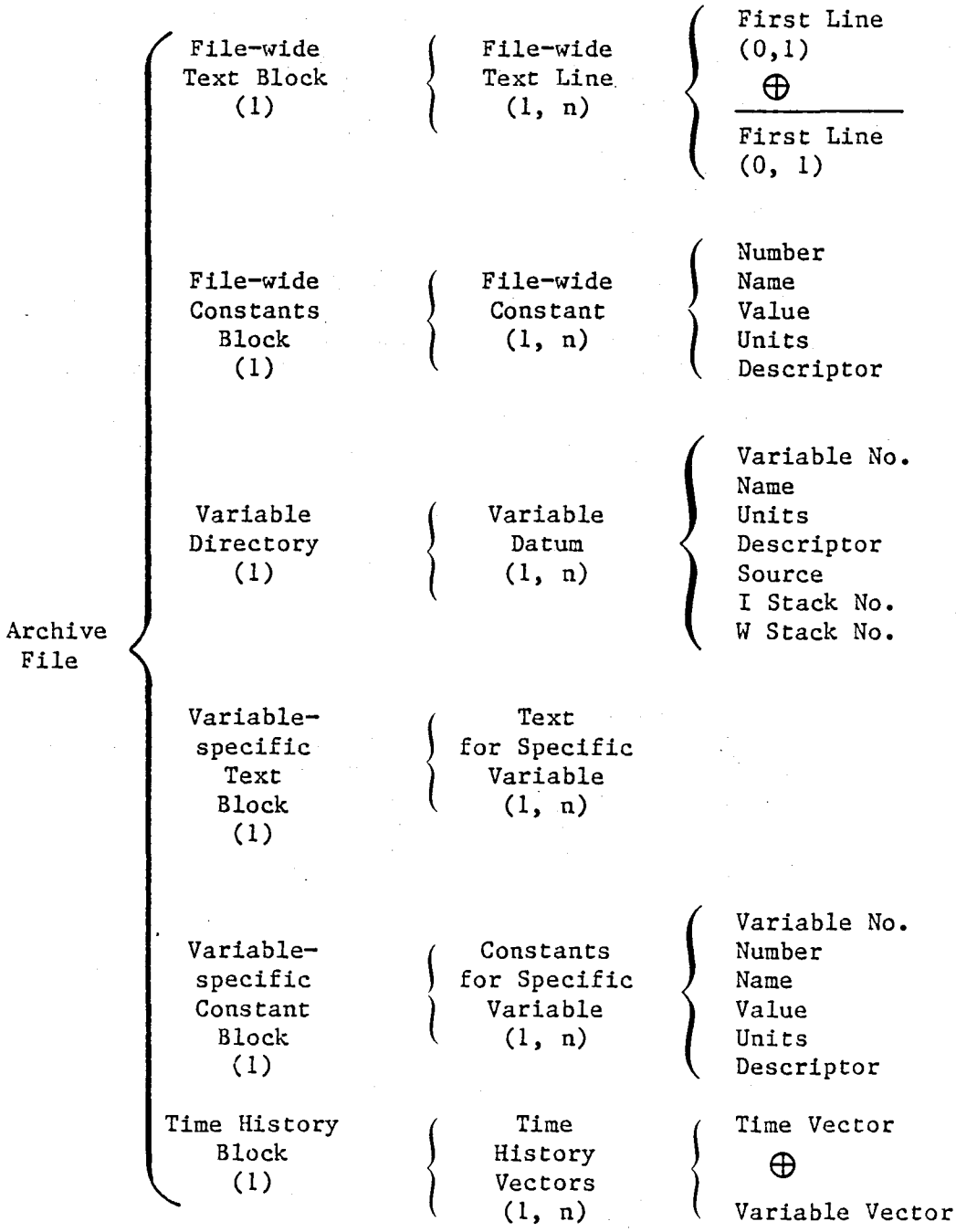

Figure 38. Logical Data Structure for the Archive Files

Constant Block contains parameters for each variable in the directory such as any necessary calibration factors.

The last block of data contains the actual time history records for the variables in the directory. This block would take the form of a matrix of time history vectors. The first vector would be a sequence of sample times at a constant sample rate. In simplest form the sample rate would be the highest needed for any variable (e.g., RHC) and all variable vectors would have elements corresponding to each time "slice." While this is the most straightforward and simplest form of data storage it may be too storage inefficient if the archive files become very large. In this event data compression may be necessary and the DEPR program developed at DFRF for the MMLE procedures would likely be useful.

At present separate archive files for each data source (and flight) reside on the STI PDP-11 computer for STS-2 through -7. Combination into a single archive for each flight has not been done pending further explanation of the SYNC program.

3. Interactive Interface

The complexities and qualitative elements of the OFQ work puts considerable emphasis on flexible and eclectic analyses which evolve as a specific line of investigation is followed. Since, as noted previously, the various steps in a particular analysis cannot be planned very far in advance, a highly interactive working environment is desired. A related feature of particular importance is the capability to use the system from locations remote from the primary DFRF computer. In the Fig. 36 structure these capabilities are provided largely by the Interactive Data Handler (IDH) software. Programs to perform the IDH function have been evolved in the previous phases of the OFQ work and have been used on both the STI and DFRF computers. The present programs are written in FORTRAN, used in a batch mode (making them more "DH" than IDH) and accommodate time history data only. In extracting a working file from the archive, defining the start and stop times requires some trial and error searching. There are a number of features desired to achieve IDH capabilities which are summarized in Table 8.

TABLE 8. DESIRED FEATURES OF THE INTERACTIVE DATA HANDLER (IDH)

- Interactive operation
- User-specified internal (I) file as subset of archive (A) file
- User-specified working (W) file as subset of internal file for specific jobs
- Specified A, I, and W files are resident until changed by user
- Directories of A, I, and W files
- Display text, constant, and time history data
- Variables specified by name (instead location in a vector)
- Search for user-specified values of any variable and time of occurrence
- Perform arbitrary transformations on variable vectors and constants
- "Calculator mode" for vector variables (to minimize "nuisance" programming)
- Interface with data presentation graphics

Achieving true interactive capability on the primary DFRF computer requires interactive (rather than batch) FORTRAN operation. Tests of the FORTRAN interactive compiler on the CYBER were made in Phase IV but this was found somewhat difficult to work with -- at least remotely from STI. Recent contacts with DFRF personnel have indicated that the ELXSI computer now coming on-line should make interactive operation much more practical.

Creation of an IDH with most of the features indicated in Table 8 would represent a very significant software development project. An attractive alternative for part of the effort which has been investigated at an initial level is the use of "integrated" spread sheet programs (such as "LOTUS 123" and "Symphony" from Lotus Development Corp.). Preliminary investigation indicates that such software would perform much of the Table 8 functions in a very efficient "user-friendly" way.

As indicated in Fig. 36, archive data can be communicated between the CYBER and remote computers including facilities outside of DFRF such as STI. Data transfer to date has been made using telephone machines and communications software ("DRY 12") on the STI PDP-11. Many commercially available data transmission packages are available and are under consideration for improvement in speed and error checking capability. Archive files at a working level (personal computers/work stations) could be maintained on floppy disks which would make data transfer by mail convenient.

SECTION V

CONCLUSIONS AND RECOMMENDATIONS

A. CONCLUSIONS

The non-intrusive analytical techniques for the OFQ continue to provide insights and deeper understanding of the critical flying qualities/flight control problem for the Shuttle -- the landing. Specific conclusions from a sample of six landings (STS-2 through -7) analyzed in the Phase IV study are:

- Distinct variations in piloting strategy and technique appear in the early Orbiter landings. The landing hodographs have been very useful in distinguishing similarities and differences.

  -- Preflare, shallow glide and final flare regions can generally be identified.

  -- The associated path variable (shallow glideslope) and "control" variables (flare altitude and final flare time constant) show considerable variation among the six landings.

  -- Yet the touchdown parameters (particularly touchdown sink rate and speed) show notable consistency with respect to estimated allowable variations.

  This demonstrates that a range of piloting techniques can produce successful Shuttle landings.

- Shallow glideslope values closer to the nominal (1.5 deg) value were achieved on the later flights (STS-5, -6, -7). This appears to be due to the improved landing aids (ball-bar indicator, HUD, and third crew member) available in these flights.

- With the exception of the anomolous STS-3 landing, touchdown sink rate (Fig. 33a) is notably low (0.86 fps mean) and consistent among the landings (0.38 fps standard deviation) particularly in comparison to the nominal design range (1.5 - 2.5 fps) for the autoland system. The (absolute) sensitivity of touchdown sink rate to

flare time constant (Fig. A-14a) is also much more constant among the six landings than other sensitivity measures.

- To achieve this consistent touchdown sink rate within speed and distance constraints, the crews used an apparent range of flare time constant from 1.26 to 4.60 sec. Basic vehicle dynamic considerations imply that the Shuttle path-to-attitude lag time constant (T_{θ_2} = 2.0 sec) should form an approximate lower bound on flare time constant. This appears to be consistent with the T_f values extracted from the flight hodographs. The first three landings were at the T_{θ_2} limit, the next two somewhat higher and STS-7 distinctly higher.

- Values of T_f close to T_{θ_2} may result from precognitive (open-loop) control built around the vehicle dynamic limitation, whereas higher values of T_f imply a closed-loop flare. Examination of both RHC activity and T_f level indicate:

  -- STS-5 and -6 appear to be largely precognitive flares

  -- STS-4 and -7 appear to be closed-loop flares

  -- STS-3 is an anomolous case with closed-loop control

  -- STS-2 is uncertain because of lack of RHC data

  These distinctions between precognitive and closed-loop control represent essential differences in piloting techniques.

- For manual closed-loop control, the flare time constant T_f is established by the ratio of the pilot's effective sink rate and altitude gains. This suggests that different sink rate gain values were used by the pilots to exercise significant closed-loop control of the final flare. This in turn emphasizes the importance of good altitude and sink rate cues near the runway.

- The autoland system is designed with a constant flare time constant (5 sec) which may be inconsistent with the apparent willingness of the crews to vary flare time constant to achieve consistently low touchdown sink rate.

- Effective vehicle dynamics, in terms of pitch rate/RHC frequency responses, from spectral analysis of data from two additional landings compare closely to that obtained previously for STS-4 in Phase III.

B. RECOMMENDATIONS FOR FURTHER RESEARCH

The non-intrusive analytical approach should be applied to later Orbiter flights to extend the data base and develop deeper understanding of how the task constraints, pilot strategies and flight mechanics impact the Orbiter flying qualities and flight control system requirements. Specific possibilities for further work include:

- Further work in refining the flight data, especially altitude and sink rate estimates, should be considered to clarify some remaining uncertainties. Complementary filtering and other estimation techniques should be considered for combining the cinetheodolite, takeoff and landing tower, and MMLE data into best estimates. The addition of ground based radar should be considered.

- Further efforts should be made to define the constraints on the landing task more precisely. Inputs from the Shuttle crews and operational groups would be valuable.

- Refinements to the procedure for fitting the glide and flare strategy model to the flight hodographs should be pursued. The next step might be to apply a low pass (digital) filter to the signals before generating the hodograph. The filter breakpoint should be below $T\theta_2$ and the pilot vehicle closed-loop attitude mode.

- A simple digital simulation model of the Orbiter in landing (which will accept flight RHC data) should be assembled. Provision for pilot models should be included for use in testing identification procedures.

- Further application of NIPIP for pilot model identification should be considered taking into account recent improvements in flight data and new strategy insights. A minimal effort could be to attempt to define the periods of open vs. closed-loop pilot activity in landings.

- Further efforts should be made to improve speed and efficiency in data handling by implementing the Interactive Data Handler functions. Use of commercially available "integrated spreadsheet/ data base manager" software for this purpose should be explored.

REFERENCES

1. Myers, Thomas T., Donald E. Johnston, and Duane McRuer, Space Shuttle Flying Qualities and Flight Control System Assessment Study," NASA CR-170391, June 1982.

2. Myers, T. T., D. E. Johnston, and D. T. McRuer, Space Shuttle Flying Qualities and Flight Control System Assessment Study - Phase II," NASA CR-170406, Dec. 1983.

3. Myers, T. T., D. E. Johnston, and D. T. McRuer, Space Shuttle Flying Qualities Criteria Assessment, Phase III, NASA CR-170407, Feb. 1984.

4. Bendot, J. S., and A. G. Piersol, Engineering Applications of Correlation and Spectral Analysis, John Wiley & Sons, N. Y., 1980.

5. Hobbs, R. L., Trajectory Analysis Report for the Space Shuttle OFT, Kentron International, Inc., K4E-103B-81, Feb. 18, 1981.

6. Covault, C., "Shuttle Crew Finds Performance Corp.," Aviation Week and Space Technology, Dec. 14, 1981.

7. Anon., "Flight Test Data Gained On Re-entry of Columbia," Aviation Week and Space Technology, Apr. 5, 1982.

8. Covault, C., "Third Shuttle Mission Being Assessed," Aviation Week and Space Technology, Apr. 26, 1982.

9. Horton, T., "STS-3 Subsystems Debriefing," Unpulished Notes, DFRF, Apr. 8, 1982.

10. Covault, C., "Shuttle Re-entry Tests Vehicle Cross Range," Aviation Week and Space Technology, July 12, 1982.

11. Scott, W. B., "Shuttle Lands on Hard Surface Runway," Aviation Week and Space Technology, July 12, 1982.

12. Horton, T., "STS-4 Systems Debriefing," Unpublished Notes, DFRF, July 15, 1982.

13. Mattingly, Capt. T. K., and Col. H. W. Hartsfield, Jr., Space Shuttle Progress Report, "Society of Experimental Test Pilots Report to the Aerospace Profession," 26th Symposium, Sept. 1982.

14. Covault, C., "Liftoff Time Pivotal to Shuttle Events," Aviation Week and Space Technology, Nov. 1, 1982.

15. Anon., "Columbia Re-entry Tests Low-Mach Characteristics," Aviation Week and Space Technology, Nov. 22, 1982.

15. Covault, C., "Shuttle Landing Shift Shows Flexibility," Aviation Week and Space Technology, July 4, 1983.

16. Looney, B. J., "Post-DETAC HUD Monitor Description," Sperry Autoland Memo 57, Nov. 4, 1980.

17. Brand, V. D., "Space Shuttle Development Update, Society of Experimental Test Pilots Report to the Aerospace Profession," 28th Symposium, Sept. 1984.

18. Myers, T. T., D. T. McRuer, and D. E. Johnston, Flying Qualities and Control System Characteristics for Superaugmented Aircraft, Systems Technology, Inc., TR-1202-1, June 1984.

19. Teper, Gary L., Richard J. DiMarco, Irving, L. Ashkenas, et al., Analyses of Shuttle Orbiter Approach and Landing Conditions, NASA CR-163108, June 1981.

20. McRuer, D. T., D. E. Johnston, and T. T. Myers, "A Perspective on Superaugmented Flight Control Advantages and Problems," AGARD Symposium on Active Control Systems - Review Evaluation and Projection, Toronto, Canada, 15-18 Oct. 1984.

21. Powers, B. G., "Active Control Technology Experience with the Space Shuttle in the Landing Regime," AGARD Symposium on Active Control Systems, Toronto, Canada, 15-18 Oct. 1984.

22. Anon., "Final Analysis Output Program (FALOUT)," Kentron International, Inc., Memo No. K4E-007B-81, 10 Dec. 1980.

23. Whitmore, S. A., "Reconstruction of the Shuttle Reentry Air Data Parameters Using a Linearized Kalman Filter," AIAA-83-2097, Aug. 1983.

24. Maine, Richard E., User's Manual for Sync, a Fortran Program for Merging and Time-Synchronizing Data, NASA TM-81355, Mar. 1981.

25. Preliminary Analysis of STS-4 Entry Flight Data, NASA TM-81375, Sept. 1982.

APPENDIX

PILOT LANDING STRATEGY: MODELING, IDENTIFICATION AND ANALYSIS

This appendix presents models, methods, and potential applications for pilot landing strategy analysis. The importance and emphasis on the landing task has been noted previously, and here consideration of this task provides a concrete example of some prototype analytical tools which may ultimately be useful for more general tasks. The emphasis here is on developing theoretical connections between the requirements of a specified task and the (implied) requirements for flying qualities and flight control system design. Such relations would be generally useful in considering the tradeoffs between vehicle design and task requirements, and would also be useful in designing simulation experiments to validate the designs. More specific applications will be noted below.

Making an analytical connection from task requirements to the flying qualities/flight control system requirements rests on quantitative definition of three elements.

- Vehicle: the aircraft can generally be quantified in precise detail. This is certainly true in the case of the Shuttle and, in addition, valuable simplifications are available from the superaugmentation model (Ref. A-1) which has been defined theoretically and confirmed from flight data analysis.

- Task: in principal the task can be defined in terms of inequality constraints on specific system variables. For the Shuttle landing task the most basic requirements will include constraints on touchdown sink rate, speed, and distance as noted previously. Realistic definition of the constraints is essential for strategy analysis, but is complicated by the fact that pilots apply weightings to physical constraints that are difficult to determine.

- Pilot: the pilot is the most difficult element to define, and the particular difficulties of the OFQ situation have led to an eclectic combination

of pilot identification methods (Refs. A-1 and A-2). For our purposes here, the identification process begins by distinguishing between the pilot's guidance strategy to accomplish the task and his inner closed-loop control activity.

Here the term "pilot strategy" is applied to the pilot's guidance activities, and the term "pilot behavior" will refer to inner-loop flight control activity performed to implement the strategy.

- Pilot strategy (guidance activity): generally refers to the pilot's plan for achieving an acceptable trajectory and energy management to meet performance constraints for the task. This is largely a precognitive plan developed from the pilot's experience and simulator training. Feedback structures associated with this activity are generally related to discrete switching from one task phase to the next. The control parameters associated with strategy are usually set in these discrete switching steps. Understanding the strategy involves separating what the pilot was attempting to do from the details of what actually happened in a particular flight. A search for landing strategy can be made in the long wavelength shape of the h, $\dot{h}$ hodograph, Fig. 32 which we expect to be roughly constant for a well trained pilot over an ensemble of flights.

- Pilot behavior (flight control activity): generally refers to the pilot's closed-loop control activity in response to internal commands derived from his strategy. The details of the behavior seen in response time histories and in the short wavelength activity in the hodographs, will vary greatly from flight-to-flight; although the spectral content of this activity can be expected to be roughly constant for a well trained pilot (see discussion in Section III-C). However, the pilot's control activity will tend to interfere with identification of strategy from the hodographs.

In this appendix, our interest is in extracting strategy from flight data, assessing the relative merits of different strategies, and developing deeper insights into how pilots evolve their strategies. The models and methods developed here are not viewed as well developed tools, but rather as prototypes which indicate what can be done with

appropriate digital flight data in a proper archive and the direction for further research. Before presenting the details of the proposed methodology, it is useful to consider the value and some possible applications of strategy models:

- Defining the theoretical range of feasible (physically possible) strategies for the Shuttle landing provides a context for the observed variations in the hodographs (Fig. 32), and provides a means of assessing the merits of the observed strategies. This will be considered in detail in Section 2.

- Understanding strategy is necessary to predict the pilot's loop structure and the internal commands to his inner control loops. These in turn are prerequisites to any rational pilot model identification, e.g., use of the "NIPIP" program as in Ref. A-2. The understanding of strategy can be gained from combining theoretical consideration of feasible strategies with observation of apparent strategies from actual flight data.

- A theoretical model of the relationship between the constraints of a specified task and the implied requirements for flying qualities and flight control systems would provide an adjunct to existing system assessment methods. Specifically for the Shuttle, the superaugmented FCS has been criticized, but a large number of successful operational landings have now been made. Quantitative strategy analysis may provide a more fundamental understanding of whether the FCS is or is not adequate for the <u>specific</u> Shuttle landing task.

- Strategy models would be useful in simulation experimental design to set up task constraints to create high stress scenarios. Conversely for any simulation experiment, the strategy model could be used to assess the robustness and generality of the simulation results.

- The ability to consider strategy from a quantitative model provides a means of considering system design tradeoffs for aircraft in development. For example, if the constraints on touchdown point must be tightened to operate on shorter runways, we would like to be able to address questions such as: what is the impact on pitch

bandwidth required? Would changes in the nominal shallow glide slope be useful, and what change should be made? How would this impact touchdown sink rate and speed control? Would the use of direct lift to alter the path-to-attitude time constant, T_{θ_2}, be warranted?

1. Landing Strategy Model

The landing strategy model presented here is viewed as a component of an overall pilot model for the Shuttle landing task. It has been evolved from earlier work (Refs. A-1 and A-2) and is based on an understanding of Shuttle operational procedures, landing aids, and Shuttle flight mechanics. It is useful to start with a review of the nominal Shuttle landing procedure.

a. Nominal Trajectory for Approach and Landing

Figure A-1a (from Ref. A-1) shows a representative trajectory for the Shuttle Orbiter approach and landing. Figure A-1b shows the corresponding nominal airspeed variation. The approach and landing phase begins with capture of the steep glide slope shortly after leveling the wings at the conclusion of the HAC turn -- nominally at 15,000 ft altitude and approximately 40,000 ft from the runway threshold. At an altitude of approximately 1750 ft, a preflare pullup maneuver is initiated, which is terminated when the flight path angle approaches that for the shallow glide slope -- nominally -1.5 deg. Most of the variation in approach and landing piloting technique occurs in the shallow glide and flare which is the sub-phase of interest here. As indicated in Fig. A-1, termination of the preflare maneuver is followed by capture of the desired shallow glide slope for a constant γ glide to a final flare. In principal, either the shallow glide or the final flare sub-phase could be replaced by an extension of the other sub-phase.

b. Strategy Model

The strategy model is developed for the shallow glide and final flare and the basic equations are summarized in Fig. A-2.

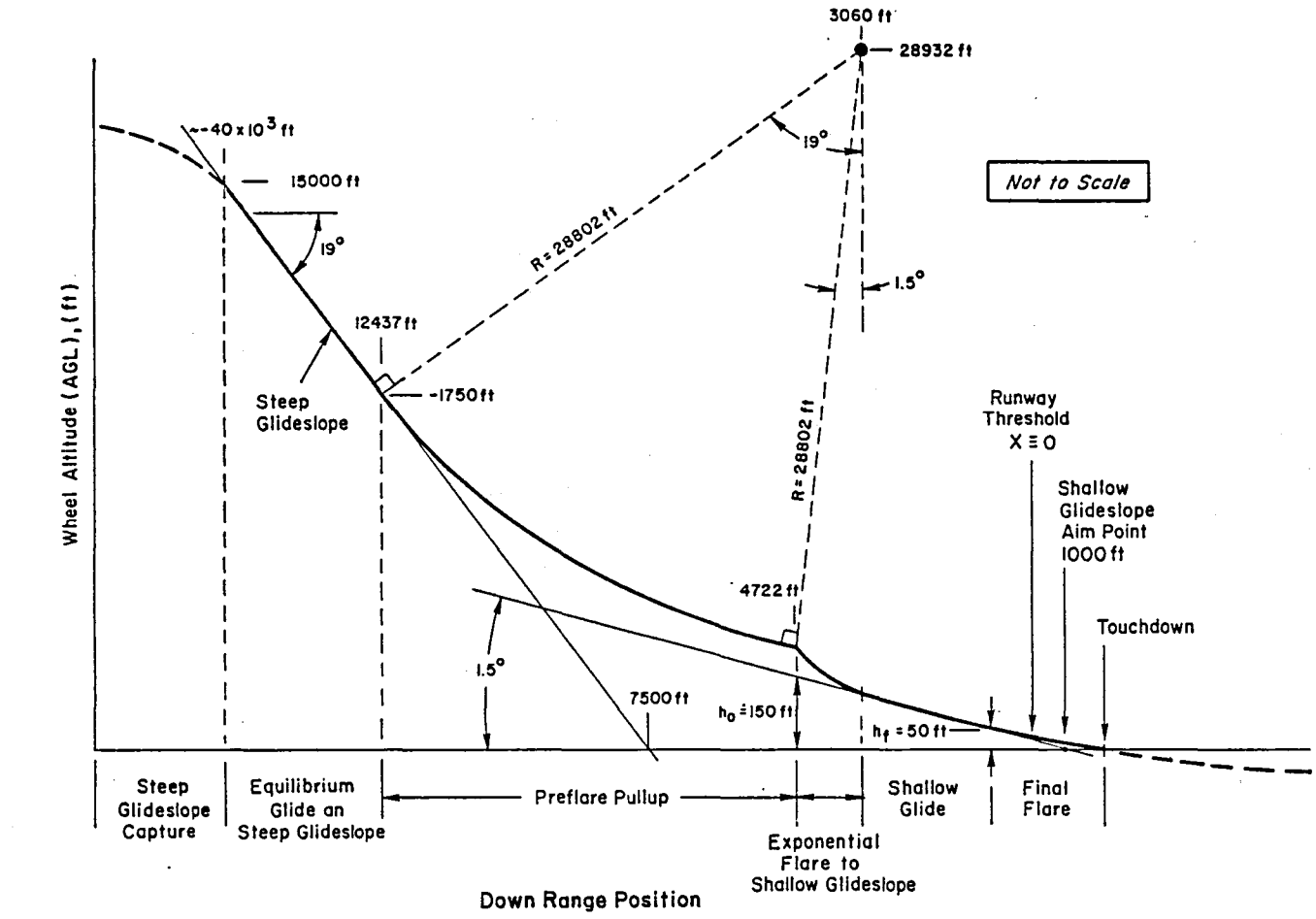

a) Trajectory

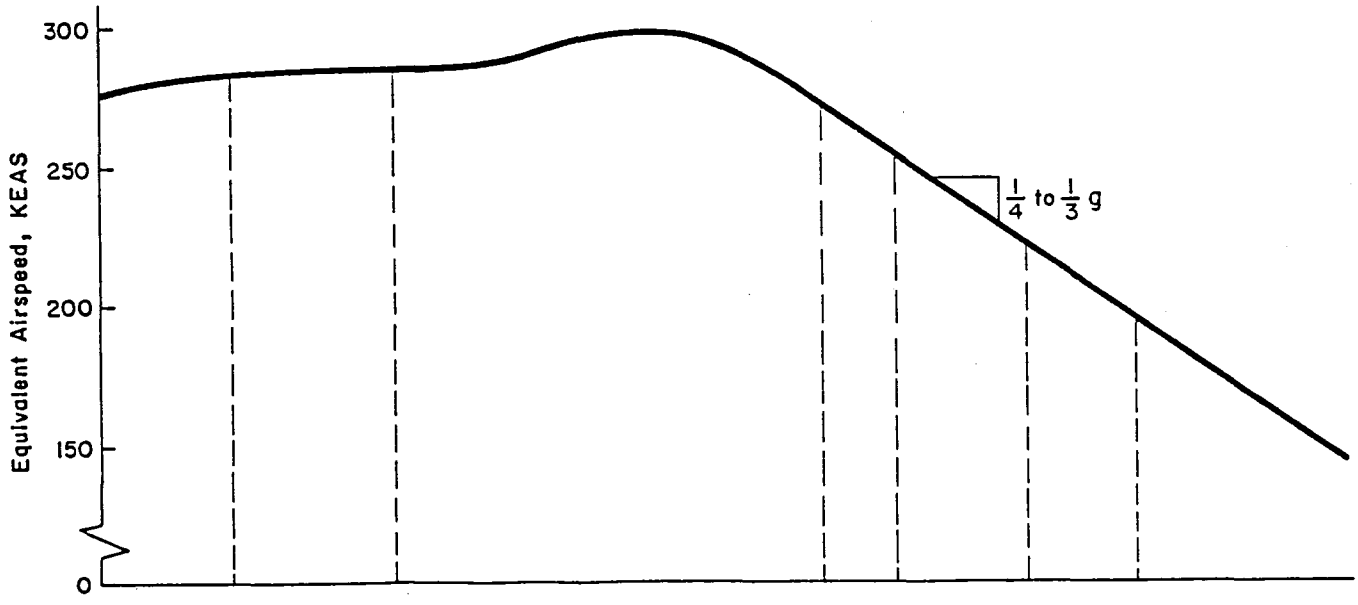

b) Equivalent Airspeed Variation

Figure A-1. Nominal Trajectory and Airspeed Variation for Shuttle Approach and Landing

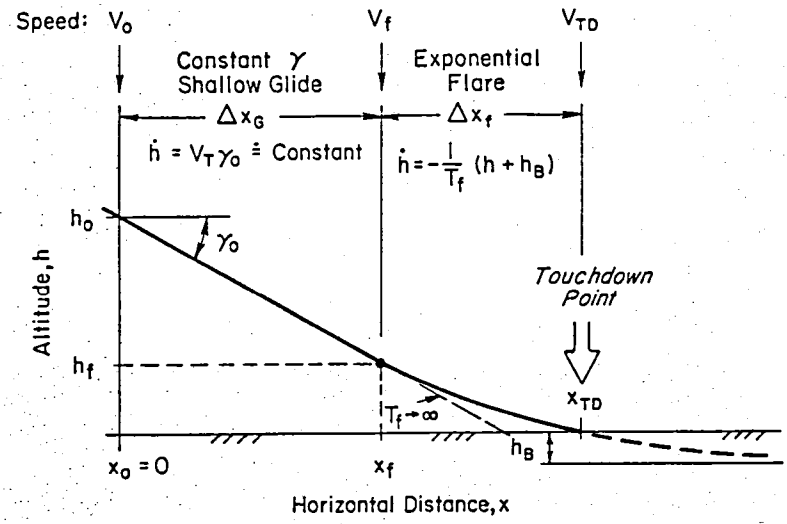

Speed at flare initiation

$$V_f = [2K_v^{\bullet}(h_o - h_f)/\gamma_o + V_o^2]^{1/2}$$

where: $K_v^{\bullet}$ = averaged (-dV/dt)

Depth of flare asymptote

$$h_B = -T_f V_f \gamma_o - h_f$$

Touchdown time measured from flare initiation

$$t'_{TD} = -T_f \ln(h_B/(h_f + h_B))$$

Touchdown speed

$$V_{TD} = V_f - K_v^{\bullet} t'_{TD}$$

Touchdown sink rate

$$\dot{h}_{TD} = \gamma_o V_f + h_f/T_f$$

Distance traveled in glide

$$X_g = (h_o - h_f)/\tan \gamma_o$$

Distance traveled in flare

$$X_f = V_f t'_{TD} - \frac{K_v^{\bullet}}{2} t'^2_{TD}$$

Glide and flare distance

$$X_t = X_g + X_f$$

Figure A-2. Summary of Glide and Flare Landing Model Speed

Analytical treatment is complicated by the fact that the Shuttle decelerates in this region, but it was shown in Ref. A-1 that the deceleration is roughly constant ($\dot{V} \doteq 1/4$ to $1/3$ g) which allowed reasonable approximate analysis. The primary impact on strategy is the creation of a relatively short "touchdown time window" to satisfy touchdown speed constraints.

The strategy model goes beyond the relationships of Fig. A-2 in the way that the various variables are classified. Here the altitude and velocity at the end of preflare (h_o and V_o) are considered initial conditions which are given (observed values for the STS-2 through -7 analysis). However, these variables are to some extent under the control of the crew through execution of the preflare and in an extended model they would become strategy variables. The touchdown sink rate, ($-\dot{h}_{TD}$), the touchdown speed, (V_{TD}), and the distance traveled in the shallow glide and flare, (X_T), are considered "constrained variables" for which the pilot's strategy must satisfy the Table A-1 constraints (introduced in Section III and actually viewed here as part of the "task model"). The constraints of Table A-1 are somewhat simplistic and further work should be done to refine them; for instance, in the distinctions between inertial speed and airspeed. However, they are adequate for a first cut study of strategy analysis. Finally, there are three "strategy variables" that the pilot has at his disposal to accomplish the task: the shallow glide slope angle (γ_o), the flare height (h_f), and the flare time constant (T_f).

Given the above definitions, the landing strategy is idealized as the sequential decision making process in which the pilot first selects a shallow glide slope, then a flare height, and finally a flare time constant to produce an exponential flare to an asymptote h_B below the runway. However, the selection of the three strategy variables for a Shuttle landing is certainly a long process which evolves over the crew's simulator and STA training, and culminates in the actual landing. The selection of shallow glide slope by the crew is largely set by the nominal value (-1.5 deg) set up by the various landing aids. However, at least in the early flights with minimal aids, glide slope is probably

TABLE A-1. CONSTRAINTS ON TOUCHDOWN PARAMETERS

Design sink rate at TD: -1.5 fps $> \dot{h}_{TD} > -2.5$ fps

Maximum sink rate at TD: $\dot{h}_{TD} = -9$ fps

Maximum sink rate at TD, crosswind: $\dot{h}_{TD} = -6$ fps

Nominal $V_{TD} = 195$ kts (329 fps)

Maximum $V_{TD} = 225$ kts (380 fps)

Minimum $V_{TD} \equiv 0.9$ nominal V_{TD} (296 fps)

adjusted by the crew and is treated conceptually as a strategy variable in the model.

The glide and flare model summarized above has intentionally been maintained as simple as possible and involves only about a half dozen parameters. The computational problems associated with the model are not particularly difficult; however, even with such a simple model, interpretation of the implications and consideration of its validity is complex. The difficulty in interpretation stems in part from the inequality constraints (Table A-1), which must be examined in multi-dimensional parameter spaces (three dimensions here). It is not assumed here that the simple glide and flare model is adequate to explain all issues of pilot strategy and technique; however, the view is taken that the simplest model with some chance of explaining the basic phenomena should be the starting point. This model leads to working hypotheses and performance measures which should be thoroughly investigated before increasing the complexity of the model.

An initial simplification that will be made here is the reduction of the model to a single strategy variable -- flare time constant, T_f -- by

fixing glide slope, and flare height at the values extracted from flight data (see Section III). Some preliminary work on the three variable (γ_o, h_f, T_f) problem has been done, but will not be discussed here. The effect of the flare time constant may be examined from the curves of Fig. A-3 computed for the nominal conditions indicated in the figure. If the flare is very slow (very large T_f), there is essentially no flare and the trajectory is an extension of the glide. Thus the minimum flare distance is

$$(X_F)_{min} \doteq -h_f/\gamma_o \qquad \text{as } T_f \to \infty$$

As T_f is reduced for a faster flare, the trajectory approaches a level parallel to h_B feet below the runway. When T_f is reduced to:

$$T_f^* = -h_f/V_f\gamma_o$$

h_B goes to zero and the runway is approached asymptotically ($X_f \to \infty$). For still lower T_f values, the runway is never reached and a "ballooning" situation results. Touchdown speed remains fairly constant until $T_f \doteq T_f^*$ at which point the increasing flare time causes considerable speed bleedoff. Touchdown sink rate is strongly affected by the trajectory slope and thus decreases steadily as $T_f \to T_f^*$.

c. Model Verification

A basic validity check of the model can be made by comparing the model-derived variation of the constrained variables ($\dot{h}_{TD}$, V_{TD}, X_T) as a function of flare time constant to the observed values of these three variables obtained from the flight hodographs (see Section III). Comparisons are shown for touchdown sink rate, touchdown speed, and the glide and flare distance in Figs. A-4 through A-6, respectively. These comparisons show that the observed T_f as extracted from the hodograph is generally consistent with the T_f from the model at the corresponding value of the observed constrained variable at touchdown. In almost all cases, the observed T_f are displaced slightly from the model curves;

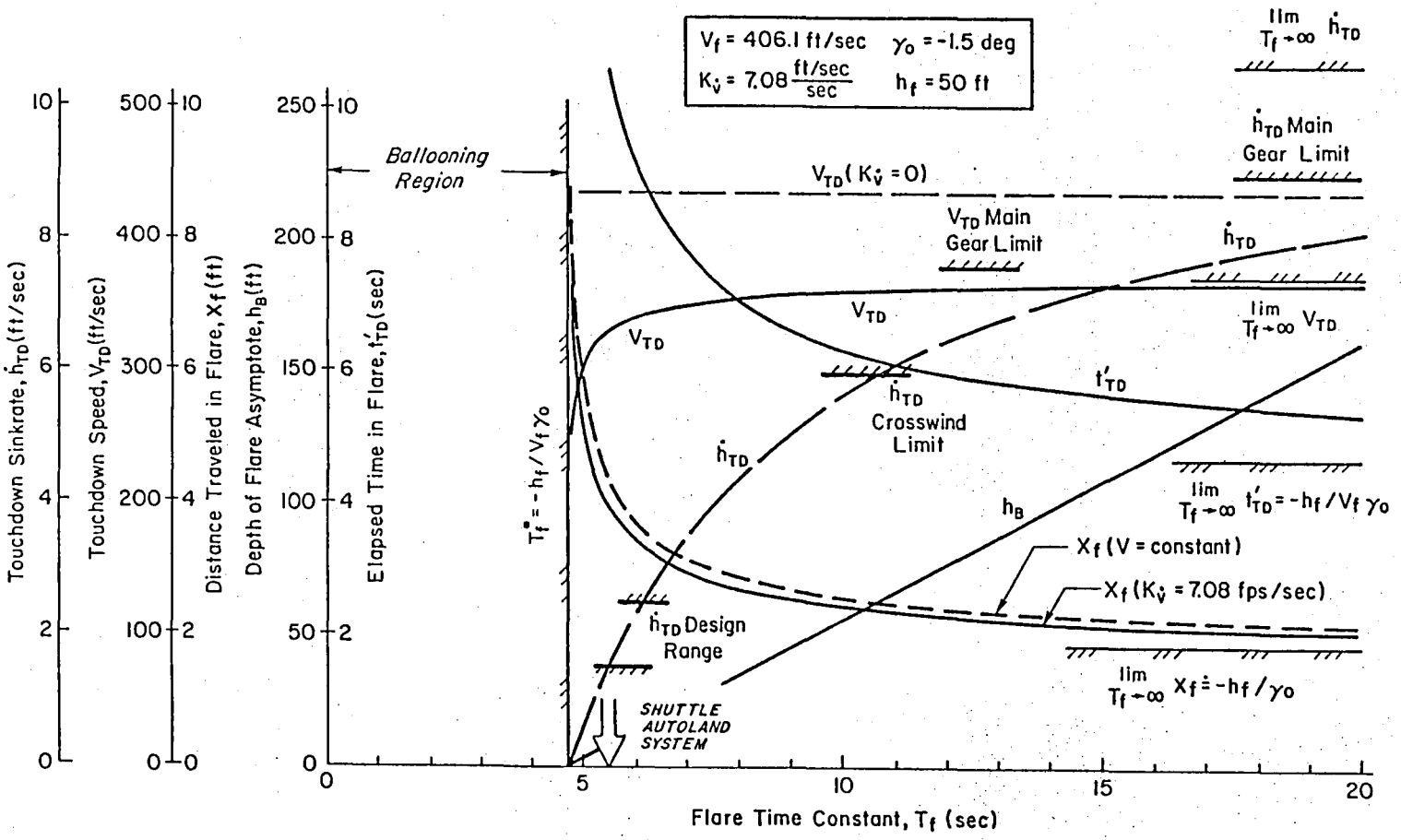

Figure A-3. Effect of Flare Time Constant on Touchdown

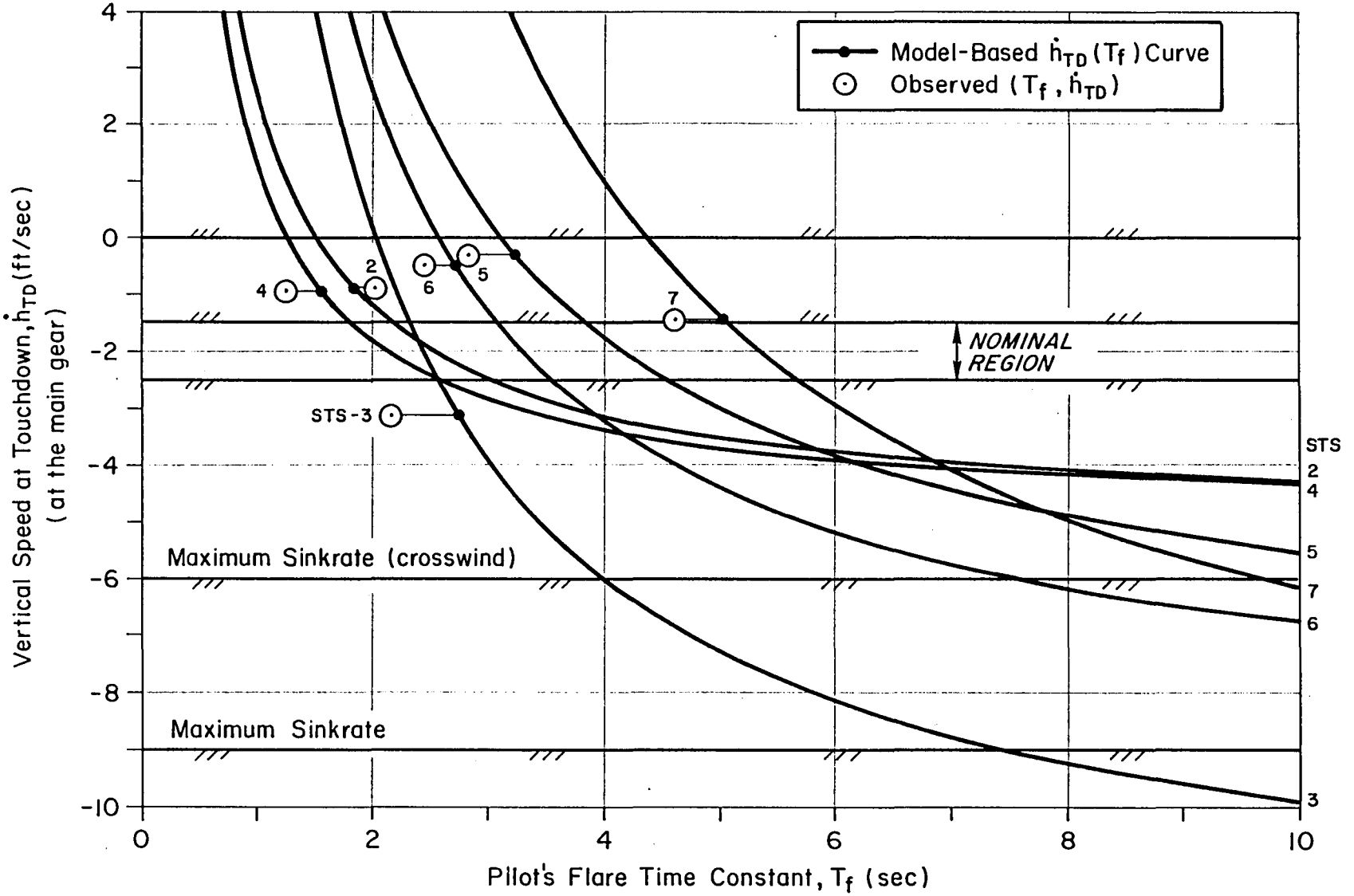

Figure A-4. Comparison of Model-Based $\dot{h}_{TD}$ (T_f) with Observed Values

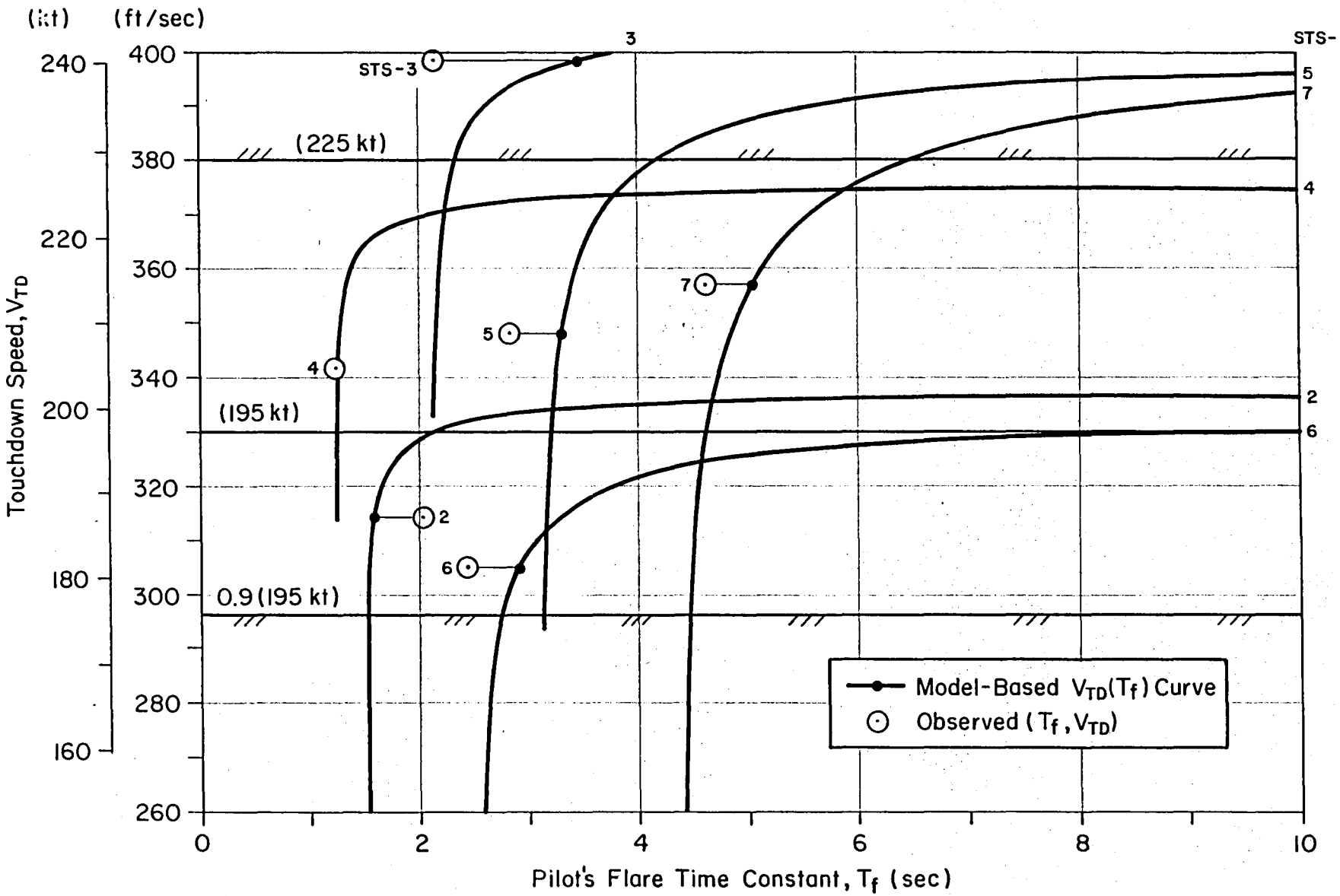

Figure A-5. Comparison of Model-Based V_{TD} (T_f) with Observed Values

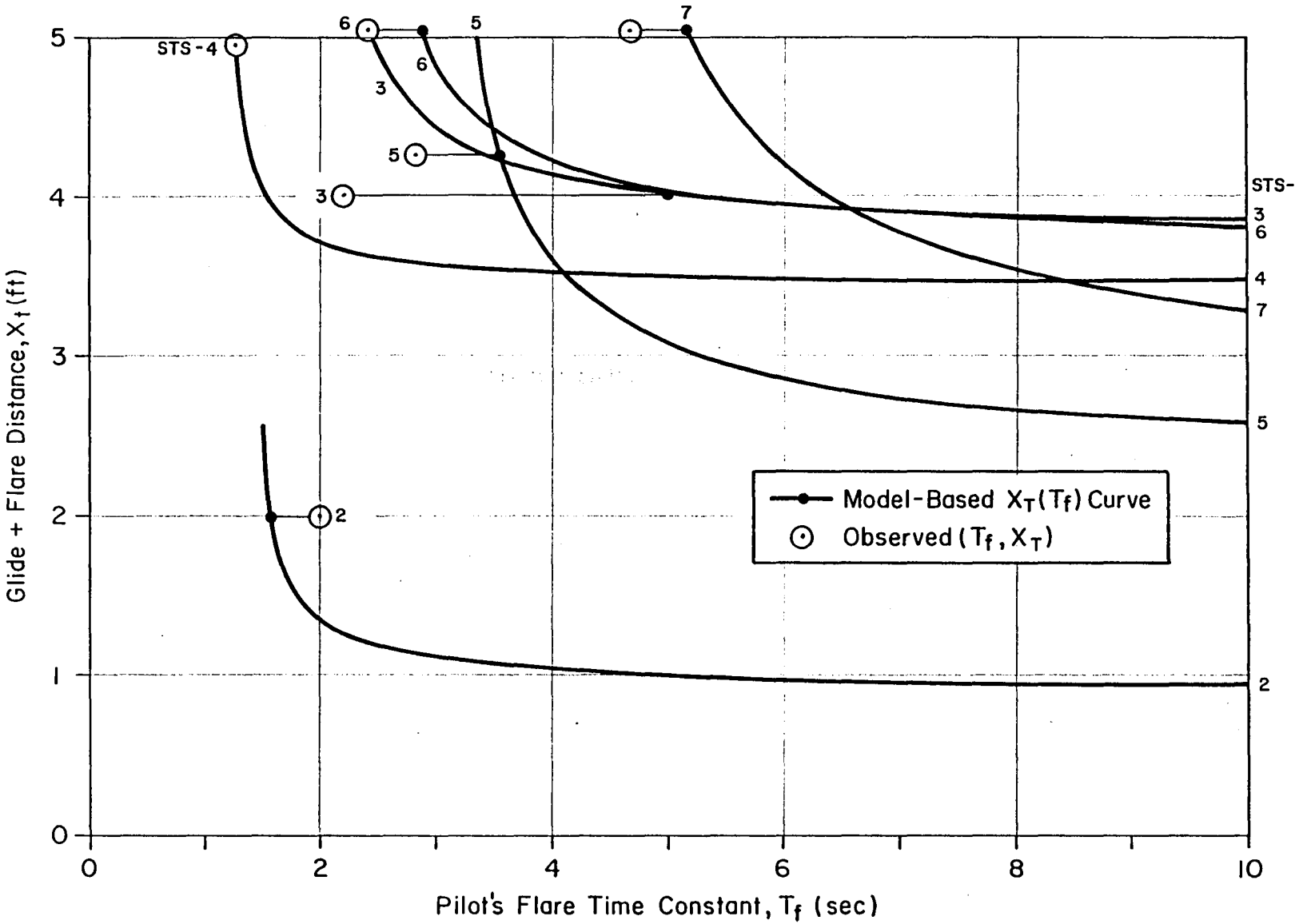

Figure A-6. Comparison of Model-Based X_t (T_f) with Observed Values

however, such displacements are to be expected given the inherent uncertainty in extracting T_f from the hodograph resulting from the short wavelength pilot activity.

Not surprisingly in Figs. A-4 through A-6, the most significant differences between model and observation occurs for the anomalous STS-3 case, which because of the oscillations seen in the hodograph, is distorted beyond the ideal glide and flare characteristics. The most compelling argument for model validity is that the difference between model and observed T_f for most landings is small compared to the range of observed T_f for the six landings examined.

No attempt has been made to "fit" the model to the flight data after the initial extraction of parameters (γ_o, h_f, etc.) as discussed in Section III. While all of the parameters defining the curves of Figs. A-4, A-5, and A-6 except T_f are extracted from flight data, it should be realized that this alone does not guarantee a good match as seen in the figures. Specifically, arbitrary models could be constructed using the same observed variable values that would not match well.

d. Asymptotes in the Constrained Variable - T_f Plane

The model based curves of touchdown sink rate, speed, and distance as a function of flare time constant shown in Figs. A-4 through A-6 each have two types of asymptotes. First, each curve has an asymptote that forms a lower bound on flare time constant which is the T_f^* noted above. Secondly, the sink rate and total distance curves have horizontal asymptotes for large T_f which form lower bounds and are denoted $\dot{h}_{TD}^*$ and X_t^*, respectively. There is a corresponding V_{TD}^* which forms an upper bound for the touchdown speed curves. Analytical expressions for these asymptotes are summarized in Table A-2. The asymptotes are of interest because they limit the achievable values of the touchdown parameters and the feasible values of T_f. Further, it may be seen from the formulas of Table A-2 and the curves of Figs. A-4 through A-6, that the asymptotes are strong functions of the initial conditions h_o and V_o, and the pilot's landing strategy as defined by γ_o and h_f.

TABLE A-2. ASYMPTOTES IN THE TOUCHDOWN VARIABLE - FLARE TIME CONSTANT PLANE

$$\dot{h}^*_{TD} = \lim_{T_f \to \infty} \dot{h}_{TD} = \gamma_o V_f$$

$$V^*_{TD} = \lim_{T_f \to \infty} V_{TD} = V_f + \frac{K_{\dot{V}} h_f}{V_f \gamma_o} < V_f$$

$$X^*_t = \lim_{T_f \to \infty} X_t = X_g - \frac{h_f}{\gamma_o} - \frac{K_{\dot{V}}}{2} \left(\frac{h_f}{V_f \gamma_o}\right)^2$$

$$T^*_f = \left(T_f \ @ \ \dot{h}_{TD} \equiv 0\right) = -h_f / V_f \gamma_o$$

There is an exception for the $\dot{h}_{TD}$ vs. T_f curves in that the vertical asymptote in this case is the $T_f = 0$ axis, and the T^*_f lower boundary is the value of T_f which makes $\dot{h}_{TD} = 0$. This can be seen by substituting $T^*_f = -h_f/V_f\gamma_o$ into the equation for the depth of the flare asymptotes in Fig. A-2. It may be seen that $T_f = T^*_f$ makes $h_B = 0$ so that the flare trajectory is asymptotic to the runway surface. Thus the aircraft touches down in infinite time and infinite distance at which point V_{TD} and $\dot{h}_{TD}$ have long since become zero. Thus T^*_f represents the transitional T_f value between touching down and not touching down.

The horizontal asymptotes indicate the touchdown situation for large flare time constants, that is when no final flare is performed and the Orbiter essentially continues on the shallow glide slope to the runway. The asymptotes lead to some useful characterizations of the curves in Figs. A-4 through A-6. It may be seen that except for small transitional regions (the "knees" of the curves), the curves rapidly approach

either the horizontal or vertical asymptotes. Thus each curve can be thought of as consisting of three regions: the vertical asymptote, an intermediate transition region, and the large T_f asymptote. The vertical and horizontal asymptotes represent regions of very high and very low sensitivity, respectively, of each touchdown variable to the flare time constant. That is, if the pilot chooses to operate in the region of the vertical asymptote, very small changes in flare time constant will produce very large changes in the touchdown parameter, i.e., high sensitivity. On the other hand, when operating in the region approximated by the horizontal asymptote, large changes in flare time constant have almost no affect on the touchdown parameter. This is of interest, since if the pilot can properly set the asymptotes as part of the landing strategy, satisfaction of one or more landing constraints could be guaranteed "automatically" (i.e., without flare). This will be considered further in the next section where it will be shown that Shuttle crews apparently do not use this strategy.

The observed values of the four asymptotes are summarized in the bar charts of Fig. A-7 for the six landings.

2. Model-Based Landing Strategy Analysis

a. Feasible T_f Ranges and Margins

The general approach to strategy analysis will involve defining the feasible ranges of the strategy variables for which the task constraints can be met. Here we consider the single strategy variable (T_f) case as discussed above. The constraints may be considered individually but ultimately they must be considered together because the pilot must find a single value of T_f that satisfies all constraints simultaneously. We can expect that good strategies would produce feasible T_f ranges which are sufficiently wide, such that extremely precise execution of the flare is not required. The widths of these feasible regions will be termed the "T_f margins." A good landing strategy must also allow the pilot to select a flare time constant which can be achieved in the given aircraft. As discussed in Section III for the Shuttle landing, this

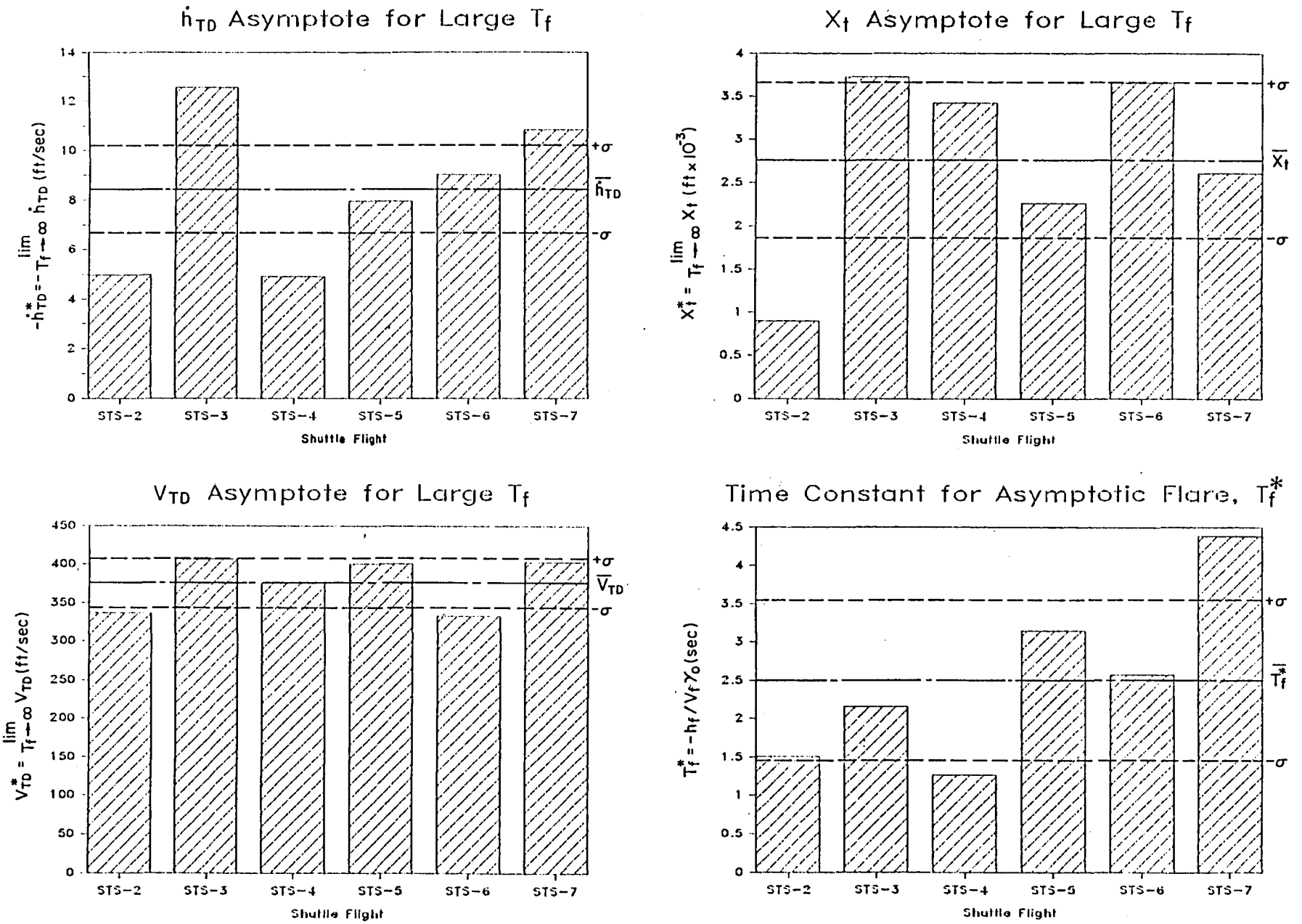

Figure A-7. Summary of Asymptote Values Extracted from Flight Data

implies a T_f greater than T_{θ_2}. Thus strategy analysis must also be concerned with the "T_{θ_2} margin," defined as the difference between a minimum feasible T_f and T_{θ_2}.

These ideas can be made more concrete by considering specific application to the Shuttle landing beginning with the sink rate margin.

(1) Feasible T_f Ranges and Margins for Touchdown Sink Rate

The touchdown sink rate constraints (Table A-1) can be used to partition the flare time constant scale into four feasible ranges or "bands" (shaded and labeled (A), (B), (C), and (D)) as indicated in Fig. A-8. The (B) band (solid band in Fig. A-8) defined by the nominal $\dot{h}_{TD}$ range is the "nominal band."

For the case shown in Fig. A-8 (STS-6), the T_f margin for the nominal band is a little less than 1/2 sec and the T_{θ_2} margin is a little over 1 sec. Band (D) would not be feasible in a crosswind, but otherwise extends to $T_f = \infty$ since the $\dot{h}^*_{TD}$ as asymptote happens to be -9 fps for STS-6.

The feasible bands corresponding to Fig. A-8 for all six landings are compared in Fig. A-9. Comparison of the six landings shows that the overall feasible regions are generally large (robust), and specifically are infinite for STS-2, -4, -6, and -7 (but not for crosswinds in STS-6 and -7). Again these infinite margins result from the position of the large T_f asymptotes ($\dot{h}^*_{TD}$) with respect to the sink rate limits (this can be seen more easily by re-examining Fig. A-4). The exception is STS-3 which has the tightest overall T_f margin and would have been the most critical for a crosswind landing. The nominal T_f margins are generally on the order of 1 sec, but again tightest for STS-3. Thus from the standpoint of requiring the most precise execution of the flare, the STS-3 strategy is indicated as the worst of the six.

The T_{θ_2} margins for the lowest (A) band and the nominal band are small or negative for the first three flights, but larger and consistently positive for the STS-5, -6, and -7 landings. This apparent improvement in strategy for the later landings is presumably a result of improved landing aids.

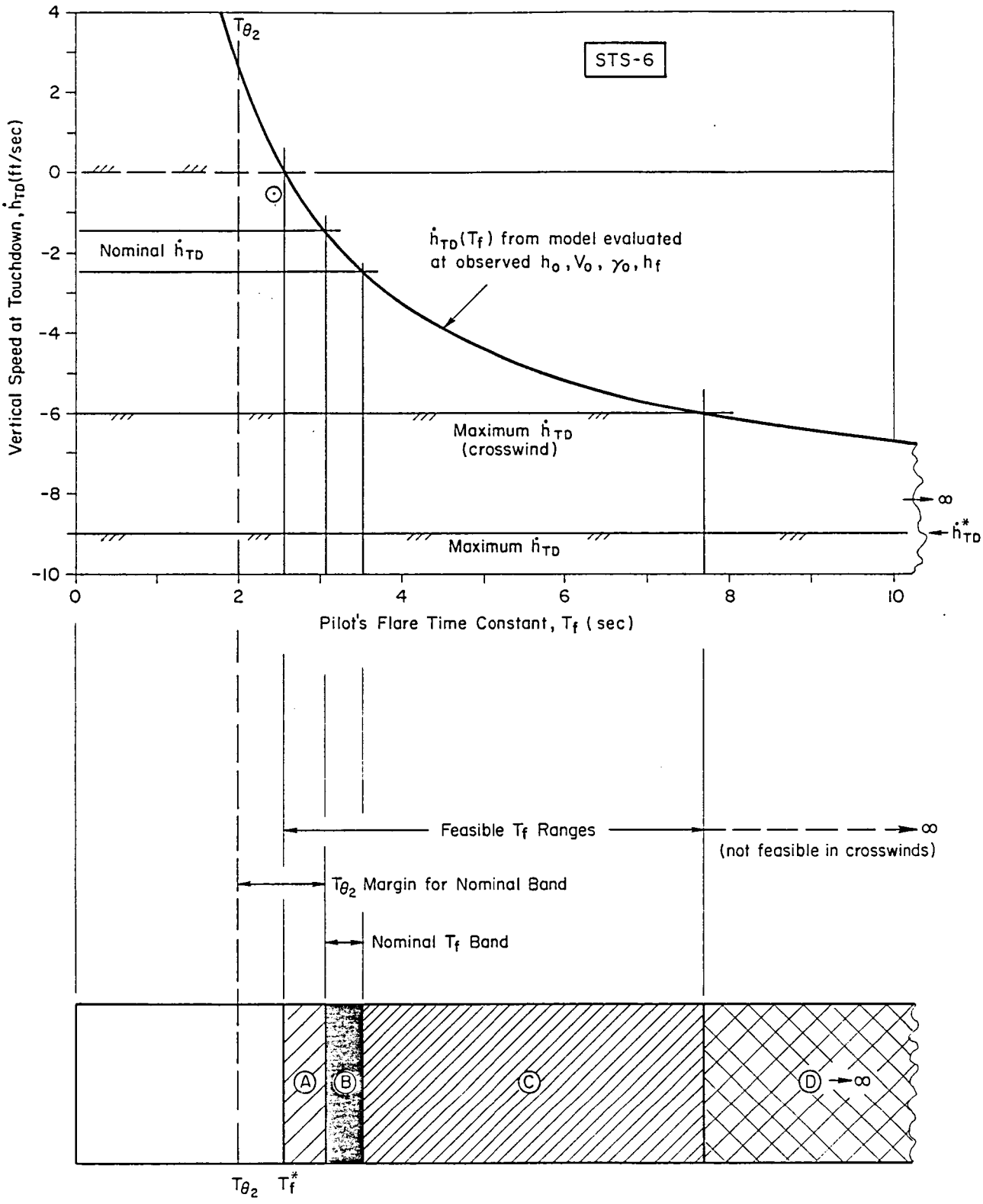

Figure A-8. Definition of the Feasible T_f Ranges and Margins

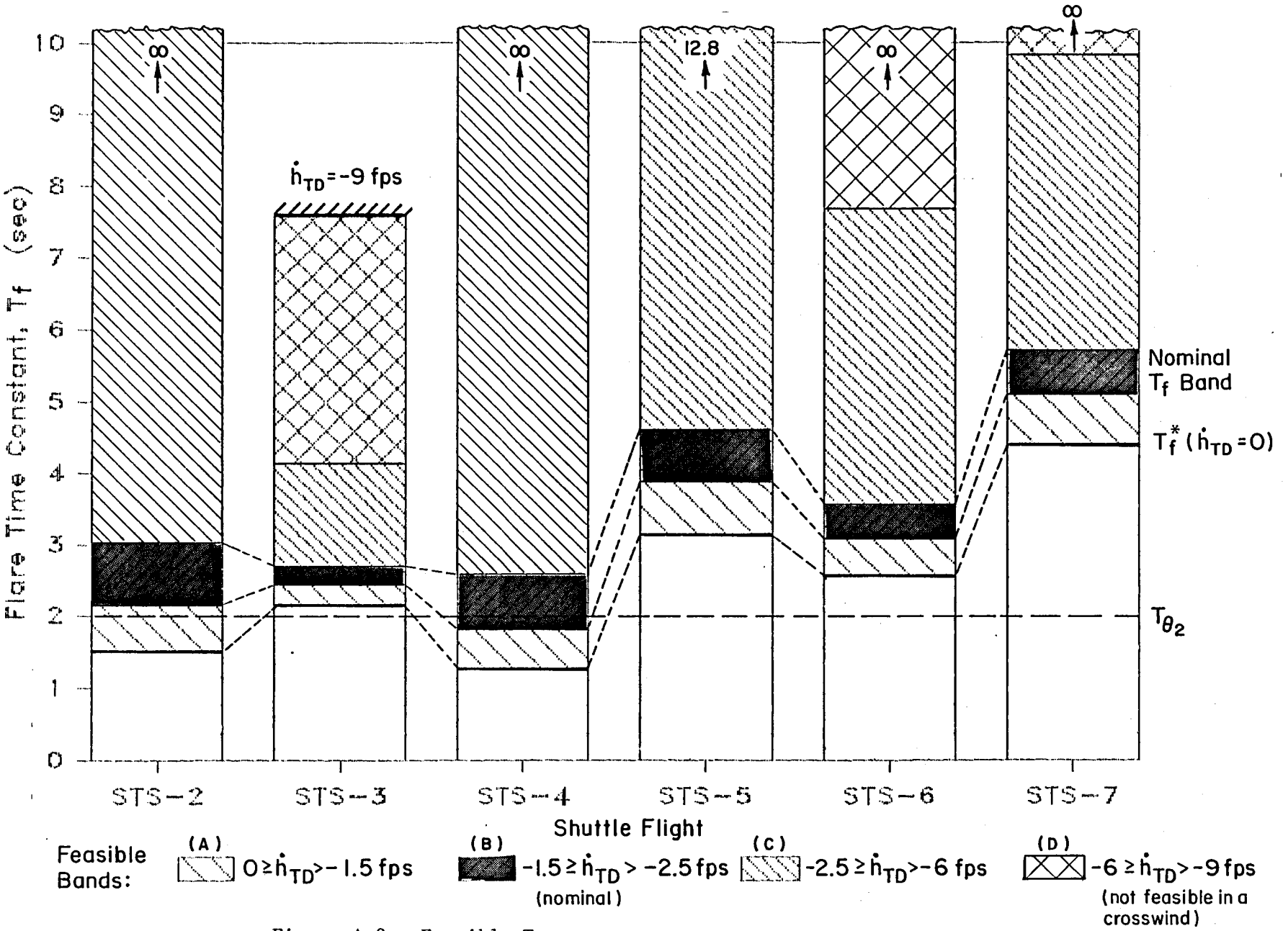

Figure A-9. Feasible T_f Ranges for Touchdown Sink Rate

(2) Feasible T_f Ranges and Margins for Touchdown Speed

The feasible ranges and margins can be defined for touchdown speed analogously to those for sink rate -- except that there are only two bands since there is no crosswind dependence and the nominal band is a single speed (195 kts). The six landings are compared in Fig. A-10. It may be seen that the T_f margins are quite small for three landings (STS-3, -5, and -7 with STS-3 clearly the tightest) and infinite for the other three. As for the sink rate margins, the T_{θ_2} margins are larger (better) for the last three flights. For STS-2 and -4, the infinite T_f margins would presumably offset the tight T_{θ_2} margin. However, the analysis does indicate that the STS-3 strategy is exceptionally poor with respect to speed control.

(3) Feasible T_f Ranges and Margins for Touchdown Distance

The touchdown distance constraints cannot be treated as precisely as those for sink rate and speed because the flight (cinetheodolite) distance data have not yet been referenced to the runway threshold where appropriate. Further, for early landings (certainly those on the EAFB lakebed), touchdown point was not considered critical by the crews. Thus for a first cut analysis, relative constraints have been defined by considering ±20% increments on the observed distance. Thus T_f margins can be viewed in terms of the potential for touchdown point adjustments in flare.

The six landings are compared on this basis in Fig. A-11. Interestingly, the STS-3 strategy is indicated as being clearly the best both in terms of overall T_f margin (the only infinite margin) and with respect to the nominal T_{θ_2} margin. By the same criteria the STS-2 and -4 situations appear to be the worst with improved situations in the last three landings.

It is of course difficult to obtain any indication from the Shuttle crews as to whether these margins are perceived as part of their landing strategies and techniques; however, one piece of indirect pilot commentary (from Ref. A-3) is worth noting with respect to the STS-4 distance margin.

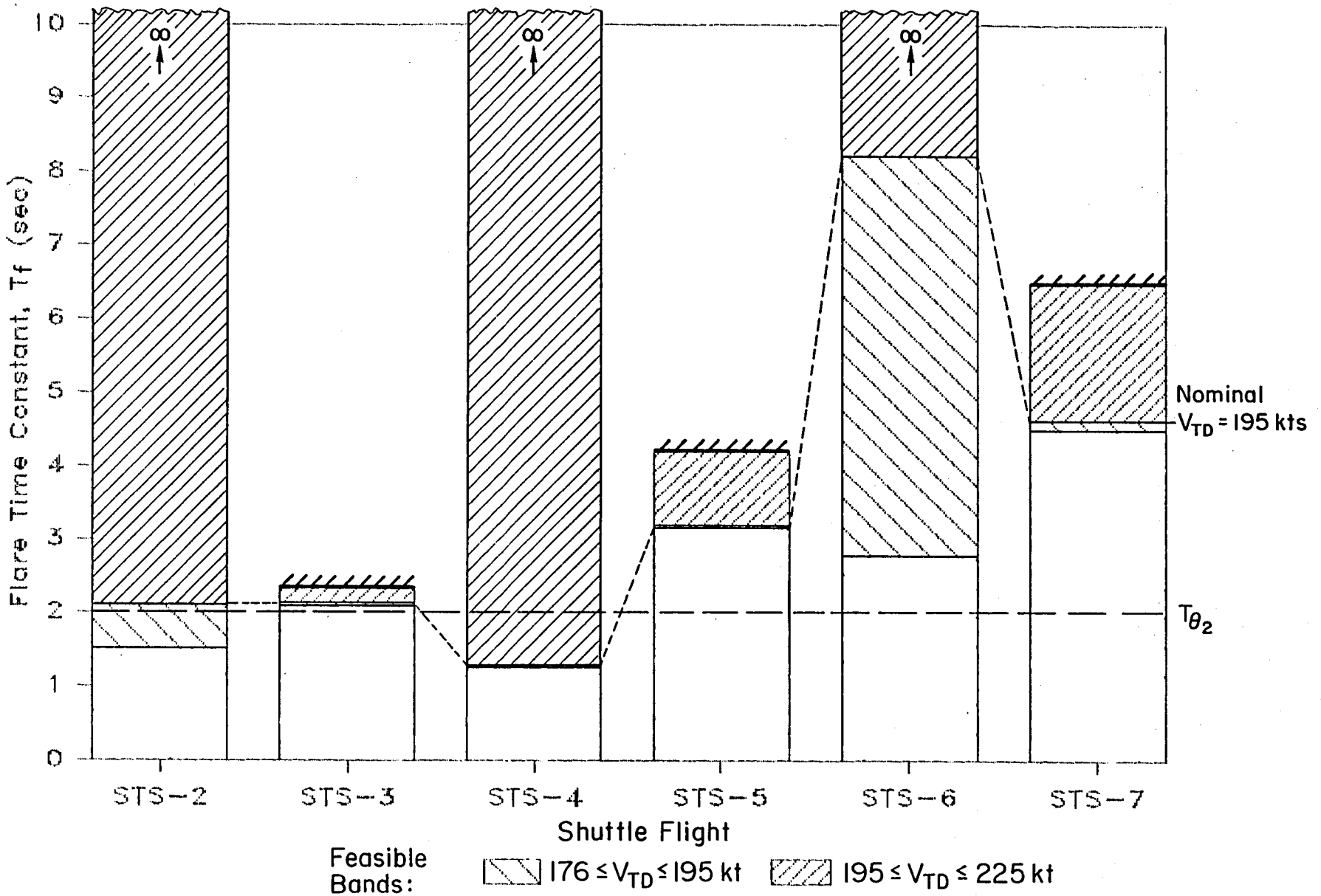

Figure A-10. Feasible T_f Ranges for Touchdown Speed

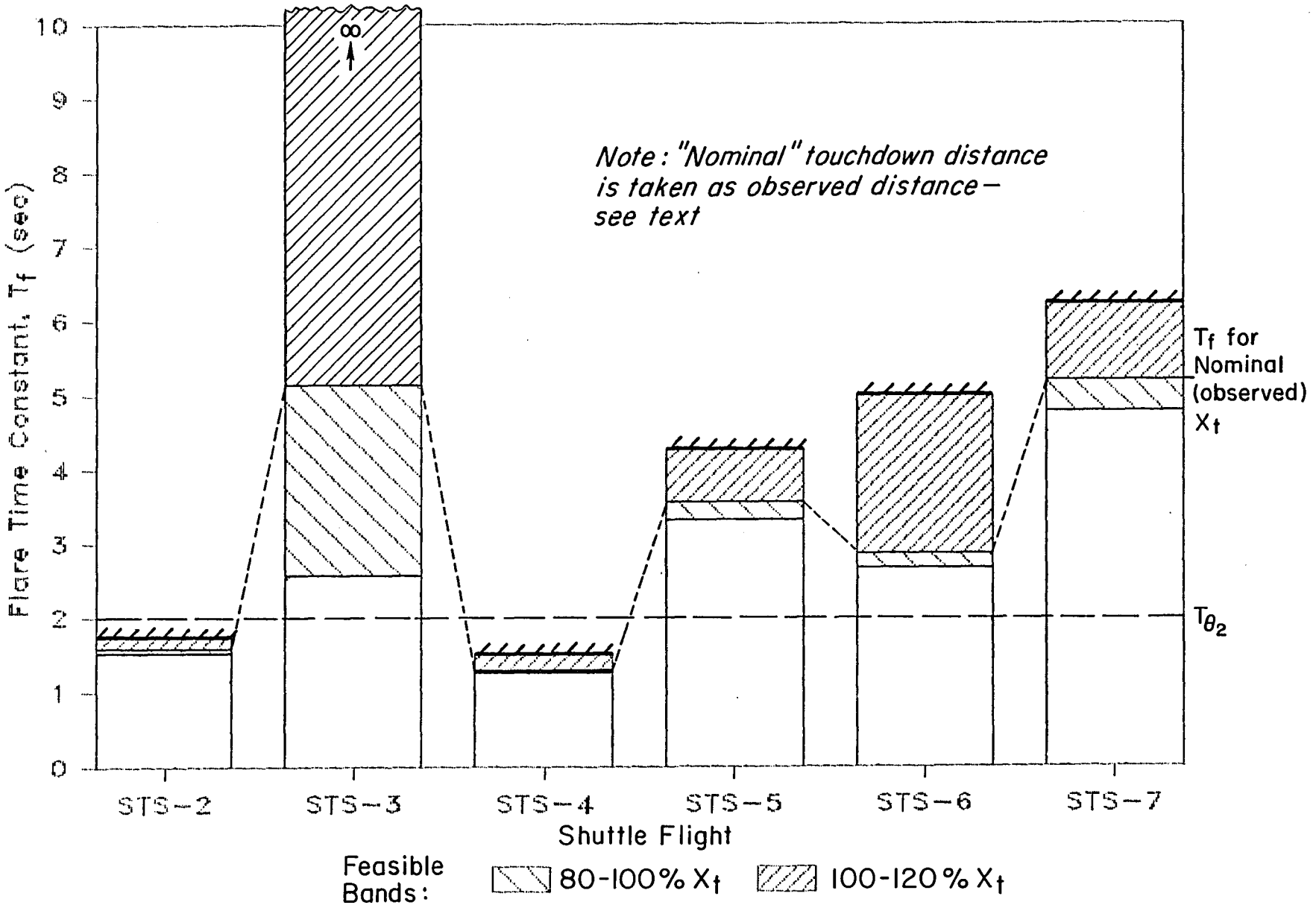

Figure A-11. Feasible T_f Ranges for Touchdown Distance

> The STS-4 Commander Mattingly indicates that "he was surprised how short he landed. (He landed 950 ft past the threshold, the expected touchdown point was 3000 ft.) He said that it was pure luck that they had landed where they did. He also said that without adequate instruments and displays, he would be uncomfortable about landing where a 1000 ft error was unacceptable."

In contrast no explicit adverse comments were made concerning speed and sink rate control by Mattingly, and corresponding debriefing documents from STS-5 and -6 do not contain pilot comments indicating concern with difficulty in precise touchdown control. Reference A-4 states that STS-5 Commander Brand said, "that he felt comfortable with landing on the concrete runway." While such commentary cannot verify the analysis leading to the margins of Fig. A-11, there is at least this consistency between the margin analysis and the limited pilot comments available.

(4) Feasible T_f Ranges and Margins with Simultaneous Constraint

As noted previously, the pilot must ultimately select a single T_f that will (if possible) satisfy all three touchdown constraints. This final consideration can be addressed by combining Figs. A-9, A-10, and A-11 into a single plot as shown in Fig. A-12. In this figure, the feasible bands for sink rate, speed, and distance are shown from left to right for each of the six landings. It can be expected that when crews face difficulties in satisfying all three constraints, they will weight each constraint differently in an attempt to find an acceptable compromise. This makes for difficulties in assessing Fig. A-12 so several alternative assessments will be examined here. The best long term approach to this issue (and all others in pilot strategy analysis) is to process as much flight data as possible through the best available strategy analysis tools and consider the long term results.

As a first assessment of Fig. A-12, we can consider the overall feasible T_f ranges simultaneously. In this case, all 3 feasible ranges overlap (implying a mutually acceptable T_f exists) for all landings except STS-3. This problem with STS-3 cannot really be considered significant since it could disappear with a slight re-definition of the

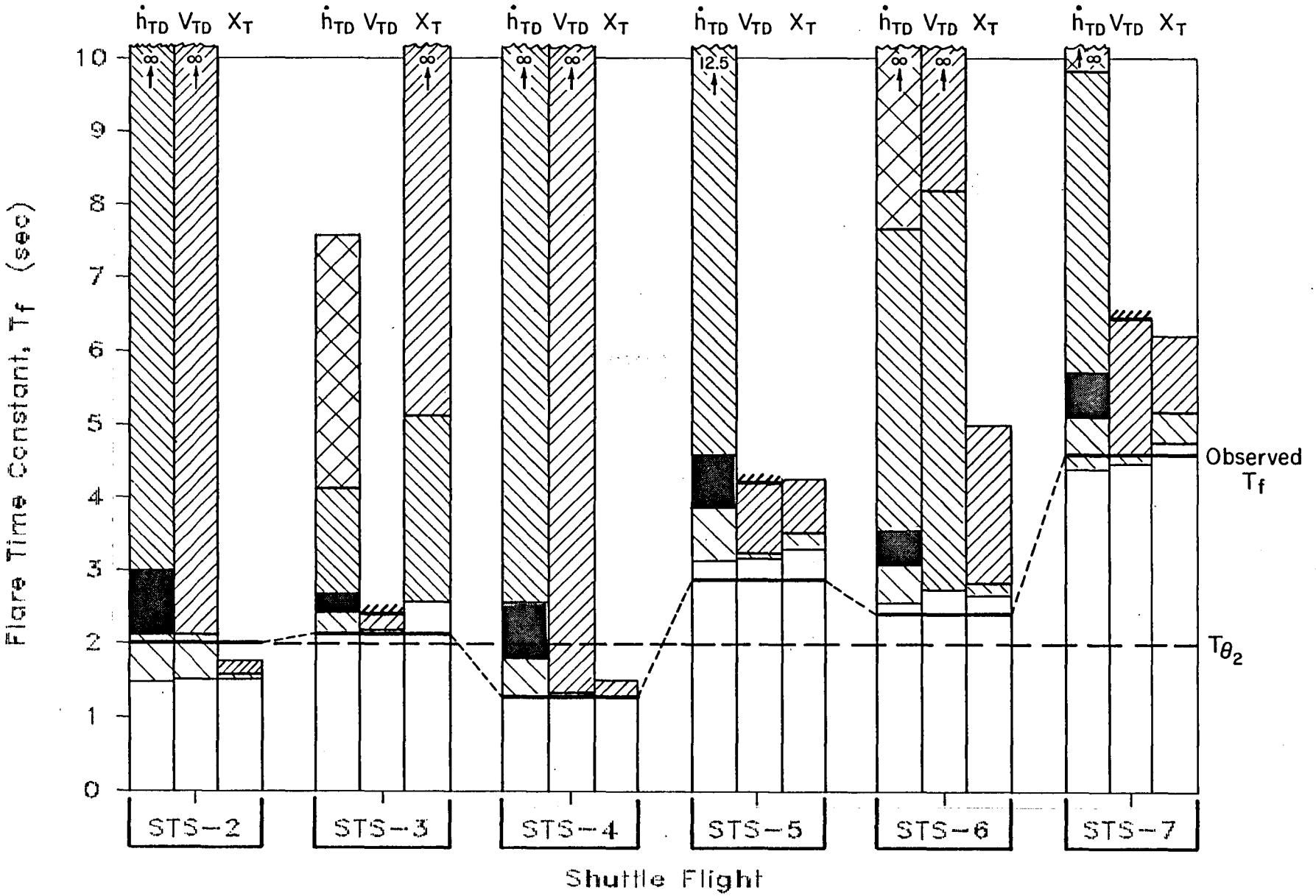

Figure A-12. Feasible T_f Ranges for Simultaneous Application of Constraints

relative distance constraints. Consistent with the analysis of the individual constraint cases, the T_{θ_2} margins, based on the simultaneous feasible bands, are improved for the last three flights.

It appears that crews apply their own tighter constraints on acceptable touchdown sink rate. Thus as a second assessment, we can focus on the nominal $\dot{h}_{TD}$ band (shown solid in Fig. A-12). Under these conditions, a slight problem is indicated for STS-3 with respect to speed and similar slight mismatches are indicated for distance for STS-2 and -4. Again the last three flights show improvements in both the T_f and T_{θ_2} margins. For the last three landings, the nominal $\dot{h}_{TD}$ margin is the limiting factor in setting the simultaneous T_f margin except for STS-5 where touchdown speed margin is the limiting factor. The observed values of $\dot{h}_{TD}$ indicate that the true nominal range accepted by the crews may be closer to $\dot{h}_{TD} = 0$. However, if this assumption were made, the above conclusions would remain except for a technical correction for STS-3.

As a final assessment, we can consider only the sink rate and speed constraints which are more well defined than the distance constraint. In this case, the STS-2, -3 and -4 landings would appear marginally better, but STS-3 would remain clearly the worst strategy.

As a final indication of the gross validity of the margin analysis, we can note that the variation in the observed T_f shown in Fig. A-12, tracks the simultaneous feasible bands (within the precision to which T_f can be extracted from flight data) regardless of the band criterion. Of course the model-based bands also depend on flight extracted parameters other than T_f, but it should be realized that an arbitrary function of the extracted parameters would not in general produce such tracking.

In summarizing the above use of margins as performance measures for strategy analysis, it seems likely that some of the recurring indications (such as general improvement in the strategies for the last three flights correlated with improved landing aids) probably are significant. However, many of the detailed interpretations are certainly open to question. The greatest value of the analysis scheme at this point is

perhaps the indication of potential developments for quantitative flight data analysis. The best route to improving the methodology is to apply it to many additional flights.

b. T_f Sensitivity Analysis

One basic limitation of margin analysis is that it does not necessarily indicate the most likely choice of T_f within a feasible range. An approach to this problem can be made by considering the sensitivity of the constrained touchdown parameters to T_f (or in a more general view any strategy variable.) Here the T_f sensitivity of any constrained variable is defined as its derivative with respect to T_f computed from the Fig. A-2 equations and evaluated at the observed value of the constrained variable. This absolute sensitivity can be normalized by multiplying by T_f and dividing by the observed constrained variable value. These definitions can be made more concrete by considering the T_f sensitivities for touchdown sink rate, speed, and distance.

The calculation of absolute sink rate sensitivity is shown graphically in Fig. A-13 for STS-6. The sensitivities for all six landings are compared in Fig. A-14a and in normalized form in Fig. A-14b. The normalized sensitivities may be interpreted as the percentage change in touchdown sink rate for a 1% change in flare time constant. As an adjunct to these bar charts, it is useful to visualize the sensitivities as slopes on the Fig. A-4 curves. The corresponding touchdown speed and distance sensitivities are summarized in Figs. A-15 and A-16, respectively. Comparison of these sensitivities shows that the absolute (but not the normalized) sink rate sensitivity is noticeably the most consistent over the six flights. The speed and distance sensitivities, both absolute and normalized, show a general pattern of variation for the early flights with an indication of more consistent medium values in the later flights. This could be a result of the growth of flight experience and the improved landing aids.

In considering sensitivity and its possible bearing on pilot strategy, it is useful to consider three basic levels of sensitivity based on the asymptotes as discussed above (Section A-1-d). If the pilot's

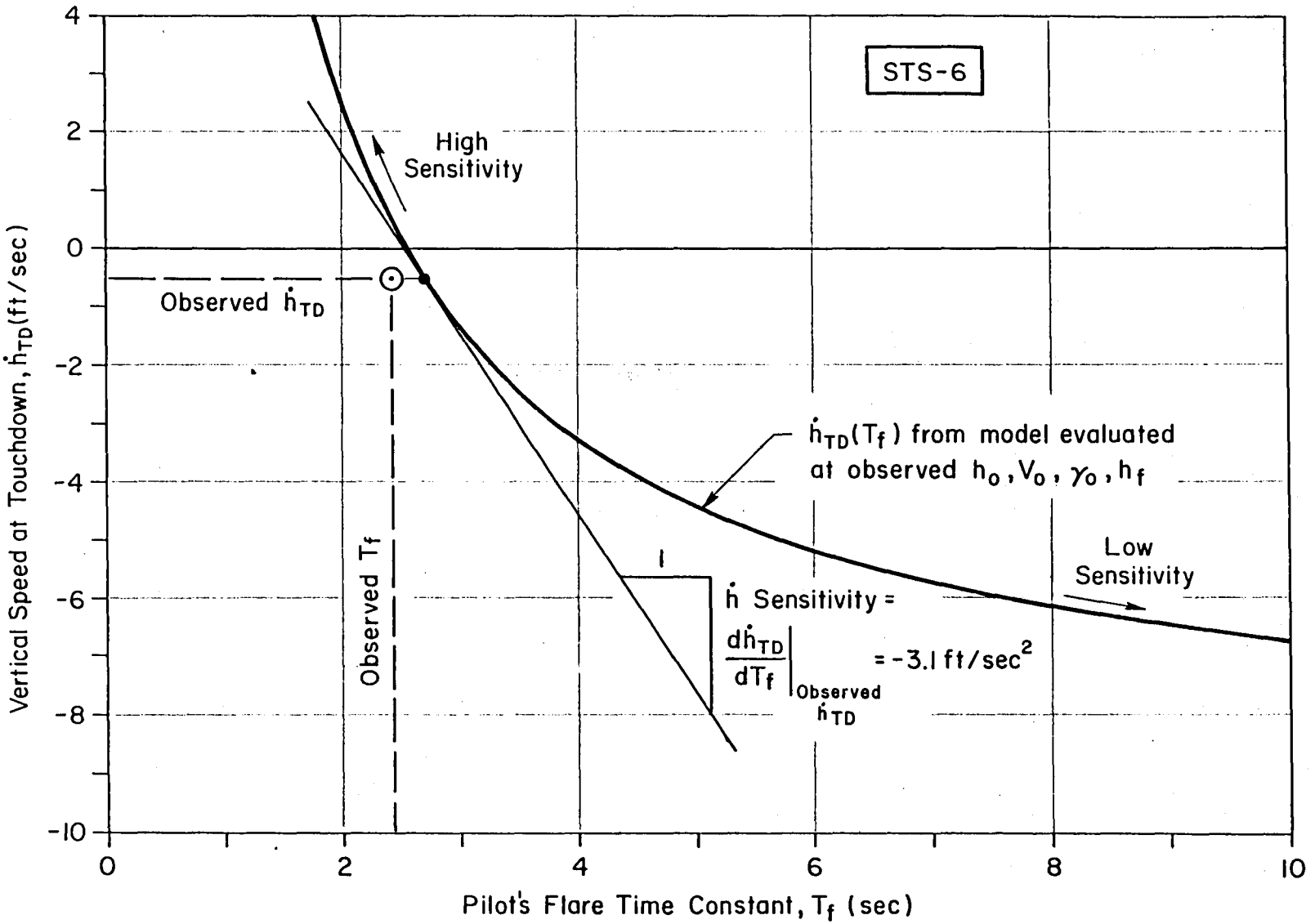

Figure A-13. Calculation of Absolute Sink Rate Sensitivity

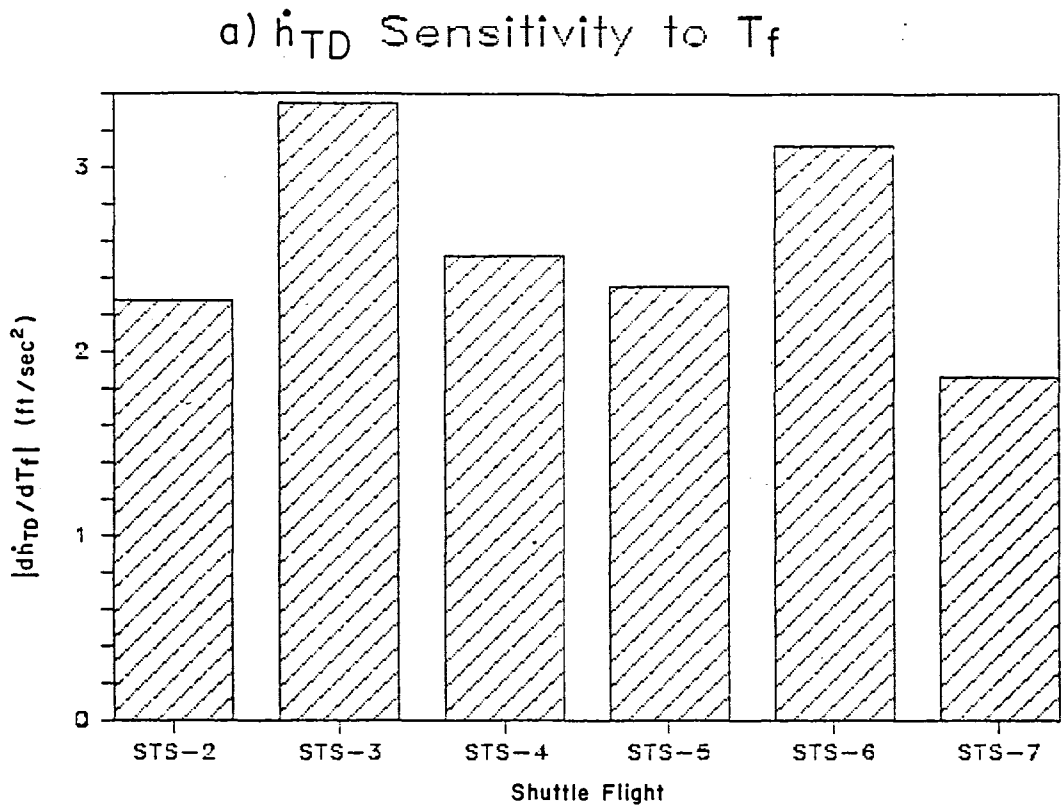

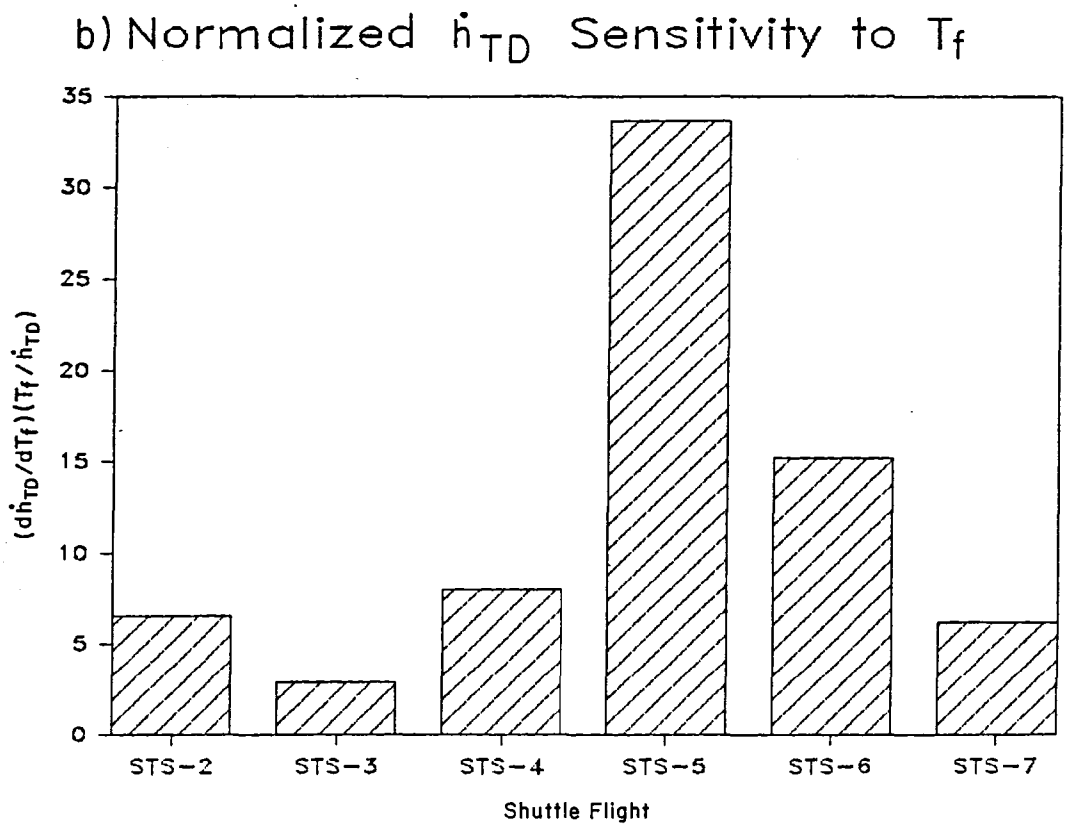

Figure A-14. Touchdown Sink Rate Absolute and Normalized Sensitivity to Flare Time Constant

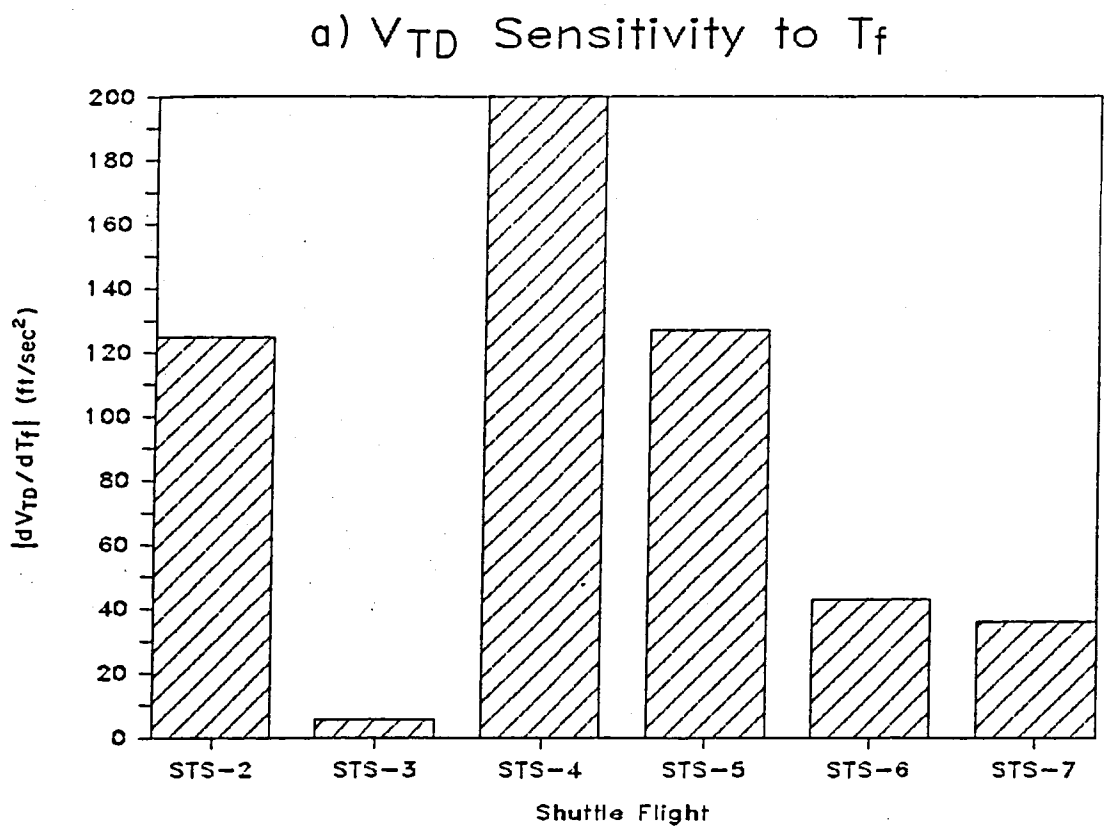

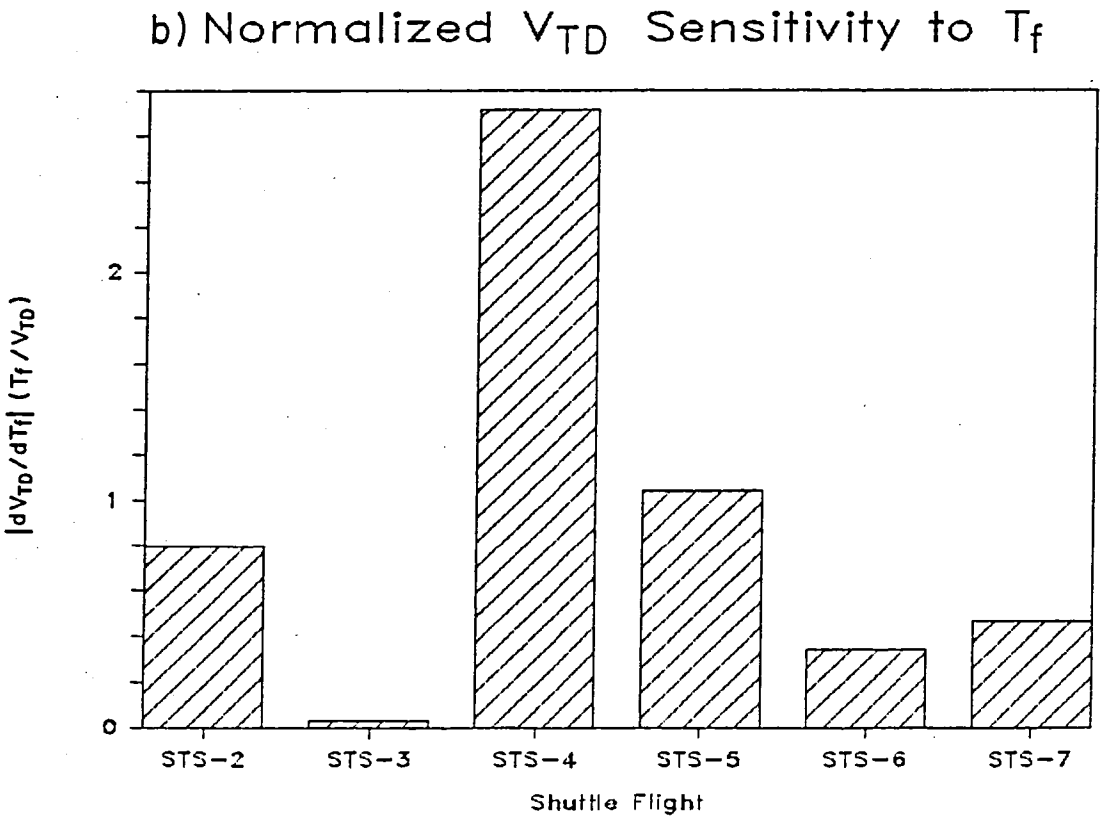

Figure A-15. Touchdown Speed Absolute and Normalized Sensitivity to Flare Time Constant

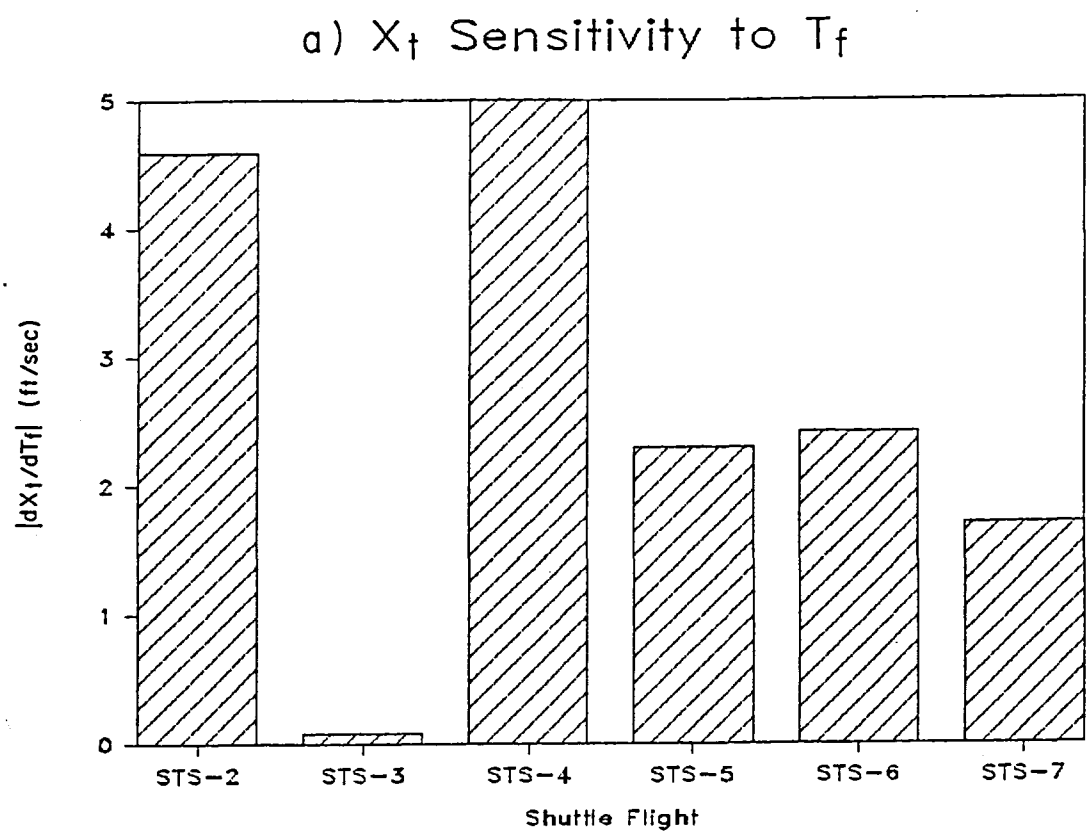

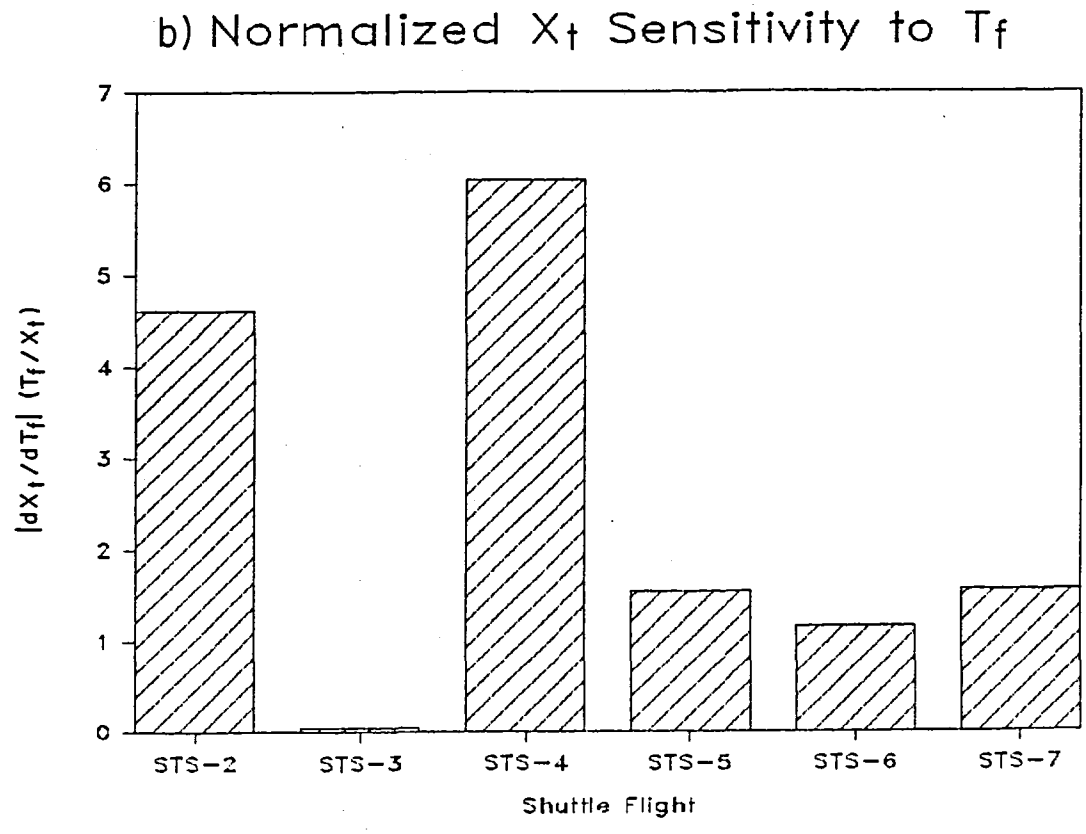

Figure A-16. Touchdown Distance Absolute and Normalized Sensitivity to Flare Time Constant

strategy results in operation near the vertical asymptotes, the sensitivities will be very high, but if he operates near a horizontal (large T_f) asymptote, the sensitivity will be very low. Medium sensitivity is achieved by operation on the "knee" of the curves. It seems likely that pilots would wish to avoid high sensitivity strategies that would require very precise inner-loop control. On the other hand, there is in principle some potential advantage for low sensitivity strategies, since if the pilot sets up to operate on the large T_f (horizontal) asymptotes, the final flare is not at all critical and becomes almost unnecessary. The critical disadvantage of such strategies is that if the setup is not correct, there is no sensitivity available to the pilot for last second corrections with T_f. Thus we may speculate that the pilots would prefer to "keep their options open" by setting up the landing with adequate or even high sensitivities. It should be emphasized that sensitivity is not a strategy variable, but rather (per the hypothesized model) a consequence of the overall strategic decisions. If sensitivity is truly a factor in the Shuttle crew's strategic planning, it would seem that its effect must be slowly perceived and accounted for during the long process of simulator and STA flight training.

The sensitivity summaries for STS-2 through -6 do indicate a general trend toward medium sensitivity as the flights progress, but notably the crews do not appear to reduce sensitivity to low levels even when it is feasible (e.g., STS-2 in Figs. A-4 and A-5). It might be speculated that the consistency seen in the sink rate sensitivities indicates that the pilot weights sink rate more heavily than speed or distance. However, it may well be that this is simply a consequence of the limited range of $d\dot{h}_{TD}/dT_f$ around the nominal feasible T_f range for $\dot{h}_{TD}$ (see Fig. A-4).

The above considerations of sensitivity provide some useful quantitative working hypotheses, but resolution of the issues raised will require analysis of a much larger sample of flight data.

3. Summary and Possibilities for Further Development

Conclusions from the Strategy Analysis

- A simple three variable model of pilot strategy has been defined and parameters of the model have been extracted from STS-2 through -7 flight data. The model was simplified to a single strategy variable, T_f, the pilot's flare time constant by setting the other two variables, shallow glide angle and flare height, to the values observed in flight. A check of model validity was made by comparing the observed T_f to the model-based value.

- The strategy model has been used to define the feasible ranges of T_f for the given touchdown constraints which allow definition of two strategy measures -- T_f margin, the width of a feasible T_f band and T_{θ_2} margin, the difference between a minimum feasible T_f, and the path-to-attitude lag, T_{θ_2}.

- Comparison of the margins for the six landings with the three touchdown constraints applied individually or simultaneously, shows a general improvement in the margins for the last three flights apparently correlated with improved landing aids and greater flight experience.

- T_f sensitivity was developed as a possible factor in the pilot's choice of T_f within a feasible range. Comparison of the six landings indicates that crews are willing to accept high sensitivity, but with an indication of a trend toward medium levels for later flights. For several landings it would have been feasible to reduce sensitivity to low levels and thus minimize the requirements for flare, but this option was not exercised by the Shuttle crews. One possible explanation is that the crews wish to maintain adequate sensitivity to allow for last second adjustments in the flare.

- While some of the primary conclusions of the strategy analysis appear valid, the concept needs to be refined from a much larger sample of landings. The primary value of the method at this point is to indicate new possibilities for quantitative manual control analysis of flight data.

Recommendations for Further Development of Strategy Analysis

- Further work in refining the flight data, especially altitude and sink rate estimates for analytical use should be considered. Complementary filtering and other estimation techniques should be considered for combining the cinetheodolite, takeoff and landing tower, and MMLE data into best estimates. The addition of ground based radar should be considered.

- Further efforts should be made to define the constraints on the landing task more precisely. Inputs from the crews and Shuttle operational groups would be very valuable.

- Refinements to the procedure for fitting the glide and flare strategy model to the flight hodographs should be pursued. The next step might be to apply a low pass (digital) filter to the altitude and sink rate signals before generating the hodograph. The filter breakpoint should be below $1/T_{\theta_2}$ and the pilot-vehicle closed-loop attitude mode.

- A simple digital simulation model of the Orbiter in landing (which will accept flight RHC data) should be assembled. There should be provision for pilot models for use in testing identification procedures.

- Further application of NIPIP for pilot model identification should be considered taking into account recent improvements in flight data and new strategy insights. A minimal effort could be to attempt to define the periods of open vs. closed-loop pilot activity in landings.

- Further efforts should be made to improve speed and efficiency of data handling. The Interactive Data Handler functions should be implemented with use of commercially available "integrated spread sheet/data base manager" software being the most practical approach.

APPENDIX

REFERENCES

A-1. Myers, T. T., D. E. Johnston, and D. T. McRuer, Space Shuttle Flying Qualities Criteria Assessment, Phase III, NASA CR-170407, June 1983.

A-2. Myers, T. T., D. E. Johnston, and D. T. McRuer, Space Shuttle Flying Qualities and Flight Control System Assessment Study, Phase II, NASA CR-170406, Dec. 1983.

A-3. STS-4 systems debriefing 15 July 1982, Tim Horten.

A-4. STS-5 systems debriefing 30 November 1982, Tim Horten.

1. Report No.	2. Government Accession No.	3. Recipient's Catalog No.
NASA CR-166618		

4. Title and Subtitle	5. Report Date
SPACE SHUTTLE FLYING QUALITIES CRITERIA ASSESSMENT PHASE IV — DATA ACQUISITION AND ANALYSIS	May 1986
	6. Performing Organization Code
7. Author(s) T.T. Myers, D.E. Johnston, and D.T. McRuer	8. Performing Organization Report No. STI TR-1206-1
	10. Work Unit No. RTOP 506-48
9. Performing Organization Name and Address Systems Technology, Inc. 13766 South Hawthorne Boulevard Hawthorne, California 90250	11. Contract or Grant No. NAS2-11431
	13. Type of Report and Period Covered Contractor Report — Final
12. Sponsoring Agency Name and Address National Aeronautics and Space Administration Washington, D.C. 20546	14. Sponsoring Agency Code

15. Supplementary Notes

NASA Technical Monitor: Donald T. Berry, Ames Research Center, Dryden Flight Research Facility, Edwards, CA 92523. Phase I of this study published as NASA CR-170391; Phase II as NASA CR-170406; Phase III as NASA CR-170407.

16. Abstract

This study continues the development of flying qualities experiments (OFQ) as a part of the Orbiter Experiments Program (OEX). Phase I reviewed flying qualities criteria and initial Shuttle Data. Phase II proposed a non-intrusive experiment program implementation in which flying qualities data and information can be extracted from onboard and ground sensing of routine Orbiter approach and landing performance measures and correlated with simulation experiments. Phase III presented a first trial of the analytic techniques required for the non-intrusive experimental approach using data from STS-4 onboard sensing and recording systems. In this Phase IV effort the data base was extended to use of ground based cinetheodolite measurements of Orbiter approach and landing. Onboard the cinetheodolite data were analyzed from flights STS-2 through -7 to identify the effective augmented vehicle dynamics, the control strategy employed by the pilot during preflare, shallow glide, and final flare segments of the landing, and the key approach and touchdown performance measures. A plan for an OFQ flying qualities data archive and processing program is presented.

17. Key Words (Suggested by Author(s))	18. Distribution Statement
Space shuttle orbiter Flying qualities Flight control Manual control	Unclassified — Unlimited STAR category 8

19. Security Classif. (of this report)	20. Security Classif. (of this page)	21. No. of Pages	22. Price*
Unclassified	Unclassified	133	A07

For sale by the National Technical Information Service, Springfield, Virginia 22161.

End of Document